UNDERSTANDING THE SYSTEMIC ROLES OF EXOSOMES IN INNATE IMMUNITY

A Dissertation

Presented to

The Academic Faculty

by

Swetha Srinivasan

In Partial Fulfillment

of the Requirements for the Degree

Doctor of Philosophy in the

School of Biology

Georgia Institute of Technology

August 2016

UNDERSTANDING THE SYSTEMIC ROLES OF EXOSOMES IN INNATE IMMUNITY

Approved by:

Dr. Fredrik Vannberg, Advisor
School of Biology
Georgia Institute of Technology

Dr. J Brandon Dixon, Co-advisor
Georgia W. Woodruff School of
Mechanical Engineering
Georgia Institute of Technology

Dr. John McDonald
School of Biology
Georgia Institute of Technology

Dr. King Jordan
School of Biology
Georgia Institute of Technology

Dr. Gregory Gibson
School of Biology
Georgia Institute of Technology

Date Approved: 06/20/2016

To Sriram (Cheelu), my brother and inspiration

ACKNOWLEDGEMENTS

There are many people without whom I would not have made it this far.

I wish to thank my advisor Dr. Fredrik Vannberg for his constant support and guidance through the entirety of my PhD. I would also like to thank my co-advisor Dr. J. Brandon Dixon for his support and this unique opportunity of being a part of his team as my second lab. Under their guidance, I have learned to become a better communicator, a better scientist – and a better person. I have learned how to think critically of my work and that of others, while maintaining "the big picture" in mind. I will forever remember their lessons and their mentorship. Additionally, I would also like to thank Dr. John McDonald, Dr. Gregory Gibson and Dr. I. King Jordan for being my committee members and for providing me with very valuable guidance for which I am thankful.

I must thank all the Vannberg and Dixon lab members, both present and past for being my lab family. Several of them have helped me immensely, and their input and/or guidance on all aspects of my project(s) is greatly appreciated. I would also like specially thank Shweta Biliya, who ensured that the lab functioned smoothly for all the work to happen and also for her help with the sequencing runs. I would also like to thanks Shashidhar Ravishankar and James Moore for their help with RNA-Seq analysis

I am grateful to the TI:GER program for giving me a different perspective and encouraging me to explore and understand the business side of science. I would specially like to thank Margi Berbari, Professor Marie Thursby and my TI:GER team(Deepa, Mark, Alex(K) and Alex(G)) for their support and participation in my TI:GER journey. Those 2 years were the best years of my PhD.

I would like to thank the support staff here in IBB that trained and helped me with a lot of my work; Andrew Shaw for confocal microscopy and imaging, Nadia Boguslavsky for flow cytometry and cell sorting, Steve Woodard and Allen Echols for their help around IBB, and Kim Benjamin, Dr Laura O'Farrell and others at the animal facility. I also want to thank the staff at the school of

Biology including Kevin Roman, Nena Gray, Alison Onstine and others for all their help. I also want to thank all the professors with whom I TA'ed; Dr. Merrill, Dr. Bardill, Dr. Shin, Dr. Choi and Dr. Gormally for their patience and support; I learnt how to instruct students communicate better as a result of my experiences with you.

I had a great time working with and mentoring several undergraduate students as a part of these projects and I want to acknowledge their contributions both intellectual and otherwise to this body of work. A special shout out to Michelle Su who perhaps spent as much time as me on some of the work done here. I would also like to take this opportunity to thank my fellow PhD students and friends for the support outside and sometimes even inside lab. They were a part of all my celebrations and are too many to name but you know who you are!

A special round of thanks to Samit and Preeti, the two people in my life have supported me without reservation or hesitation, not just during my time here, but always. Whenever I made a misstep, or when times were tough, they always helped guide me back to where I needed to be.

Lastly, I would like to thank all my parents for their patience, understanding, and encouragement. They kept me going with their positive attitude and strong belief in my work and this thesis is a result of their backing and support.

TABLE OF CONTENTS

LIST OF TABLES

LIST OF FIGURES

LIST OF SYMBOLS AND ABBREVIATIONS

Abbreviation	Description
AF #	Alexa fluor, common fluorophore used in secondary antibodies
ALIX	Protein of the ESCRT pathway, important for intralumenal endosomal vesicle formation
APC	Antigen presenting cells
BCA	bicinchoninic acid assay
BSA	Bovine serum albumin
CCD	charge-coupled device
CCL19	Chemokine (C-C motif) ligand 19, pro-inflammatory
CCL21	Chemokine (C-C motif) ligand 21, binds to CCR7 for cell migration
CCL3	Chemokine (C-C motif) ligand 3, inflammatory cytokine
CCR7	C-C chemokine receptor type 7
CD11B	Murine macrophage surface marker
CD14	cluster of differentiation 14, cooperates with other proteins to recognize LPS
CD169	Sialoadhesin found on subcapsular sinus macrophages
CD19	Murine B-cell surface marker
CD4	Helper T-cell marker
CD63	Tetraspanin membrane protein found on exosomes
CD8	Killer T-cell marker
CD81	Tetraspanin membrane protein found on exosomes
CD86	Membrane protein of the immunoglobulin superfamily expressed by antigen-presenting cells
cDNA	Complementary DNA
CEL	file that stores results of the intensity calculations on the pixel values of the DAT file from microarray chips
CIBERSORT	method for characterizing cell composition of complex tissues from their gene expression profiles
CT	Computerized tomography
CTL	cytotoxic T cell
CV	Collecting vessel
CXCL2	Chemokine (C-X-C motif) ligand 2 (CXCL2), macrophage inflammatory cytokine
DAPI	4',6-diamidino-2-phenylindole) is a fluorescent stain that binds strongly to DNA
DC	Dendritic cells
DiL/DiO	Lipophilic Tracers to stain lipid membranes
DMEM	Dulbecco's Modified Eagle Medium
DNA	Deoxy ribose nucleic acid
dsRNA	double stranded RNA
EBM	Endothelial Cell Growth Medium
EBV	Epstein-Barr virus
EDTA	Disodium Ethylenediaminetetraacetic acid
ESCRT	endosomal sorting complexes required for transport

FACS	Fluorescence activated cell sorting
FBS	Fetal bovine serum
GCRMA	Background Adjustment method for microarrays
HBSS	Hank's Balanced Salt Solution
HEPES	(4-(2-hydroxyethyl)-1-piperazineethanesulfonic acid, a buffer
HEV	high endothelial venules
HIV	human immunodeficiency virus
HSP	Heat shock protein
ICG	indocyanine green
IFN	Interferon, cytokine that plays critical roles in innate immunity to pathogens
IL12	Cytokine expressed by activated macrophages, serves as an essential inducer of Th1 cells development
IL1b	Interleukin 1 beta, cytokine that mediates inflammation
ILV	intraluminal vesicles
iNOS	Nitric oxide synthase
IRAK4	Interleukin-1 Receptor-Associated Kinase 4
IRDye	Near infrared dye that conjgates with n-terminal proteins
IRF	interferon regulatory factor
LBP	LPS Binding Protein
LBPA	lyso-bis-phosphatidic-acid
LEC	lymphatic endothelial cells
LN	Lymph node
LPS	lipopolysaccharide
LRR	leucine-rich repeat
LSM	Laser scanning microscope
M1 STATE	Macrophages reprogrammed to respond by secretion of inflammatory molecules
MAMP	Microbe Associated Molecular Patterns
MAPK	Mitogen-activated protein kinases
MART1	melanoma antigen recognized by T-cells
MAVS	mitochondrial Antiviral Signaling Protein
MD-2	protein that associates with toll-like receptor 4 on the cell surface and confers responsiveness to lipopolysaccharide
MDA5	Innate immune receptor which acts as a cytoplasmic sensor of viral nucleic acids
MHC	Major histocompatibility complex
MRI	Magnetic resonance imaging
MVB	Multi-vesicular bodies
Myd88	myeloid differentiation primary response protein 88
NF-κB	Nuclear Factor- kB
NIK	NF-κB-inducing kinase
NIR	Near Infra-red
NK	Natural Killer cell
NKG2D	Membrane protein expressed on natural killer cells
NO	Nitric oxide

OCT	Optimal cutting medium
PAM	synthetic triacylated lipopeptide (LP) that mimics the acylated amino terminus of bacterial LPs.
PAMP	Pathogen Associated Molecular Patterns
PBS	Phosphate buffered saline
PCR	Polymerase chain reaction
PE	Phycoerythrin, common fluorophore used in secondary staining
PET	Positron emission tomography
PFA	paraformaldehyde
pIC	Poly (I:C)
PKH67	Fluorescent cell membrane stain
PLA	Proximity Ligation Assay
PRR	Pattern Recognition Receptors
QD	quantum dots
RIG-1	Protein involved in cytoplasmic viral double-stranded (ds) RNA recognition
RIPA	Radioimmunoprecipitation assay buffer, protein extraction buffer
RNA	Ribonucleic Acid
RNA-Seq	RNA sequencing, aka whole transcriptome shotgun sequencing
ROI	regions of interest
RP105	Co-protein required for recoginition of lipopolysaccharide by TLR4
RPMI	Roswell Park Memorial Institute medium
SCS	subscapular sinus
SEM	Scanning electron microscopy
SIRT1	Sirtuin 1, regulates epigenetic silencing via deacetylation
SNR	Signal to noise ratio
SRA	Sequence read archive
STAT	Signal transducer and activator of transcription , transcription factor
TAK1	Protein kinase required for NF-κB induction
TGF-B	transforming growth factor beta
TIR	Toll/IL-1 receptor
TIRAP	Toll-like receptor adaptor protein, responsible for signal transduction
TLR	Toll-like receptor
TLR3	Toll-like receptor 3
TLR4	Toll-like receptor 4
TNFA	Tumor necrosis factor
TOLLIP	Toll-Interacting protein
TRAF6	TNF Receptor-Associated Factor 6,
TRIF	Toll-Like Receptor Adaptor Molecule , mediates protein-protein interactions between the Toll-like receptors (TLRs) and signal-transduction components
TSG101	Tumor Susceptibility gene 101, Component of the ESCRT-I complex, a regulator of vesicular trafficking process.
UV	Ultraviolet

SUMMARY

The ability of the immune system to recognize and respond to pathogenic organisms is essential for the body's ability to control an infection. The broad and prompt innate immune response primes the acquired branch eliciting protection against most pathogenic invaders. Cell-cell communication is critical for rapidly spreading the message of infection and enabling the innate immune system to mount a broad response against the pathogen. While cytokines and chemokines have been extensively characterized for the roles as messengers in innate immunity, exosomes are emerging as key players in this field.

Exosomes are nanovesicles (~50nm in diameter) that are released extracellularly by all cell types. They carry functional cargo in the form of mRNA, microRNA and proteins that reflect the host cells molecular composition and can transport this cargo to recipient cells where it is functional_and has the ability to affect the phenotype of the cell both transcriptionally and biochemically. Their ability to transmit messages between cells at a distance and their rapid transport through the body makes them ideal messengers for establishing innate immune responses.

Lymphatic flow is an important component of the circulation and serves to transport of antigens, immune cells and large macromolecules from the periphery to the lymph nodes where innate and adaptive immune responses are elicited. While exosomes have been seen to modulate lymph node function, their ability to use the lymphatics was unknown. Using an in vitro model of lymphatic uptake, we have shown that lymphatic endothelial cells actively enhanced lymphatic uptake and transport of exosomes to the luminal side of the vessel. Furthermore, we have demonstrated a differential distribution of exosomes in the draining lymph nodes that is dependent on the lymphatic flow. Lastly, through endpoint analysis of cellular distribution of exosomes in the node, we identified macrophages and B-cells as key players in exosome uptake. Together these results suggest that exosome transfer by lymphatic flow from the periphery to the lymph node

could provide a mechanism for rapid exchange of infection-specific information that precedes the arrival of migrating cells, thus priming the node for a more effective immune response.

Toll-like receptors (TLR's) are a family of receptors play a central role in the host cell defense against disease by detecting highly conserved pathogen associated molecular patterns. This results in a localized inflammatory response that results in the production of a broad range of molecules including cytokines and chemokines, which are essential for host response to infection as well as for the development of an adaptive immune response. However, it is unknown if exosomes play a role in propagating the local TLR response to distal cells, aiding in the rapid spread of the message of infection as well as the establishment of a pathogen specific response.

Here we demonstrate the distal recapitulation of the local toll-like receptor response via exosomes. We further delineate the kinetics of the response and show that we can abrogate the action-at-a-distance signaling of exosomes by UV irradiation, demonstrating that RNA is crucial for their effector function. We also show that exosomes derived from TLR stimulated cells epigenetically modify distal cells to be refractory to further LPS stimulation (i.e. undergo endotoxin tolerance), thus protecting these distal cells from uncontrolled inflammation.

We show a striking increase in total lymphatic transport and nodal retention of pIC exosomes within minutes of injection. The data shown here is the first evidence that exosomes could directly be involved in modulating flow to the lymph node. We further expand the impact of exosome uptake by lymph node macrophages to demonstrate that TLR-exosomes are capable of inducing an inflammatory response via *Il12 and Nos2* in murine macrophages *in vivo*. We also analyzed the whole lymph node milieu by next generation sequencing to find evidence of neutrophil, mast cell and monocyte recruitment in the pIC-exosomes and polarize the node to a pro-inflammatory state.

CHAPTER 1: BACKGROUND AND LITERATURE REVIEW

1.1 Immune system

The immune system is a complex network of cells and organs that protects the organism against infectious agents such as bacteria, viruses and other pathogens. This is achieved with a combination of the two arms: humoral immunity and adaptive immunity. Innate or humoral immunity is an antigen non-specific, evolutionarily conserved system in most multicellular organisms that attacks common human pathogens. Adaptive Immunity on the other hand is mediated by lymphocytes and is characterized by specificity and memory(1).

1.1.1 Adaptive Immunity

Adaptive immunity relies on the generation of a random and diverse repertoire of antigen receptors followed by clonal selection and expansion of receptors with high specificity resulting in immunological memory. The main limitation of the adaptive immune system is that specific clones need to expand and differentiate into effector cells before they can participate in the host's defense. This process usually takes 4-7 days and the source and biological context of the antigen remains undetermined(2).

1.1.2 Innate immunity

Innate immunity involves the sentinel cells of the immune system that are initial responders upon microbe entry into the body. The host uses innate immunity immediately on exposure to any pathogen and is an initial response to prevent infection. It does not recognize every possible antigen and relies on a variety of distinct, constitutive and conserved molecules that are characteristic of common microbes that infect mammals. These unique microbial molecules can be thought of as molecular signatures of microbial invaders and are called *P*athogen *A*ssociated *M*olecular *P*atterns

(PAMP's) or *M*icrobe *A*ssociated *M*olecular *P*atterns (MAMP's). They include a large number of molecules including lipopolysaccharide (LPS) from Gram negative bacteria, Peptidoglycans from Gram positive Bacteria, and unmethylated CpG DNA from bacteria and viruses. PAMP's are invariant, are essential for microbial survival and are unique to microbes(3).

Most immune cells such as natural killer cells, phagocytic cells (macrophages, monocytes) have a variety of *P*attern *R*ecognition *R*eceptors (PRR's) for common PAMP's and respond immediately against the invading microbe. These receptors are located on the cell surface where they interact with extracellular PAMP's or within phagolysosomes where they interact with phagocytosed pathogens. Binding of PAMP's to the corresponding PRR results in the synthesis and secretion of regulatory molecules such as cytokines that are essential for initiating an immune response(4).

A complete list of PAMP's, their microbial origin, along with the cognate PRR that recognizes them is given below in Table 1

Table 1: Recognition of microbial components by PRRs(5)

Receptor	Cellular localization	Microbial component(s)	Origin(s)
TLRs			
TLR1/TLR2	Cell surface	Triacyl lipopeptides	Bacteria
TLR2/TLR6	Cell surface	Diacyl lipopeptides	*Mycoplasma*
		Lipoteichoic acid	Gram-positive bacteria
TLR2	Cell surface	Lipoproteins	Various pathogens
		Peptidoglycan	Gram-positive and -negative bacteria
		Lipoarabinomannan	Mycobacteria
		Porins	*Neisseria*
		Envelope glycoproteins	Viruses (e.g., measles virus, HSV, cytomegalovirus)

Table 1 Continued

		GPI-mucin	Protozoa
		Phospholipomannan	*Candida*
		Zymosan	Fungi
		β-Glycan	Fungi
TLR3	Cell surface/endosomes	dsRNA	Viruses
TLR4	Cell surface	LPS	Gram-negative bacteria
		Envelope glycoproteins	Viruses (e.g., RSV)
		Glycoinositolphospholipids	Protozoa
		Mannan	*Candida*
		HSP70	Host
TLR5	Cell surface	Flagellin	Flagellated bacteria
TLR7/8	Endosome	ssRNA	RNA viruses
TLR9	Endosome	CpG DNA	Viruses, bacteria, protozoa
RLRs			
RIG-I	Cytoplasm	dsRNA (short), 5′-triphosphate RNA	Viruses (e.g., influenza A virus, HCV, RSV)
MDA5	Cytoplasm	dsRNA (long)	Viruses (picorna- and noroviruses)
NLRs			
NOD1	Cytoplasm	Diaminopimelic acid	Gram-negative bacteria
NOD2	Cytoplasm	MDP	Gram-positive and -negative bacteria
NALP1	Cytoplasm	MDP	Gram-positive and -negative bacteria
NALP3	Cytoplasm	ATP, uric acid crystals, RNA, DNA, MDP	Viruses, bacteria, and host
Miscellaneous			
DAI	Cytoplasm	DNA	DNA viruses, intracellular bacteria
AIM2	Cytoplasm	DNA	DNA viruses
PKR	Cytoplasm	dsRNA, 5′-triphosphate RNA	Viruses

1.1.2.1 Toll-like receptors

The Toll-like receptors (TLRs) are an evolutionarily conserved pattern recognition receptor family and consist of type-I trans-membrane receptors, which are characterized by an extracellular leucine-rich repeat (LRR) domain and an intracellular Toll/IL-1 receptor (TIR) domain. The namesake of the family, Toll, is a *Drosophila* protein with an immune function and responds to fungal and gram positive bacterial signals. LRR's are involved in ligand recognition and signal transduction while the TIR region is a conserved protein-protein interaction module(6).

In mammalian species, there are at least 10 distinct TLR's and each has a distinct function in mammalian immunity (Table 1). Several TLR ligands are known and are diverse in structure and origin. However, some common attributes are that TLR ligands are conserved microbial products (PAMP's), TLR's can recognize several structurally unrelated ligands, and some TLR's need accessory proteins to recognize their ligands(7).

Activation of signaling pathways by Toll like receptors results in the induction of various genes for host defense like cytokines, MHC complex, chemokines, and co-stimulatory molecules. Multiple effectors such as antimicrobial peptides and nitric oxide synthase are also induced(8).

1.1.2.2 LPS signaling pathway

Human TLR4 was the first characterized mammalian Toll and is expressed predominantly in macrophages and DC's but is found in a variety of cell types(9). It serves as the signal transducing receptor for LPS(10). Recognition of LPS by TLR4 is complex and requires several accessory proteins such as LPS Binding Protein (LBP), MD-2 and RP105. Once bound by LBP, LPS is transferred to CD14 (TLR4 co-receptor), a high affinity LPS receptor(11).

Post-receptor signal transduction by TLR4 requires the function of several conserved proteins since TLR's don't have any enzymatic activity. Instead stimuli induced

dimerization/oligomerization rearranges the TIR domains such that they act as a scaffold for recruiting adaptor proteins. This leads to Myd88 recruitment, a TIR domain protein which interacts with IRAK4. This complex (Myd88-IRAK4) activates TRAF6, NIK and TAK1 sequentially and this in turn results in MAPK and NF-κB activation. TNF is an important endpoint of LPS response as a result of NF-κB translocation to the nucleus(12).

Figure **1** shows classical TLR4 signaling mediated by LPS that results in a pro-inflammatory response resulting in the secretion of *TNFA,* IL1B and *IFNG.*

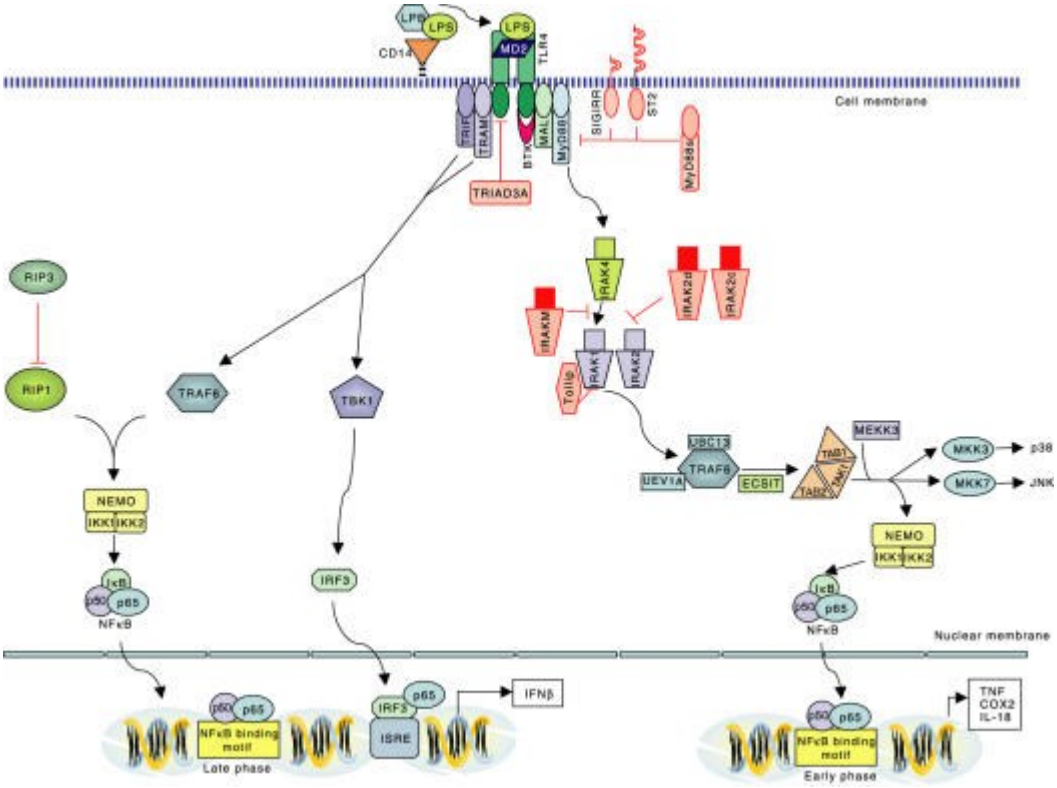

Figure 1: Model of LPS signaling through TLR4 binding in the cell(13)

1.1.2.3 Regulation of TLR signaling

The inflammatory cytokines and chemokines produced as a result of TLR engagement, if released in excess have the potential to induce serious systemic disorders including chronic inflammation, autoimmune disorders(14) and endotoxin shock(15). Thus the tight regulation of toll-like receptor

maintains the balance between immune activation in response to microbial pathogens and overt systemic inflammation.

Toll-Interacting protein (TOLLIP) interacts with IRAK and suppresses its activity resulting in the blocking of TLR4/LPS signaling(16).NF-κB is a key transcription factor that is held inactive by bound Iκ-Bα in the cytoplasm. It is activated in response to a pro-inflammatory signal such as LPS or TNFA and translocates to the nucleus where it activates the transcription of several pro-inflammatory cytokines and chemokines(17). It plays a key role in both TLR 4 and TLR3 response to infection. SIRT1, a NAD+ dependent histone deacetylase physically binds to the p65/RelA subunit of NF-κB and deacetylates it at a critical Lysine residue (K310) resulting in NF-κB inactivation and suppression of the pro-inflammatory response(18).

1.1.2.4 TLR3 signaling pathway

TLR3 is expressed predominantly in dendritic cells(19). It functions as a cell surface receptor for double stranded RNA (dsRNA) which is a molecular pattern produced by most viruses at some point in their life cycle(20). Several synthetic dsRNAs, like PIKA, Ampligen [Poly(I:C12U)] or polyriboinosinicacid-polyribocytidylic acid – commonly denoted as poly(I:C) efficiently mimic viral dsRNA. This results in the activation of TLR3 and an initiation of the host anti-viral response.

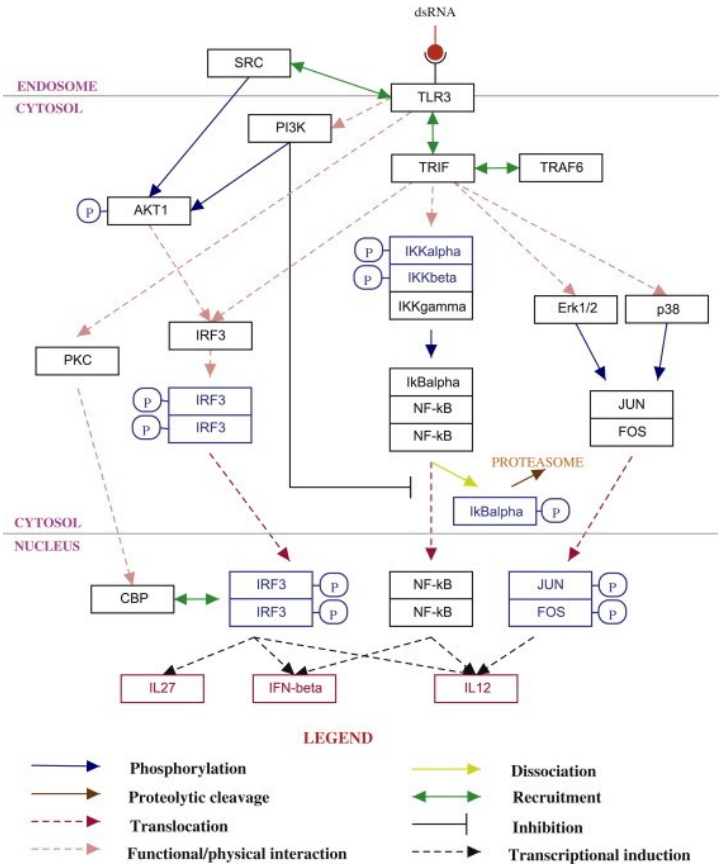

Figure 2: The TLR3 signaling pathway in dendritic cells (57).

Physiologically, TLR3 encounters dsRNA in the endosome since viruses are taken up by the endocytic pathway (

Figure 2). CD14 binds to Poly I: C and mediates its cellular uptake where it transfers it to TLR3 in intracellular compartments (21). This is followed by phosphorylation of TLR3 resulting in initiation of downstream signaling leading to activation of interferon regulatory factor(IRF)-3 and NF-κB-dependent gene expression via TRIF(22). The outcomes of TLR3 engagement are IL-12 and Type I IFN induction, both key molecules in antiviral defense and immune activation(23) in addition to production of inflammatory chemokines and cytokines.

1.1.2.5 Other RNA recognition modules

TLR3 is mainly expressed endosomally where it recognizes viral RNA (Figure 3a). However, RIG-1 and MDA-5 are cytoplasmic receptors for the recognition of RNA(24). Both these receptors signal to a mitochondrial protein IPS-1 (MAVS), which results in the activation of IRF1 (for an antiviral response) and NF-κB (for a pro-inflammatory response)(25). (Figure 3b)

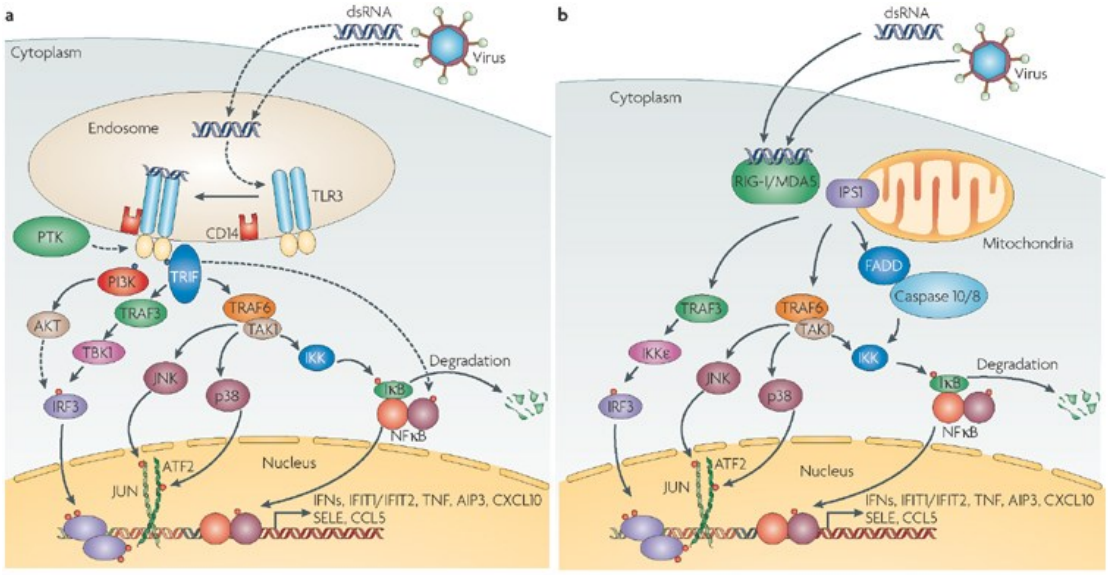

Figure 3: dsRNA recognition pathways in the cell(25)

1.1.3 Local ccellular response to TLR agonist stimulation *in vitro*

Response to direct stimulation of cells with TLR agonists is very well studied. Bone marrow derived dendritic cells when stimulated with LPS, pIC or PAM (a TLR2 agonist) *in vitro (*

Figure 4) showed distinct expression of distinct gene regulatory networks; pIC induced an antiviral program and LPS induced both an inflammatory and antiviral program and PAM induced an inflammatory program(26).

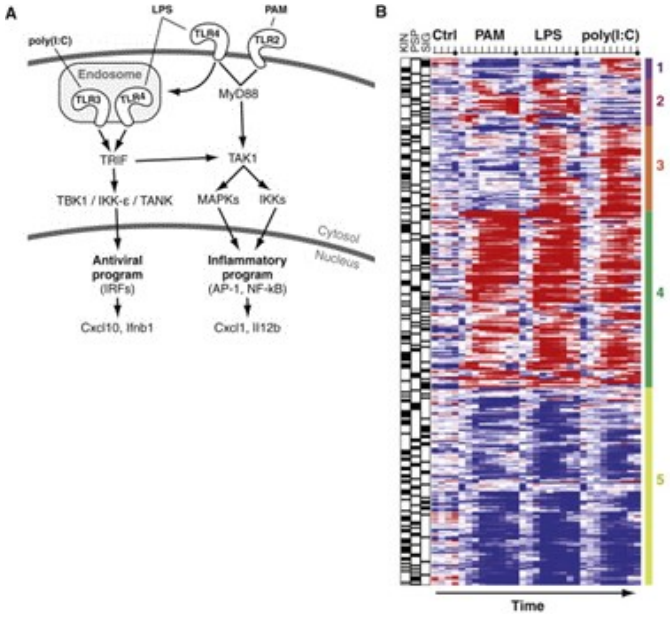

Figure 4: Differential response to TLR stimulation in dendritic cells(26)

Macrophages when stimulated with pIC expressed IFN-β in an IRF3 and NF-κB independent manner whereas they responded to LPS in a NF-κB dependent manner resulting in the production of TNF-α(27). Several other cell types have also been extensively characterized for their responses to poly I:C and LPS(11).

1.1.4 TLR response and innate immune response *in vivo*

The TLR response has been studied extensively *in vivo* in several immune subsets including natural killer cells(28), mast cells(29), macrophages(30), dendritic cells(31) and neutrophils(32) under physiological(33) and pathological conditions(34). Similar to the observed *in vitro* responses, stimulation of TLR signaling *in vivo* results in a tightly controlled and well established pro inflammatory pathways and are critical in maintaining host tissue/organism health under conditions of infection(35).

1.1.5 Dual role of TLR signaling in cancer progression and immunotherapy

TLR signaling is severely deregulated in several cancers since the inflammatory response has a strong effect on the survival of tumors at several stages including initiation, metastasis and malignancy(36). e.g. LPS stimulation of a mammary adenocarcinoma cell line increased

migration, invasion and metastasis(37), TLR stimulation of multiple myeloma cell lines lead to increased proliferation and survival(38) and activation of TLR4 signaling on tumor cells promote evasion of CTL cells and increased survival *in vivo*(39). Additionally, constitutive NF-κB due to aberrant TLR activation results in chronic inflammation which results in a poor outcome for many hematological tumors(40).

Some TLR agonists are also actively being used in cancer immunotherapy for their ability to activate immune cells and promote both innate and adaptive immune responses against cancers. Breast and bladder cancer cells when stimulated with TLR3 activated IFN-α resulting in the apoptosis of human and mouse cancer cells(41). A summary of the role of poly (I:C) and LPS in tumor outcome is summarized below in Table 2.

Table **2:** Summary of the effects of *TLR3* and *TLR4* Signaling in tumor Cells(41)

TLR	Type of Cancer	Protumor effects	Anti-tumor effects
TLR3	Breast cancer		Apoptosis, ↑type I IFN
	Colon cancer		Apoptosis
	Cervical cancer		Apoptosis
	Head and neck cancer		Apoptosis, necrosis, ↑ICAM-I
	Hepatocellular carcinoma		Apoptosis
	Melanoma		Decreased proliferation, apoptosis
	Myeloma		Apoptosis, ↑type I IFN
	Lung cancer	Proliferation and survival	Apoptosis
	Prostate cancer		Inflammation, apoptosis
TLR4	Breast cancer	Viability, immune evasion, ↑VEGF, NO, IL-6, IL-12, MMPs	
	Colon cancer	Inflammation, tumor growth, immune evasion, ↑B7-H2, B7-H2, ↓Fas	
	Gastric cancer	Proliferation	
	Hepatocellular carcinoma	Carcinogenesis	
	Lung cancer	Immunosuppression, immune evasion, reduced apoptosis, ↑TGF-β, VEGF, IL-8	Decreased lung permeability and inflammation
	Melanoma	Carcinogenesis	

1.1.6 Organs of the innate immune system

The effector cells of immunity are all produced within lymphoid organs in the body. The immune system is divided into primary and secondary organ systems; the primary lymphoid organs are the bone marrow and the thymus where lymphocyte production and maturation occurs. The secondary lymphoid organs include lymph nodes, the spleen, the tonsils and other specialized tissues in the mucous membranes of the bowel where an immune response is mounted.(42)

1.2 Lymphatic System

The lymphatic system consists of a network of vessels, nodes, and accessory organs that play a vital role in the body's balance of interstitial fluid volume to maintain protein concentration and oncotic pressure gradients(43) It operates as an open system that returns excess interstitial fluid and proteins to the blood stream via a lymphatic duct in the left subclavian vein(44). Additionally the system is essential to a wide variety of physiologic and pathophysiologic processes including immune cell trafficking and regulation of immunity(45, 46), lipid transport(47) progression of autoimmunity, cancer metastasis (48), and tissue inflammation(49).

1.2.1 Structure of the lymphatic system

The lymphatic system is composed of initial collecting lymphatic capillaries which converge intro collecting lymphatic vessels which transport fluid via lymph nodes back into circulation (Figure 5). These initial capillaries collect undrained interstitial fluid, called lymph once it enters the lymphatic system; and propel it forward by contraction of the smooth muscle cells embedded in the walls of the collecting vessels thereby carrying large proteins and immune cells. They contain one- way valves that prevent retrograde flow and thus propel lymph through the lymph nodes(50).

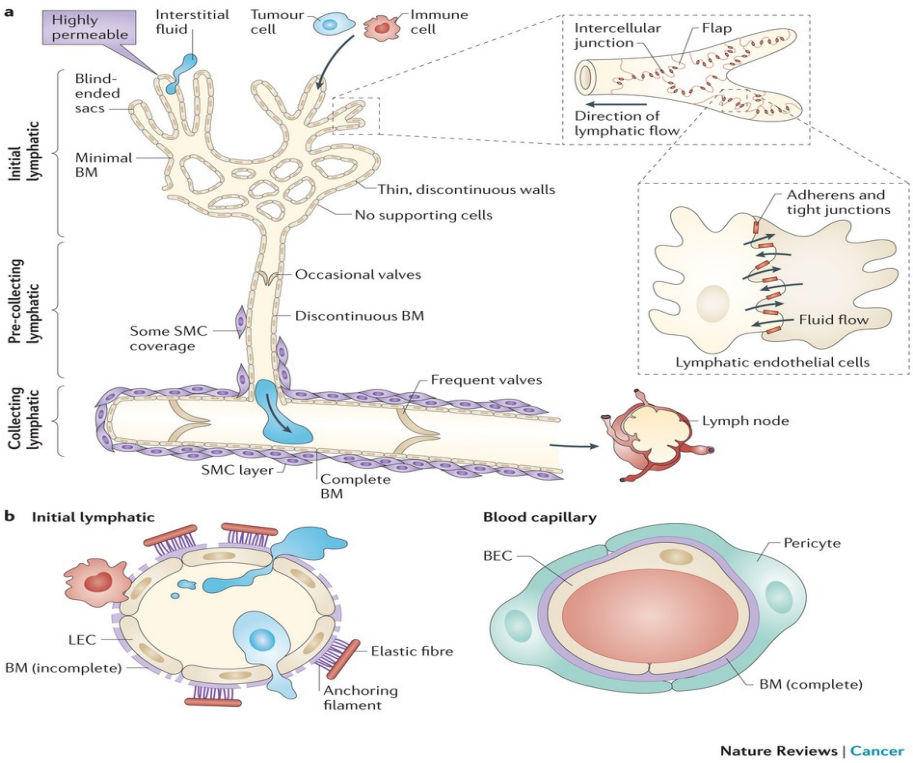

Figure 5: Structure of the lymphatic system and its components(51).

The lymph nodes are sites where large groups of macrophages, antigen presenting cells and leukocytes are present. Lymph enters via the afferent vessel, is filtered through the sub capsular sinuses, and around the lymphoid compartment which has high resistance due to the packed cells contained within(52). Macrophages and antigen presenting cells present in this compartment samples the afferent lymph for antigens and can initiate an immune response if they detect signs of infection(53). Most of the lymph exits via the efferent lymphatics without entering the lymphoid compartment. Large particles (>70 kDa or with a hydrodynamic radius >4 nm)cannot cross the subcapsular sinus and exit via the efferent lymphatics, whereas small particles can cross the floor of the sinus and enter the lymphoid zone(54). While cells can cross the subcapsular sinus by active movement, fluid can only enter though small collagen tubules that connect the between sinus lining cells and the high endothelial venules (HEV's) in the lymphoid compartment(54). The fluid in the lymphoid compartment can then enter the bloodstream thought the HEV's. A general structure of the lymph node is shown in Figure 6. Mice have 22 identifiable lymph nodes(55)

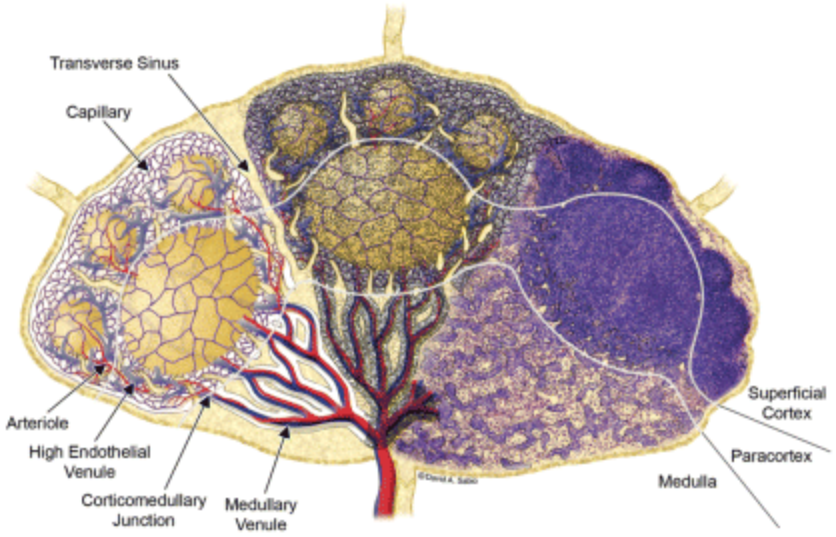

Figure 6: Structure of a lymph node(56).

1.2.2 Imaging lymphatics

Given the central role played by lymphatics in the development of immunity, imaging the transport of antigens, and immune cells is essential to monitor health and the development of disease. Systemic lymph node imaging was limited to Magnetic resonance imaging (MRI) and Computerized tomography (CT) but they are cost prohibitive and lack the required sensitivity to image initial and collecting lymphatics(57). Positron emission tomography (PET), has been used to image the lymph nodes and although non-invasive suffers from a lack of sensitivity(58) Current methods of intra-lymphatic imaging rely on the presence of a contrast agent. Lymphoscintigraphy is the gold standard of imaging to investigate lymphatic function but suffers from a lack of spatiotemporal resolution(59).

1.2.2.1 Near Infra-red (NIR) Imaging

NIR imaging, is an emerging non-invasive imaging technology that collects tissue-scattered light to assess conducting and collecting lymphatic vessels at greater penetration depths enabling detection of lymph drainage and lymph nodes. NIR light resides in the optimal wavelength, where there light absorption and scattering by biological tissue are low, auto fluorescence is minimal and offers excellent spatiotemporal resolution(60). NIR imaging with an FDA-approved fluorescent

dye, indocyanine green (ICG), has recently emerged as a novel method for quantitative assessment of lymphatic function in animals and humans. Upon illumination of tissue surfaces with NIR excitation light, contrast agent (typically ICG or Licor IR dyes) fluorescence is collected using charge-coupled device (CCD) cameras and can be used to visualize the initial lymphatics, collecting and conducting lymphatics, and draining LNs across wide fields of view that can encompass entire limbs(61, 62).

NIR images are collected at high speeds (every millisecond) which allows for real-time noninvasive assessment of lymphatic functions(63). It enables quantitative measurements of lymphatic pump function such as pumping pressure, packet frequency, packet velocity and total lymphatic transport(61, 64, 65) as well as dysfunction as in the case of lymphedema(66). NIR imaging has also been successfully used to assess tissue rejection in an animal model of hind limb transplantation showing applications in regenerative medicine(67).

While NIR imaging is ideal for studying superficial lymphatic drainage and lymphatic fluid transport in small animals, it lacks the ability to generate strong fluorescent signals through deep tissue sections(68). Recent advances in nanotechnology has led to development of small semiconductor crystals (5-20nm) called quantum dots (QD's) whose emissions can be fine-tuned to emit in the NIR range (69). QD's enable the use of multicolor imaging along with increased tissue depth penetration to study multiple lymphatic vessels/components simultaneously(70)

1.2.3 Role of lymphatics in the establishment of immunity

The lymphatic system is extremely important in immune surveillance because the collecting vessels traffic both antigens and antigen-presenting cells from peripheral tissues to lymph nodes(53).

The continuous circulation of lymph through the lymph nodes allows for enrichment of rare antigens and provides more opportunity of antigen-specific lymphocytes to encounter their cognate antigen from any part of the body creating an efficient sampling system for foreign pathogens or abnormal self-antigens as in the case of cancer. Immune cells and several types of cancer cells

secrete the chemokines CCL19 and CCL21(71). Several cancer cells also have the corresponding receptor CCR7 to the chemokines which, eventually leads to the cancer cells migrating towards the draining lymphatic vessel and are transported to the lymph nodes(72).

The immune response is initiated when antigen presenting cells and soluble antigens reach the sub-capsular sinus within the lymph node. Small antigens are able to directly enter the B-cell follicles via a system of conduits formed by the stromal cells while larger antigens need to taken up by macrophages or dendritic cells and trafficked there(73). Recently, lymphatic endothelial cells and stromal cells themselves have been shown to play a role in the transport of antigens and communicating with immune cells regulating their functions(74).

1.3 Exosomes

It has been long known that vesicles of various sizes are released form cells. Exosomes were first discovered while studying the differentiation of sheep reticulocytes which involved the shedding of transferrin receptors on small vesicles of endocytic origin(75). They were initially thought to be a method of removing unwanted proteins from cells, and the term 'exosomes' had also been used to refer to vesicles from various normal and neoplastic lines that possessed 5'nucleotidase activity(76). They were later shown to play an important role in immune regulation, when B-cell exosomes were found to contain MHC II molecules that could present antigens to $CD4^+$ T-cells(77).

Exosomes are released by diverse cell types including immune cells such as B-cells(77), T-cells(78), dendritic cells(79), mast cells(80) and macrophages(81), epithelial cells(82), neurons(83), adipocytes(84), tumor cells(85) and stem cells(86). They are also found in a number of bodily fluids such as saliva, urine, breast milk, broncho-alveolar lavage fluid, amniotic fluid, synovial fluid, epididymis fluid, serum, and ascites under both physiological and pathological

conditions(87). Exosome presence in bodily fluids indicates the potential of exosomes to be used as non-invasive diagnostic tool to check for biomarkers of diseased states.

1.3.1 Exosome Biogenesis

Membrane vesicles are classified as spherical structures composed of lipid bilayers containing hydrophilic soluble components. In eukaryotic cells, intracellular transfer is mediated by carrier vesicles which bud from a donor compartment and fuse with a target compartment, thereby delivering luminal material from the donor compartment to target compartments. Intercellular trafficking of soluble proteins is accomplished by secretory vesicles which contain intraluminal material. Large secreted vesicles (size>100nm) containing cytosol called macrovesicles are also released from several cell types and are formed by the budding or shedding of the plasma membrane.

Distinct from other secreted vesicles, exosomes are formed by the invagination of endosome membranes to give rise to intraluminal vesicles (ILV's). ILV's contain cytosol, are enclosed within larger membrane bound intracellular structures called Multi-vesicular bodies (MVB's) and are released from the cell by the fusion of the MVB with the plasma membrane(88).

MVB's were well known for their functions as intermediates in protein degradation. They carried proteins internalized from the cell surface or from the trans-Golgi network and fused with the lysosome initiating degradation(89). Pioneering studies in reticulocytes showed an alternate fate for the MVB's in aiding release of exosomes extracellularly(75).

In addition to mode of formation, these vesicle types also differ in size, biophysical and biochemical properties. Figure 7 below shows the formation and release of exosomes via MVB formation and other types of vesicles as outlined above.

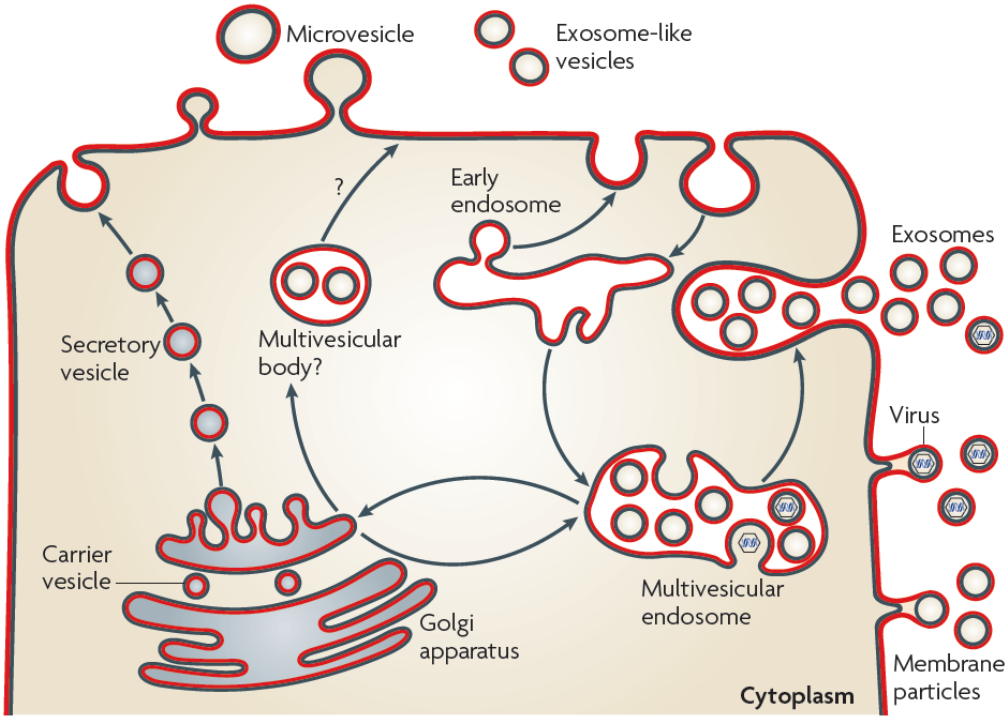

Figure 7: Schematic depicting the formation and release of exosomes from a cell(90).

1.3.2 Exosome composition

Exosomes range in size from 30-120 nm and are composed of a lipid bilayer containing functional biomolecules like proteins, mRNA and miRNA that can be delivered to a target cell by fusion and thus play an important role in cell-cell communication(88). Electron microscopy reveals saucer shaped vesicles with a diameter of 50-100nm(91).

While the molecular composition of exosomes varies depending on cell type of origin, they contain a number of biomolecules in common. Proteomic profiling has revealed characteristic protein markers on the surface such as tetraspanins (CD63, CD81), components of the ESCRT machinery (Alix, Tsg101), heat shock proteins (Hsc70, Hsp 90), cytoskeletal proteins (Actin, tubulin) ,and membrane proteins (Lamp2, Rab5b, annexin II)(90).

Exosomes also contain proteins that are specific to cell type, e.g. exosomes from antigen presenting cells carry MHCII molecules(92). Characteristic of their endosomal origin, they do not contain any nuclear, mitochondrial or endoplasmic reticulum proteins.

Figure 8 below shows the proteins present in and on the exosomal membrane. Not all cellular proteins found in exosomes suggesting a specific loading mechanism which is as yet unknown. Protein sorting requires the machinery of the endosomal sorting complex required for transport machinery (ESCRT). Studies in *Saccharomyces cerevisiae* showed that monoubiquitinated proteins are sorted into ILV's while oligoubiquituination increases chances of ILV incorporation(93). Ubiquitination is however only one of the mechanisms of exosomal protein inclusion. Additional ubiquitination independent mechanisms such as the ability of tetraspanins to partition in lipid rafts and to independently sort into ILV's(94) or incorporation of Transferrin receptor by Alix association(95) also contribute to exosomal sorting.

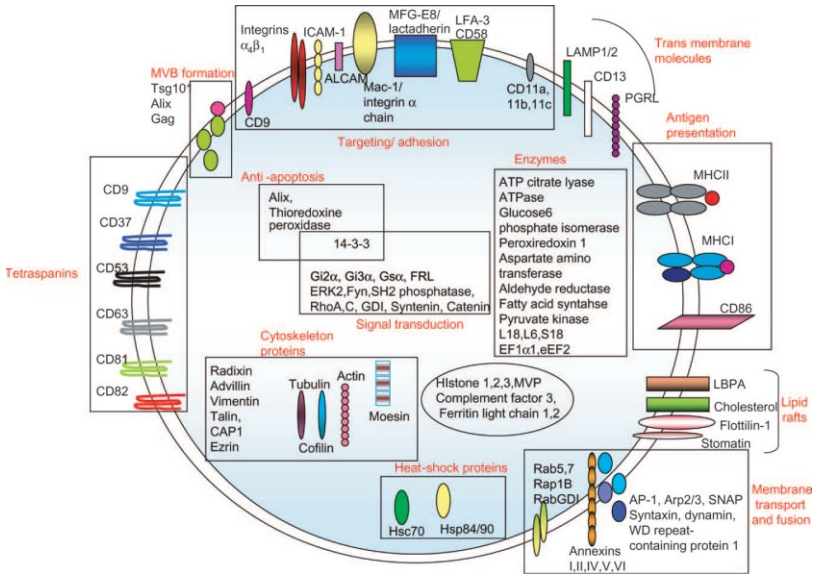

Figure 8:Typical molecular composition of an exosome (22)

Exosomal membranes are similar to the plasma membrane and some reports suggest that they are enriched in sphingomyelin, cholesterol(96), lyso-bis-phosphatidic-acid (LBPA)(97) and

ganglioside GM3, lipids that are typically enriched in detergent-resistant membranes(98). Lipid flip flopping is increased in exosomes as compared to plasma membranes and exosomal membranes show an increase in rigidity between pH 5 and 7(97). High membrane rigidity has implications for exosome stability and prevents its degradation in circulation.

1.3.3 Functions of exosomes:

Exosomes are involved in a multitude of biological processes and facilitate intercellular communication. Although the initial role of exosomes was attributed to removal of unwanted proteins from the cells, they have since expanded to include a wide variety of functions that encompass normal physiology, disease pathology, immune modulation and cancer diagnostics and therapeutics. A few of their key roles are outlined below

1.3.3.1 Exosome Functions in physiology

Exosomes have a number of functions in maintaining homeostasis and normal organism physiology(99). They have been discovered in a number of biological fluids including cerebrospinal fluid where they play roles in neural development(100), saliva where contributed to cell free clotting(101), and amniotic fluid where they play important role in maternal tolerance to the fetus(102). Exosomes are also implicated in embryonic development with roles in processes like morphogenetic gradients formation, cell migration and the development of cellular polarity(103). They are also shown to play important roles in tissue repair and regeneration. E.g., mesenchymal stem cell derived exosomes when injected in mice models of myocardial infarction, reduced infarct size and helped in tissue repair(104). Overall, the functions of exosomes in physiology are diverse and an active area of research with new functions being discovered every day.

1.3.3.2 Exosomes functions in immunity

The role of exosomes in immunity are very well characterized and have been shown to have both immunostimulatory and immunosuppressive effects. The immunostimulatory properties of exosomes were first discovered in the context of antigen presentation in a landmark study which showed that exosomes derived from EBV transformed B-cells were shown to stimulate primed $CD4^+$ T-cells in an antigen specific manner. This study also showed the release of MHC II on exosomes derived from murine and human T-cells(77). By contrast, exosomes cannot activate naïve T-cells and deliver their contents to dendritic cells in the vicinity(105).

Further evidence for their immunostimulatory effects came from studies in which exosomes from mouse dendritic cells pulsed with tumor peptides were shown to be capable of priming cytotoxic T-cells and suppress tumor growth in a T-cell dependent manner (106).However, T-cell activation by exosomes also depends on the physiological state of the cell of origin. Naïve dendritic cell derived exosomes activate T-cells less effectively than those derived from mature DC's(107). Exosomes from pathogen infected cells can such as Cytomegalovirus infected endothelial cells allow induction of pathogen specific T-cell responses(108) (Figure 9).

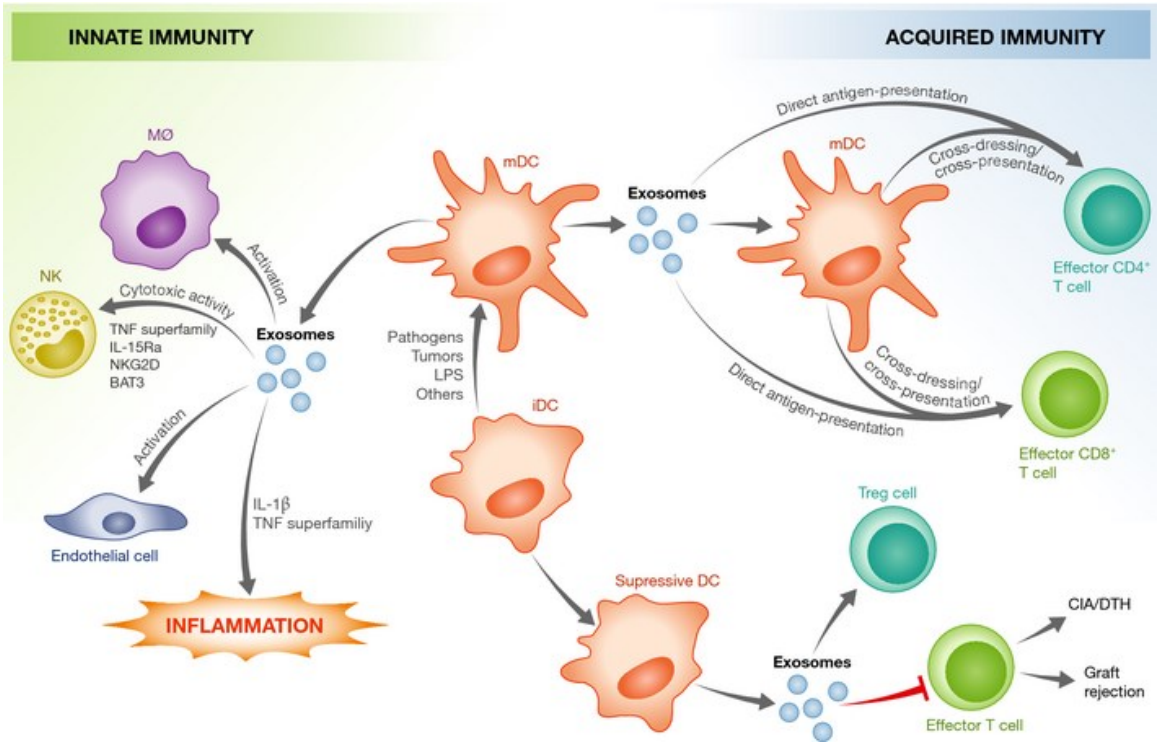

Figure 9: The roles of exosomes in innate and adaptive immunity(109)

The immunosuppressive effects of exosomes are best understood in the context of pathogens and intracellular infection. Exosomes from HIV-1 infected macrophages crucial viral proteins such as Gag and nef to uninfected cells aiding the rapid spread of HIV to nearby cells(110). While several factors impact the activity of exosomes, there have consistent reports of bacterial pathogens such as *Leishmania* spp. and fungal pathogens such as *Cryptococcus* spp secrete immunosuppressive molecules on secreted vesicles to suppress the immune response against them resulting in enhanced pathogen survival and poor host prognosis(111, 112) (Figure 9).

Exosomes also play important roles in induction of immune tolerance in an antigen specific manner in mice(113) which has been further exploited to benefit transplant patients. Exosomes from donor bone marrow dendritic cells, when administered prior to transplantation, were shown to increase allograft survival in mice after a heart transplant.(114)

1.3.3.3 Exosomes function in cancer

Exosomes have been best characterized in the context of tumor development and immune evasion. They transfer antigens from tumor cells to dendritic cells(115), which in turn can induce $CD8^+$ T-cell dependent anti-tumor effects and thus play a role in T-cell cross priming. Tumor derived exosomes carry tumor specific antigens like MART1 (melanoma) that are delivered to dendritic which cross prime cytotoxic T-cells (116).Thus exosomes can aid in antigen presentation, boost host immunity and provide us with potential vaccination strategies particularly for targeting tumors(Figure 10)

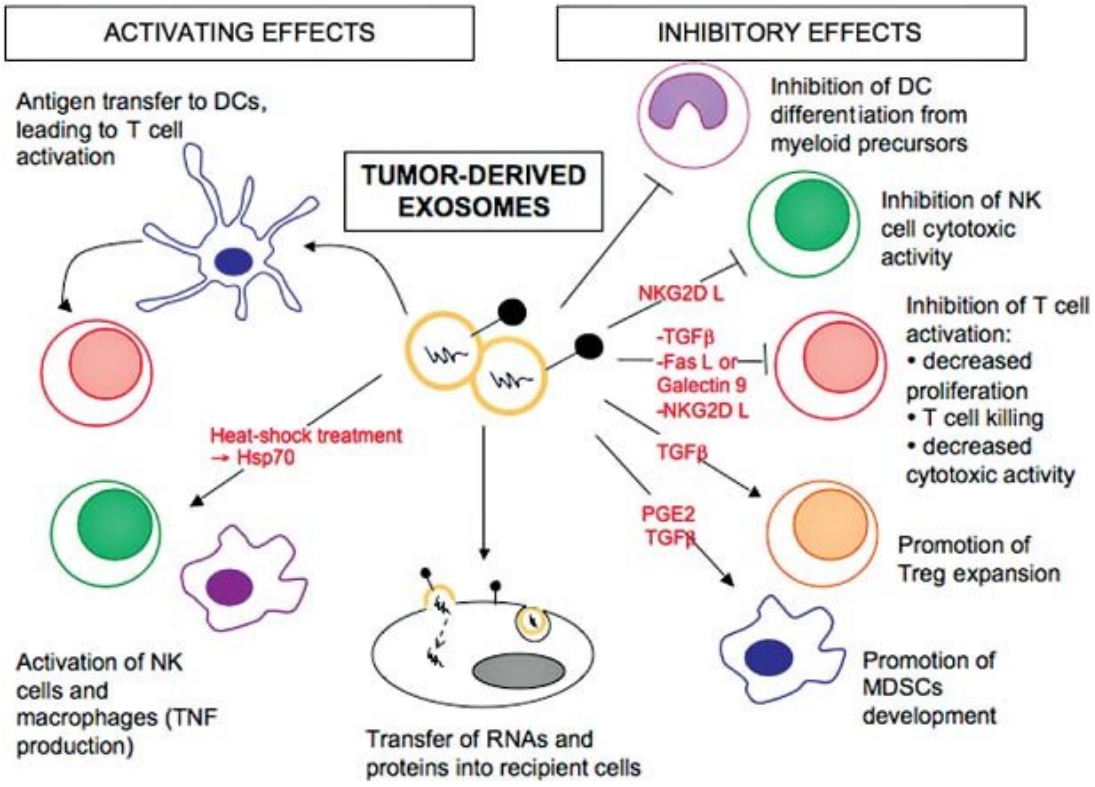

Figure 10: Some functions of exosomes secreted by tumors (32).

Exosomes also play a role in the suppression of immune response, since they carry various immunosuppressive molecules such as the Fas-L ligand on melanoma exosomes which can lead to T-cell apoptosis(117). Tumor exosomes expressing TGFβ1 and ligands for NKG2D were also

able to inhibit Natural Killer (NK) cell proliferation impairing the ability of immune cells to recognize and destroy the cancer(118). This results in increased tumor growth, invasiveness and metastasis. (Figure 10).

They are also capable of modifying the transcriptional profile of the target cells by delivering functional payloads of biomolecules as demonstrated in exosomes derived from colorectal cancer cells, (119) lung(120) and prostate cancer cells(121). Glioblastoma derived exosomes carry mRNA and miRNA that are capable of inducing cell migration, proliferation and angiogenesis in brain microvascular endothelial cells (122) (Figure 10: Some functions of exosomes secreted by tumors (32).Figure 10). This demonstrates a clear role for exosomes as important players in cell-cell communication as they carry functional messages between cells with pleiotropic effects.

1.4 Exosome trafficking through the body

Exosomes travel to distal target cells upon being secreted by the cell of origin via circulation and other body fluids. Body fluid-derived exosomes have been found in all biological fluids and are a mixture of vesicles originating from different sources such as the cells found in the body fluids and/or the cells lining the cavities of extruded body fluids. The two most important body fluids for the development of an immune response are blood and lymph, and the exosomes within them are described below.

1.4.1 Exosomes in circulation

The first report of the existence of EVs in blood was almost 70 years ago and was later described as platelet “dust”(123). There have been innumerous reports of exosomes in the circulation since where they have been shown to play a number of roles(124-126). Studies with fluorescent exosomes have enabled systemic tracking of exosomes in circulation which revealed their organ biodistribution and rapid clearance from the body via the liver(125). Exosome movement through

the circulation is well established and current research is focused on understanding the many functions of exosomes and the potential to harness exosomes in circulation to deliver therapeutic molecules.

1.4.2 Exosomes in lymphatics

Exosome trafficking through the lymphatics came to the forefront when research showed the strong presence and localization of both tumor derived exosomes and B-cell derived exosomes in lymphoid organs such as the spleen and lymph nodes(124, 127). However, the presence of exosomes in the lymph or trafficking through the lymphatic system has been undemonstrated.

1.5 Research Goals

The overall research goals of this thesis can be divided into two primary objectives:

1) The role and kinetics of lymphatic transport of exosomes in the establishment of an innate immune response both *in vitro* and *in vivo* (Chapter 2)
2) The systemic roles of exosomes in the context of innate immunity, specifically in the dissemination of the Toll-like receptor response and the contribution of exosomal cargo to this process *in vitro* and *in vivo* (Chapter 3).

CHAPTER 2: SPECIFIC AIMS AND HYPOTHESES

Multicellular organisms rely on cell-cell communication for information exchange in order to promote survival, and appropriate development and functioning of tissues. This communication occurs either through direct physical contact via nanotubes(128), secreted chemical signals like cytokine, chemokines, or small molecule mediators (proteins, nucleic acids), or exchanging information via exosomes (129). Exosomes provide the ability to transmit messages between cells at a distance and their roles in long distance communication have been well established(130). The discovery of functional, transportable mRNA and miRNA within exosomes further increases the complexity of cell-to-cell communication. They can fuse with the recipient cells and deliver their contents into the cytoplasm of the recipient cell and perturb the recipient cell, especially since miRNA can mediate RNA interference (88).They can also bear combinations of ligands to engage several cellular receptors at once modulating changes in the recipient cell.

Exosomes play a wide variety of roles in the body including immunity and it is critical to dissect their contribution to the development of innate immunity. One of the biggest unknowns in the field, is the routes of transport utilized by exosomes in the body while transferring immune related information systemically. Exosomes have been demonstrated to have functional consequences in the lymph node drained by both blood and lymph. While exosomal trafficking in circulation is well known, the contribution of lymphatic transport needed to be ascertained. We also wanted to understand the effector functions of exosomes in the context of pathogen recognition and response by the toll-like receptor pathway. We modeled this response using LPS and poly (I:C), agonists that activated the bacterial response via TLR 4 and the viral response via TLR 3 respectively. We further characterized the role of exosomes in the dissemination of the TLR activation state of the cell of origin distally in a mouse tail lymphatic model and elucidated the immune response within the lymph node at both the cellular(macrophage) and organ (whole node) levels.

2.1 Aim 1: Establishing and characterizing exosome transport through the lymphatics *in vivo*[1].

Hypothesis: Exosomes are taken up and transported by the lymphatics to the lymph node.

Long distance cell-cell communication is particularly important when cells are exposed to infection and helps in mounting a coordinated response against the invading pathogen. Exosomes are particularly well suited to transmit messages of infection from exposed cells to distal cells which are as yet uninfected(131). The lymphatic system is found in most tissues of the body, and plays important roles in maintaining fluid balance, immune cell trafficking from the periphery to lymph nodes, and lipid transport from the intestine to the circulation(44). A few salient features that make it likely that exosomes utilize the lymphatic system as a route for rapid cell-cell communication are: a) The lymphatics can transport large molecules, b) The lymphatics provide direct access to lymph nodes which are immune cell hubs. C) Exosomes have a number of immunomodulatory effects and d) Exosomes exist in the ideal size-range for lymphatic transport

Exosomes secreted antigen presenting cells (APC) stimulate T-cells *in vitro* and *in vivo*(132). However, they cannot activate the T-cells directly; they must be captured by an antigen presenting cell proximal to the naïve T-cells for activation. The speculated reason for this alternate route is that APC's in the periphery could use exosomes as a rapid means of priming the downstream lymph node instead of directly migrating there themselves since exosomes are in the ideal range of lymphatic transport (133). Here we have definitively shown the lymphatic transport of exosomes both *in vitro* and *in vivo*. Using an *in vitro* model of lymphatic uptake, we have shown that lymphatic endothelial cells actively enhanced lymphatic uptake and transport of exosomes to

---

[1] Srinivasan, S. et al. Lymphatic transport of exosomes as a rapid route of information dissemination to the lymph node. Sci. Rep. 6, 24436; doi: 10.1038/srep24436 (2016).

the luminal side of the vessel. Furthermore, we have demonstrated a differential distribution of exosomes in the draining lymph nodes that is dependent on the lymphatic flow. Lastly, through endpoint analysis of cellular distribution of exosomes in the node, we identified macrophages and B-cells as key players in exosome uptake.

2.2 Aim 2 Elucidating effector functions of exosomes under bacterial and viral infection states *in vitro* and *in vivo*.

Hypothesis: Exosomes from infected cells have distinct functional effects on downstream cells and will differ in their (RNA) contents between control and TLR stimulated cell derived exosomes. The biological functions of the exosome is essentially dependent on the biological state of the parental cells that produces it. E.g. Cells under oxidative stress release exosomes that can transmit resistance to oxidative stress in recipient cells (134). This protective effect on growth conferred by exosomes was annulled by exposing the exosomes to UV implicating exosomal RNA as the causal agent. Therefore exosomes released under different conditions have different effects on recipient cells due to varied exosomal RNA content. While the responses of cells exposed to LPS and Poly I:C are well elucidated *in vitro* (135)and *in vivo*(136), these studies don't take the role of exosomes into account. Exosomes have the ability to transmit messages of infection from the location of stimulation to a distal location rapidly because of their ability to move through the body rapidly. It is as yet unknown if exosomes can transmit differential signals based upon specific TLR agonists. This study is the first to explore the importance of exosomes in spreading the message of infection to naïve cells and facilitating a rapid response by the innate immune system.

Here we show that exosomes from TLR stimulated cells can largely recapitulate TLR activation in distal cells *in vitro*. We can abrogate the action-at-a-distance signaling of exosomes by UV irradiation, demonstrating that RNA is crucial for their effector function. We are the first to show that exosomes derived from poly (I:C) stimulated cells induce *in vivo* macrophage M1-like polarization within murine lymph nodes. These poly (I:C) exosomes demonstrate enhanced

trafficking to the node and preferentially recruit neutrophils as compared to control exosomes. This work definitively establishes the differential effector function for exosomes in communicating the TLR activation state of the cell of origin.

CHAPTER 3: LYMPHATIC TRANSPORT OF EXOSOMES FOR RAPID INFORMATION DISSEMINATION TO THE LYMPH NODE

3.1 Abstract

It is well documented that cells secrete exosomes, which can transfer biomolecules that impact recipient cells' functionality in a variety of physiologic and disease processes. The role of lymphatic drainage and transport of exosomes is as yet unknown, although the lymphatics play critical roles in immunity and exosomes are in the ideal size-range for lymphatic transport. Through *in vivo* near-infrared (NIR) imaging we have shown that exosomes are rapidly transported within minutes from the periphery to the lymph node by lymphatics. Using an *in vitro* model of lymphatic uptake, we have shown that lymphatic endothelial cells actively enhanced lymphatic uptake and transport of exosomes to the luminal side of the vessel. Furthermore, we have demonstrated a differential distribution of exosomes in the draining lymph nodes that is dependent on the lymphatic flow. Lastly, through endpoint analysis of cellular distribution of exosomes in the node, we identified macrophages and B-cells as key players in exosome uptake. Together these results suggest that exosome transfer by lymphatic flow from the periphery to the lymph node could provide a mechanism for rapid exchange of infection-specific information that precedes the arrival of migrating cells, thus priming the node for a more effective immune response.

3.2 Introduction

Multicellular organisms rely on cell-cell communication for information exchange in order to promote survival and appropriate development and functioning of tissues. This communication occurs either through direct physical contact via nanotubes(137), secreted chemical signals like cytokine, chemokines, or small molecule mediators (proteins, nucleic acids), or exchanging information via exosomes(138). Exosomes provide the ability to transmit messages between cells

at a distance and their roles in long distance communication have been well established(4). The discovery of functional, transportable mRNA and miRNA within exosomes further increases the complexity of cell-to-cell communication. They can fuse with the recipient cells and deliver their contents into the cytoplasm of the recipient cell and perturb the recipient cell, especially since miRNA can mediate RNA interference(88). They can also bear combinations of ligands to engage several cellular receptors at once modulating changes in the recipient cell.

Exosomes are credited with several roles in modulating immune response *in vivo* :a) dendritic cell derived exosomes carried antigens and present them to T-cells(139), b) exosomes from macrophages infected with intracellular pathogens induced a pro inflammatory response in uninfected macrophages thereby activating the immune response(140) and c) tumor derived exosomes carry a variety of immunosuppressive molecules to suppress the immune response to the tumor by decreasing proliferation of various immune subsets like natural killer cells, regulatory T-cells or myeloid cells(132).

Lymphatic flow is an important component of circulation as it serves to return interstitial fluid from tissue back to the circulation via the lymph nodes(141). Lymphatic drainage from tissue results in transport of antigens, immune cells and large macromolecules from the periphery to the lymph nodes where innate and adaptive immune responses are elicited. Thus, each lymph node obtains region specific antigenic information through the lymphatic capillaries that drain the periphery allowing antigen presenting cells (APCs) to initiate an immune response(142). Interestingly, the intrinsic physical barriers created by the interstitium and vascular exclusion of large proteins, create an “optimal” size range for lymphatic transport of 5-100 nm which is primarily the size range of exosomes. Particles smaller than this are easily taken up in the blood capillaries and larger particles typically become trapped in the extracellular matrix(143, 144),

although more recent evidence suggests that particles as large as 1 micron could be taken up by lymphatics(145).

It is likely that one of the primary advantages of exosome size is that they are small enough to convect through the interstitial matrix with interstitial flow, yet large enough to partition their uptake into the lymphatic circulation, thus making them an ideal vehicle through which a peripheral cell can rapidly signal and transport information to the lymph node. Interestingly, melanoma-derived exosomes were able to prime the sentinel lymph node for tumor metastasis by initiating a proangiogenic program and remodeling the tissue matrix(24) and $CD169^+$ cells were identified as the target cells for B-cell derived exosomes in the lymph nodes and spleen(124) implicating the lymphatic system in playing an important role in exosome transport from the periphery to lymphoid organs and the nodes. However, experiments involving exosome signaling in the node are typically conducted over the course of hours or days and thus it is unclear how rapidly exosome trafficking and uptake into cells in the node can occur, a process in which speed should be of particular importance if exosomes are utilized to enhance innate immunity.

Near-infrared imaging is an emerging technology and has been used to non-invasively image and quantify functional lymphatic transport(61) and perform sentinel lymph node mapping(146) as it offers maximum tissue penetration with minimal autofluorescence(147). Exosomes on the other hand have been imaged by either covalently labeling with a fluorophore(148) or with a variety of lipid dyes such as DiL or DiO(24) in the visible range, which allows for trafficking of exosomes in cell cultures or endpoint in-vivo biodistribution studies of exosomes, but suffers from depth penetration limitations making them ill-suited for *in vivo* imaging. We have successfully labeled exosomes with a near-infrared dye which enables us to monitor exosome trafficking *in vivo* using near-infrared imaging. Thus, we can establish and

quantify the kinetics of lymphatic transport of exosomes from the peripheral tissue to the lymph node, which is particularly important in the context of innate immunity where rapid antigen transport can be crucial to the establishment of host immunity and limiting pathogen spread(149). Characterizing exosome trafficking through the lymphatics and the resulting cellular uptake in the lymph node provides several key insights into both the role of lymphatic drainage as well as paracrine effects of exosomes in the context of immunity.

3.3 Materials and Methods

3.3.1 Cell culture

Fetal bovine serum (Atlanta Biologicals, Lawrenceville, GA) was centrifuged for 15 hours at 120,000g, 4^{O}C to remove exosomes and was used to make exosome free cell culture media. Human neonatal dermal lymphatic endothelial cells (LECs) were originally harvested as described previously(150). LECs were expanded in flasks coated for 1 h with 50 μg/mL type I rat tail collagen (BD Biosciences, Bedford, MA) in 0.1% acetic acid and were cultured in EBM (Lonza, Walkersville, MD) supplemented with 20% exosome free FBS, 1% penicillin-streptomycin-amphotericin, 1% Glutamax (both from Life Technologies, Grand Island, NY), 25 mg/mL cyclic-AMP, and 1 mg/mL hydrocortisone acetate (both from Sigma, St. Louis, MO). Media was changed every 2–3 days and LECs were used for experiments at passages 9 and 10. Human ovarian adenocarcinoma cell line, HEY cells (Cedarlane Labs, Ontario, Canada) were cultured in RPMI 1640 (Mediatech, Manassas, VA) supplemented with 10% exosome free fetal bovine serum, 2 mM L-glutamine, 10 mM HEPES buffer (both from Mediatech), penicillin (100 U/ml), and streptomycin (100 μg/mL) (Life Technologies) for 48 hours and the culture media was used for isolation of exosomes by ultracentrifugation. SV-LECs were cultures as previously described(151) and were used as a source of mouse exosomes.

3.3.2 Exosome isolation and characterization

Conditioned media was collected from HEY cells at 90% confluence for exosome isolation. Briefly, the culture media was spun at 300g, for 10 min to remove dead cells followed by a spin at 16,500g, 20 min. The supernatant was then filtered through 0.22µm filters and centrifuged at 120,000g for 120 min. The pellet containing exosomes was re-suspended in a suitable volume of PBS.

The size homogeneity of vesicles obtained was checked using a Zetasizer Nano ZS90 (Malvern Instruments Ltd, Worcestershire, UK) and quantified using Pierce BCA Protein assay kit (Thermo Fisher Scientific, Waltham, MA). To analyze the expression of exosomal surface markers, 4 µm aldehyde/sulfate latex beads (Life technologies) were coated with Anti-CD9 antibody (BD Biosciences, San Diego, CA) overnight and incubated with 30 ug of exosomes. The beads were coated with biotin and the streptavidin-coated fluorescent beads were captured and assessed for surface marker expression. The exosome-bead complexes were probed with Anti Human CD81-PE or Anti human CD63-PE (BD Biosciences, San Diego, CA) and data was acquired on a BD LSR II Flow cytometer. Data analysis was performed using the FloJo software (FlowJo version 10, Ashland, OR).

3.3.3 Scanning electron microscopy

Exosomes were fixed with 3.7% glutaraldehyde (Sigma–Aldrich GmbH, Taufkirchen, Germany) on carbon stubs for 15 min. After washing twice with PBS, the fixed exosomes were dehydrated with an ascending sequence of ethanol (40%, 60%, 80%, and 98%). After evaporation of ethanol, the samples were left to dry at room temperature for 24 h on a glass substrate and then analyzed by Hitachi Cold Field Emission SEM SU8200 (Hitachi High-Tec, Tokyo, Japan).

3.3.4 Fluorescent labeling of exosomes

Exosomes were labeled using PKH67 Green Fluorescent Cell Linker Kit for General Cell Membrane Labeling (Sigma-Aldrich) as per the manufacturer's instructions. Briefly, exosomes in PBS were added to 500 µL of Diluent C and 2 µL of PKH67 dye was added to 500 µL of Diluent C. The two solutions were mixed and incubated for 5 min at room temperature. 1 ml of 1% BSA was added to stop the reaction. The labeled exosomes were centrifuged at 120,000g for 70 min and washed twice with PBS to remove excess dye.

PKH labeled exosomes were labeled with the near-infrared dye using IRDye® 800CW Protein labeling kit (Licor, Lincoln, NE) according to the manufacturer's instructions. Briefly, exosomes in PBS were mixed with the IRDye® 800 CW NHS ester and overnight and free dye was removed using Zeba desalting spin columns (Pierce).

3.3.5 Transport assay and data analysis

Transwell® permeable membrane supports with 3 µm pores (Corning Life Sciences, Corning, NY) were coated for 1 h with 100 µg/mL type I rat tail collagen in PBS and LECs were seeded at a density of 100,000 cells/cm^2 and cultured for 48 h (Figure 12a). A fraction of the transwells were not seeded with cells and were used to determine membrane permeability ($P_{eff\_cell\text{-}free}$).). Prior to transport experiments, cells were incubated for 1 h in serum-free, phenol red-free EBM (Lonza). The basal side of the monolayer was incubated with a fluorescent mix containing 20 µg/mL PKH labeled exosomes, 20 µg/mL FluoSpheres® Carboxylate-Modified 40nm Microspheres, 5 µg/mL 3 kDa Cascade Blue dextran (both from Life Technologies) for 1 h. Samples containing transported fluorescent exosomes and beads were collected from the apical side. In a subset of experiments, transport time varied from 10 to 30 min instead of 1 h. Fluorescence was measured using a Synergy™ H4 Multi-Mode Plate Reader (Biotek, Winooski, VT) and was used to calculate

relative concentration based on a standard curve generated from the fluorescent mix. The effective permeability of exosomes, beads and dextran were calculated using the following equation: P_{eff}=$Js\Delta C \cdot S$, where Js is the flux, ΔC is the concentration gradient, and S is the surface area(150). Transport is represented as either cellular effective permeability (P_{eff_cell}) which was calculated using the equation: $1/P_{eff\_total} = 1/P_{eff\_cell} + 1/P_{eff\_cell\text{-}free}$ or as a ratio of cellular transport to cell free transport ($P_{eff\_total} / P_{eff\_cell\text{-}free}$). After samples were removed from the apical side of the transwell for fluorescence measurement and the calculation of P_{eff}, membranes containing LECs were rinsed twice with PBS, fixed with 4% PFA, stained with DAPI and Alexa Fluor® 647 Phalloidin (Thermo Fisher Scientific) and mounted on glass slides for imaging on a Zeiss LSM 700 (Zeiss, Thornwood, NY). The fluorescence in the images was quantified using the Image J analysis software (v 1.4.1, NIH)

3.3.6 Optimization of Near-infrared (NIR) imaging of exosomes

In order to characterize the parameters of exosome imaging in the dermis using NIR, a tissue phantom was created as described previously (Figure 43a)(61). Additionally a node phantom was also created with two fixed depth settings; 5mm and 7mm to characterize the imaging setup for exosome detection at the node. The node phantom was molded in a standard petri dish using a mixture of 97.52% silicone elastomer base (Sylgard 184, Dow Corning), 2.22% Aluminum Oxide (Sigma Aldrich), and 0.26% cosmetic powder (Max Factor Crème Puff Deep Beige 42) according to previously published methods(152)

3.3.7 Near-Infrared imaging of mice

The NIR imaging system was set-up as described previously(61). The camera was connected to a computer where the videos were acquired and analyzed by a custom LabView VI (National instruments).

Lymphatic transport of exosomes was quantified *in vivo* in the tail of eight-week-old male Balb/C mice (Charles River Laboratories, Wilmington, MA) according to procedures approved by the Georgia Institute of Technology IACUC Review Board. To minimize light scattering, a depilatory lotion was used to remove hair in the region of interest on the tail and back 1 day prior to experimentation.

The mice (n=10) were anesthetized with Isoflurane continuously delivered through a nose cone and intradermally injected with 10 ug (10 ul of 1 ug/ul) of exosomes labeled with both PKH67 and IRDye 800CW in PBS. Care was taken to position the injection as close to the midline of the tail as possible to avoid favoring one collecting vessel over the other. The small volume of fluid injection and the use of NIR to enhance tissue penetration ensures that only fluorescence in the deeper collecting lymphatics is visible downstream of the injection site. Image acquisition began just prior to intradermal injection of the dye and the animals were imaged continuously for 20 min post-injection with a frame rate of 1 fps with a camera exposure time of 50 ms. Draining vessels, the injection site and the draining lymph nodes were imaged regularly to monitor movement of exosomes from the periphery to the nodes.

To evaluate lymphatic function in each of the mice, two parameters were measured as previously described: transport time and the average velocity of the packets traveling through the field of view of the recording site[64]. An example of fluorescence arrival in the collecting vessel can be seen in Supp video 1, and a plot of fluorescence intensity over time during fluorescence arrival can be seen in Figure 14a. The number of packets was measured using the plots of fluorescence intensity over time generated from two regions of interest (ROIs) in a collecting vessel and was termed the packet frequency.

3.3.8 *Ex vivo* node analysis

Mice were euthanized in 2 groups; group1 (n=5) was monitored and imaged for 2 hours post injection before euthanasia and group 2 (n=5) was imaged for 2 hours post injection and again on days 1 and 2 before being euthanized. The draining (sacral) lymph nodes, control (axillary) lymph nodes were harvested from both the groups of mice after euthanasia. Additionally the liver, spleen, pancreas, kidney, heart, lungs, stomach, intestines, thymus and injection site were excised from one mouse in each group and was homogenized using 1.4 mm Zirconium Beads Pre-Filled Tubes (OPS Diagnostics, Lebanon, NJ) in a FastPrep 24 homogenizer (MP Biomedicals, Santa Ana, California). The supernatant was used to measure fluorescence in a Synergy™ H4 Multi-Mode Plate Reader (Biotek) to calculate exosome retention by each organ. One set of lymph nodes (both sacral and axillary) from both groups were snap-frozen in Tissue-Tek OCT (VWR, Radnor, PA) and sectioned at the Winship Cancer Institute's Pathology Core.

3.3.9 Fluorescence Confocal microscopy of lymph node sections.

Frozen sections of excised sacral and axillary nodes were blocked in 10% BSA in PBS and incubated with primary antibody overnight, followed by secondary antibody for 2 h. Primary antibodies were Anti-mouse CD19, Anti-mouse CD4, Anti-mouse CD8A(all from Life Tech), Anti mouse CD14 (Sigma), Anti-mouse CD169 (Thermo Fisher Scientific), Anti-Human CD81 (BD Biosciences). These sections were detected using secondary antibodies conjugated with Alexa Fluor 647 or Alexa 680 (Life Tech) and imaged by confocal microscopy using a Zeiss LSM 700.

3.3.10 Flow cytometry of nodes

Harvested lymph nodes from both group 1(n=3) and group 2 (n=3) were digested with collagenase D (Roche Ltd., Mannheim, Germany) and homogenized using 70 μm pore size strainers. Cell pellets were washed staining buffer with BSA (BD Pharmingen, San Jose, CA) and centrifuged at

300g for 1 min. To quantify exosome retention in the whole node, cells were analyzed for PKH67 positive populations using a LSR II flow cytometer (BD Biosciences, San Jose, CA). To identify cellular subsets responsible for exosome uptake, PKH67 positive cells were sorted on a FACS Aria II cytometer (BD Biosciences) and stained with monoclonal antibodies against mouse CD14, Anti-mouse CD19 and Anti-Human CD81 conjugated with, PE or AF647 for 30 min at 4 °C in the dark. Data was acquired in a LSR II flow cytometer (BD Biosciences) with compensation using single-stained cells. Data analysis was performed using FlowJo software (version 10).

3.3.11 Statistical analysis

T-tests were used to compare the expression levels of tetraspanin markers between exosomes and beads (unpaired), exosome and bead transport at 37^0C and 4^0C (paired), arrival times for dominant and non-dominant vessels and nodes (paired). Exosome retention in the node and uptake by macrophages and B-cells was analyzed using paired t-tests. All analyses were run in Prism 6 (GraphPad Software Inc, La Jolla, CA) and significance was defined as $p > 0.05$ (not significant - ns) $p \leq 0.05$ (*), $p \leq 0.01$ (**), $p \leq 0.001$ (***), and $p \leq 0.0001$ (****). All data is presented as mean ± standard deviation.

3.4 Results

3.4.1 Characterization of exosomes and beads

Exosomes from the HEY cell line were isolated and characterized along with size and density matched polystyrene beads using dynamic light scattering, scanning electron microscopy and for surface marker expression using flow cytometry. The average size of HEY exosomes was 78.82±19.17SD nm as compared to the beads which had an average size of 67.34±13.7SD nm (Figure 11a). Exosomes had a spherical shape with a diameter of ~60-75 nm as seen from scanning electron microscopy which agreed with previous reports of exosome shape and size reported in literature (153)(Figure 11b). The classical tetraspanin surface markers CD63 and CD81, which are known to be enriched on exosomal membranes(88), had an ~80% expression level on HEY exosomes (Figure 11c-e). Thus, the HEY exosomes used in this study conformed to known exosomal size ranges, expressed the classical tetraspanin markers and were spherical in shape as previously reported.

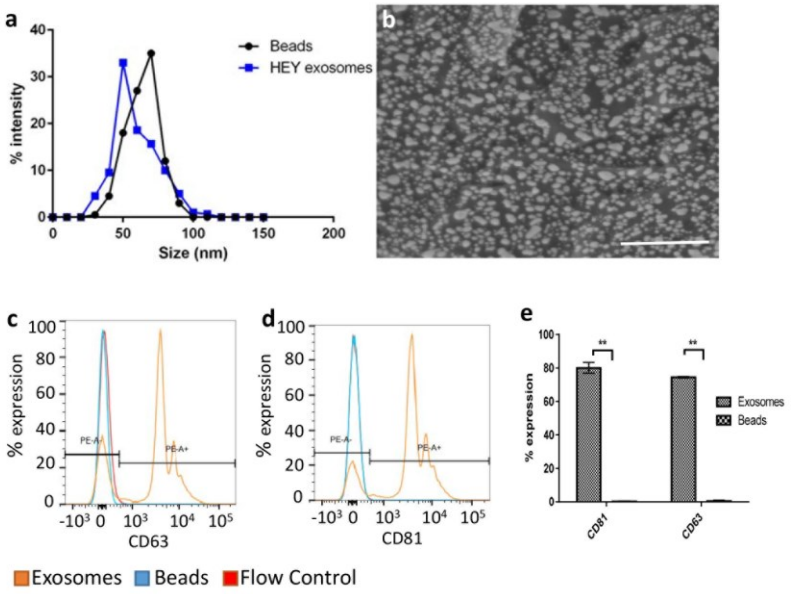

Figure 11: Characterization of exosomes and beads. a) Size distribution of HEY exosomes as compared to that of beads b) Scanning electron micrograph of exosomes c) Expression of CD63 and d) CD81 on exosomes and beads. e) Quantitation of CD63 and CD81 on exosomes and beads by flow cytometry (p-value <0.01)

3.4.2 Exosomes are transported rapidly and selectively through the lymphatic endothelium *in vitro*

To test the hypothesis that transport of exosomes across the lymphatic endothelium is higher than size and density matched beads, the effective permeability of cells (P_{eff_cell}) to the fluorescently labeled exosomes and beads in the basal to apical direction was measured using a transwell system as described previously(84) (Figure 12a). Exosomes, beads and dextran were freely transported across the membrane in the absence of cells (Figure 12b, dotted lines) and neither exosomes nor beads stuck to the membrane (Figure 42d).

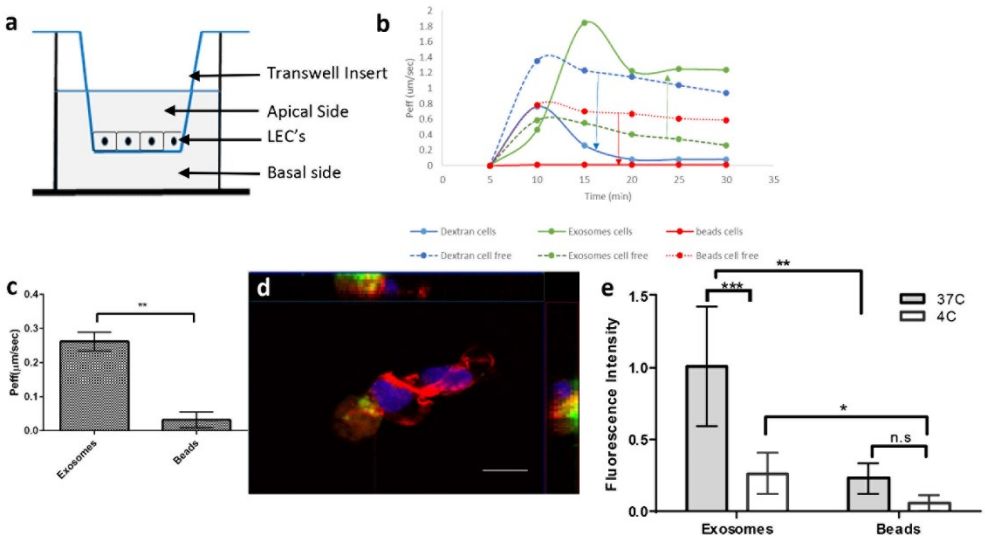

Figure 12: Exosomes transported rapidly and selectively through the lymphatic endothelium *in vitro* a) Schematic of experiment, b)Transport of exosomes across the lymphatic endothelium occurs rapidly (t=5-30mins) and is enhanced in the presence of cells, c) Exosomes are selectively transported into the lymphatic endothelium (versus beads), d) Confocal images of LEC's (nuclei stained with DAPI) with PKH67 exosomes and beads at 37^{O}C. Scale= 20 µm

Additionally, the size ranges of the exosomes collected on the apical side were similar to that on the basal side, further confirming exosome trafficking from the basal to apical sides of the LECs (Figure 42e). To understand the kinetics of exosome transport by LECs, transport was assessed every 5 min. The beads were excluded from this study as their transport was below the detection limit at 30 min. Flux was calculated both in the presence and absence of cells to determine the extent that LECs enhanced or alternatively provided a barrier to selective transport. Dextran, being extremely small (3kDa) freely diffused through the Transwell membrane at the roughly the same rate in the presence and absence of LECs and rapidly reached equilibrium at about 15 min. Exosomes were rapidly detected across the lymphatic endothelium at 5min and transport in the presence of cells was much higher than in the absence of cells (~2 fold) with transport reaching equilibrium at ~20 min (Figure 12b, solid lines). In order to quantify this difference, the effective permeability of cells was calculated after incubation with exosomes and beads for 75mins so

transport could attain equilibrium at 37^{O}C and 4^{O}C. Exosomes were transported across the lymphatic endothelium ~10 times more as compared to the fluorescent size matched beads (p-value < 0.01) at 37^{O}C (Figure 12c). When the cells were fixed and examined using confocal microscopy, exosomes were seen within cells at 37^{O}C (Figure 12d, Figure 42c) whereas beads were not (Figure 42b). However, exosome uptake was greatly reduced at 4^{O}C (Figure 42a). The fluorescence in the images that corresponded to exosomes and beads was quantified at 37^{O}C and 4^{O}C which showed that exosome transport was reduced by ~80% at 4^{O}C (Figure 12e, p-value< 0.001). Collectively this data suggests that the lymphatics actively transported exosomes *in vitro*.

3.4.3 Exosomes are rapidly transported into lymphatics *in vivo*

The tissue phantom was to test the sensitivity of the NIR imaging system for detecting dual labeled exosomes. Exosomes were detected at a signal-to-noise ratio >4 at depths of 1-6mm (Figure 43b). We tested the limit of detection of exosomes within the vessels by running several dilutions of the exosome solution through the tissue phantom and were able to detect 0.1μg/ul of exosomes which is 1% of the injected dose (Figure 43c). Lastly the lymph node phantom was able to detect an exosome concentration of 0.01μg/μl exosomes, or 1% of the injected dose of 1μg/μl (Figure 43d). To track the movement of exosomes real time *in vivo*, a near-infrared fluorophore was conjugated to the N-terminal of exosomal membrane proteins. A second fluorophore was added in the lipid bilayer of the exosomes to enable *ex-vivo*, multi scale analysis of cellular exosome uptake and transport (Figure 13a). Mice were injected intradermally with a 10ug bolus of dual labeled exosomes in PBS. The near-infrared excitation source and the field of view of the CCD emission detector were centered on the mouse tail 10 cm downstream (toward the base of the tail) from the injection site at the tip of tail (Figure 13b). This location ensured that only the downstream

collecting lymphatics would be visualized so as to maximize detection sensitivity and avoid image saturation form the injection site (Figure 13i).

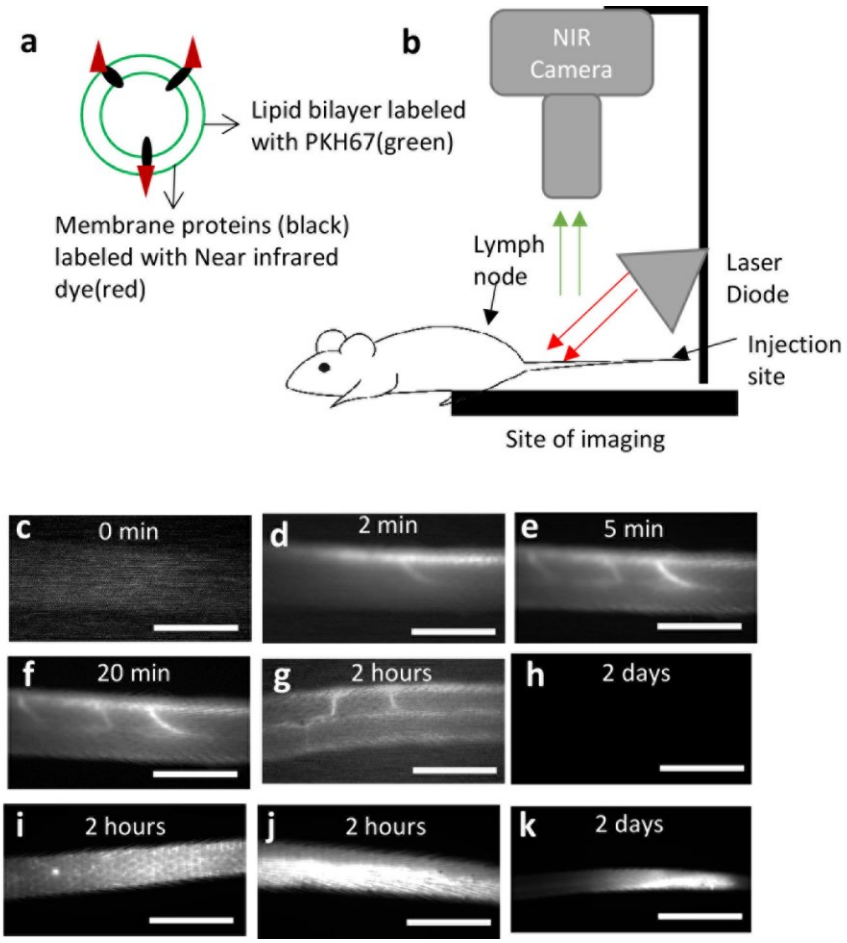

Figure 13: Exosomes are transported rapidly through the lymphatic endothelium *in vivo*. a) Dual labeling of exosomes, b) injection and visualization scheme in mice. Exosomes are detected in the lymphatics rapidly c) vessel at 0 mins, d) vessel at 2 mins, e) vessel at 5 mins, f) vessel at 20 mins g) vessel at 2 hours, h) vessel at 2 days, i) lymphatic capillaries seen close to the injection site at 2 hours, j) injection site at 2 hours, and k) injection site at 2 days. Scale bar =5mm.

Exosomes were seen in the lymphatic collecting vessels within 2 min of injecting the bolus in the tip of the tail 10cm downstream of the injection site (Supp Video 1). Exosomes were first detected first in the dominant vessel draining the tail, and then in the non-dominant vessel about 2.5 min later. Both vessels reaching a steady state value of fluorescence by 20 min after injection (Figure 13c-f) T. his result agreed with previous findings that reported lymphatic transport in rodent tails

and mouse hind limbs where the two collecting vessels had varying functional capacity as measured by NIR imaging(64, 154). The collecting vessels maintained these steady state values for up to 6 hours post injection however there was no detectable signal that remained in the vessel 24 hours after injection. Representative images of the collecting vessels are shown at the 2 hour and 2 day time points, the end points of our study (Figure 13g and h respectively). The injection site continued to retain a fraction of the injected exosomes at 2 hours and 2 days (Figure 13j and k respectively).

3.4.4 Characterization of exosomes transport *in vivo*

The fluorescence arrival in the dominant and non-dominant collecting vessels were analyzed and quantified from the time of injecting the exosome bolus until steady state fluorescence was achieved. The dominant vessel always had significantly higher fluorescence in all trials as compared to the non- dominant vessel (Figure 14a; p- value <0.05) and representative line intensity profiles are shown for both vessels (Figure 14b). The fluorescence arrival in the draining lymph nodes were analyzed and similarly, the dominant node (drained by the dominant collecting vessel) was visualized first and was brighter than the non-dominant node which was visualized later and was fainter (Figure 14c). Representative line intensity profiles are shown for both the draining lymph nodes (Figure 14d). There are two distinct regions in the line intensity graphs that corresponding to a) "arrival" where there is a rapid increase in exosome transport and b) "steady state" where the exosomal transport is stable. The packet frequency in the dominant vessel was significantly higher (p-value <0.05) at arrival as compared to the steady state while the difference in non-dominant packet frequency was not significant (Figure 44a, p-value = 0.068). The packet frequency in the lymph nodes followed a similar pattern with a significantly higher frequency in the dominant node as compared to the non-dominant node at both the arrival and steady states (p-

value<0.05, Figure 44b). The transport times of the dominant vessel was significantly lower with fluorescence first appearing in the dominant vessel at least 30 seconds ahead of the non-dominant vessels [p-value<0.05], and this trend was replicated in the lymph nodes with fluorescence in the dominant node appearing about a 1.5 min before the non-dominant node (Figure 14e).

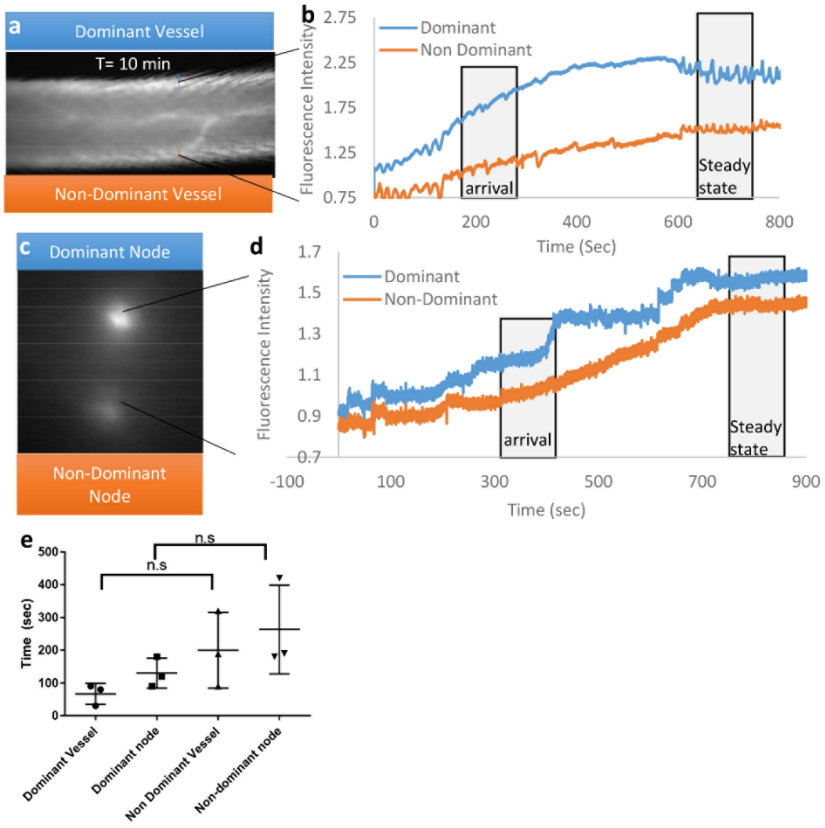

Figure 14: Characterization of exosomes transport in vivo a) Steady state fluorescence in the lymphatic collecting vessel b) Intensity profile of a specified region of interest of exosome transport in a representative vessel over a 10 minute period, c) Steady state fluorescence in the draining lymph node, d) Intensity profile of a specified region of interest of exosome transport in a representative lymph node over a 10 minute period, e) Arrival time of detectable levels of fluorescence for dominant and non-dominant collecting vessels and draining lymph nodes

To verify that the transport characteristics seen with HEY exosomes were features of lymphatic transport rather than specific to the cellular source, we injected exosomes from mouse lymphatic endothelial cell line (SV-LEC). We were able to recapitulate the collecting vessel and lymph

node transport kinetics and characteristics (Figure 45a-d). The arrival time in the collecting vessels and draining lymph nodes was comparable (Figure 45e) and the packet frequency (Figure 45f) is comparable between HEY and SV-LEC exosomes.

3.4.5 Characterization of exosome retention *in vivo*

The exosome bolus was rapidly seen in the sciatic lymph nodes drained by the collecting lymphatics with the fluorescence arriving in both the dominant (Figure 15a) and non-dominant node within 5 min (Figure 15b, Supp. Video 2). The nodes reached a steady state of fluorescence much like the collecting vessels by 30 min post injection; however unlike the vessels where the fluorescence disappeared within 24 hours, the lymph node fluorescence was detectable through the skin for at least 2 days after injection (Figure 15c and e respectively). The nodes upon excision at 2 hours and 2 days were strongly fluorescent (Figure 15d and f respectively).

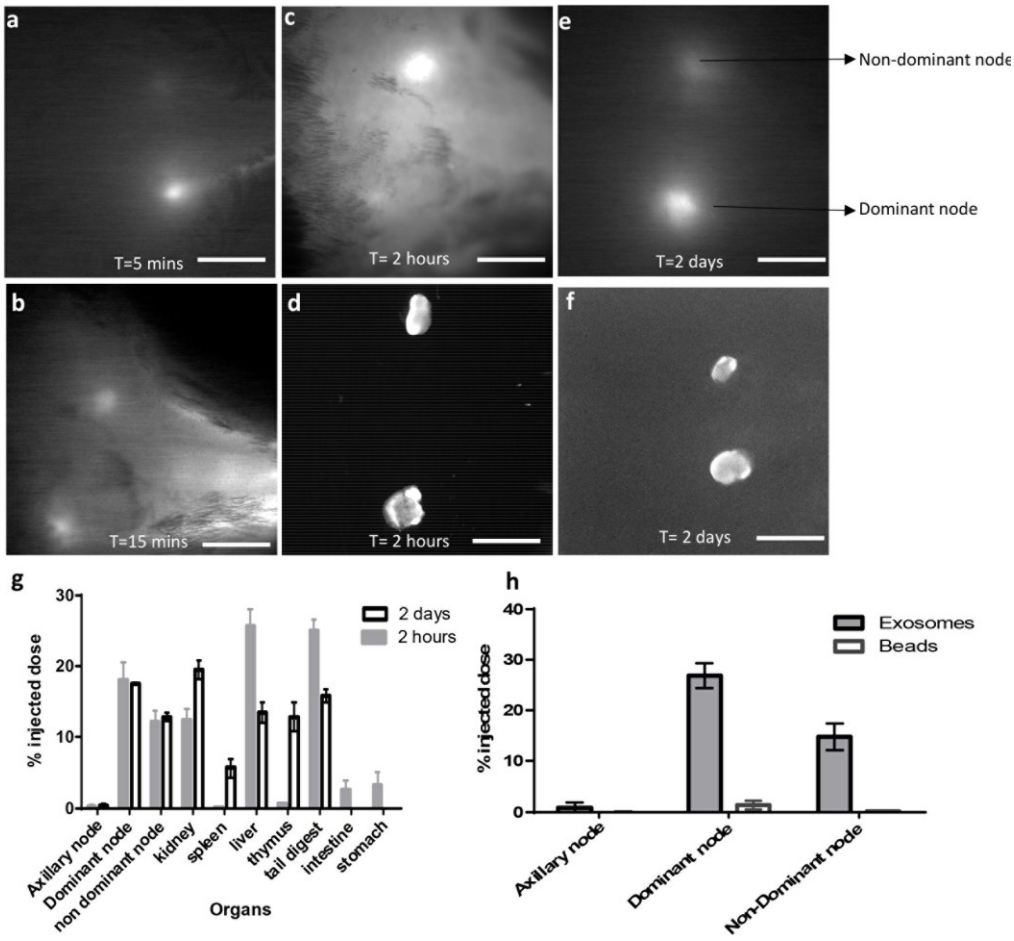

Figure 15: Characterization of exosome retention *in vivo*. Exosomes are detected in the node rapidly: a) Only dominant node is seen at 5 mins *in vivo*, b) Both nodes seen at 15 mins *in vivo*, c) Draining lymph nodes visualized at 2h pre-excision (in animal), d) Excised lymph nodes at 2h post injection, e) Draining lymph nodes visualized at 2d pre-excision (in animal) f) Excised lymph nodes at 2 days post injection, Scale =5 mm. g) Biodistribution of exosomes in mice organs analyzed at 2 hours and 2 days post injection and h) quantitation of exosomes and beads retained in the lymph node 1 hour post injection as determined by fluorescence

Several organs including the heart, lungs, kidney, spleen, liver, and pancreas were harvested from both mice at 2 hours and 2 days post injection and digested. The fluorescence was measured in each organ to quantify exosome retention by each organ. Exosomes were predominantly found in the injection site, draining lymph nodes, kidney and liver at 2 hours post injection and accumulated

in the lymph nodes, spleen, thymus and kidney at 2 days. A significant portion was still present in the injection site in the tail (Figure 15g).

We injected beads and SV-LEC exosomes together in mice to compare lymphatic uptake characteristics and quantified the percent of the injected dose in the lymph nodes using fluorescence on a plate reader 1 hour after injection. While exosomes were retained to a similar degree, the beads were poorly retained with the dominant node contributing to only 2% of the uptake. The non-dominant node had very poor (<1%) retention of the beads (Figure 15h).

3.4.6 Characterization of exosome retention in the draining lymph node

To investigate the cell populations that were responsible for uptake and retention of the exosomes in the draining lymph nodes, the dominant and non-dominant nodes were analyzed either by immunostaining or digesting the nodes and quantifying co-localization of the exosome signal with immune cells markers using FACS (Figure 16a). The dominant lymph node contained a significantly higher proportion of exosomes than the non-dominant node (p-value < 0.05) a phenomenon that was observed at both 2 hours and 2 days (Figure 16b and c respectively). Although the amount of exosomes retained in the node slightly decreased from 2 hours to 2 days post injection in both the dominant and non-dominant nodes, they still contained 10-15% of the injected exosomes and contained 1500-fold higher concentration of exosomes than the axillary lymph node which served as a control for the study as it did not directly drain the site of local exosome injection (Figure 15g, Figure 16d). Within the draining lymph node, exosomes were predominantly present in 2 specific areas: the entire periphery of the node and in small circular areas near the periphery that corresponded to the subscapular sinus (SCS) and the follicular regions of the lymph node respectively (Figure 16e-g).

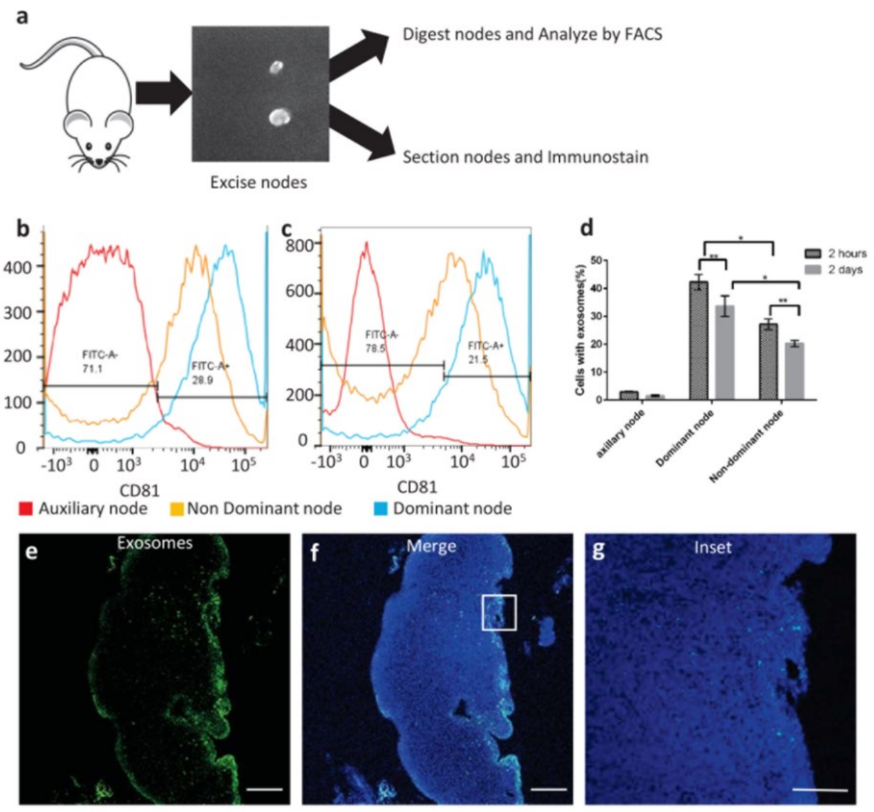

Figure 16: Characterization of exosome retention in the draining lymph node. a) Schematic of node procession post excision from mouse b) Dominant node retains a larger quantity of exosomes at 2 hours c) Dominant node retains a larger quantity of exosomes at 2 days, d) Quantitation of exosome retention by the dominant and non-dominant nodes at 2 hours and 2 days respectively, e) Exosome localization within the node; f) Merged image with whole node nuclear staining and exosome localization, g) magnified area in the node showing exosome localization (Scale =10um)

3.4.7 Role of CD11b+ and CD19+ cells in exosome uptake

To determine the primary *in vivo* targets of exosomes, we sorted the PKH positive cells and quantified the co-localization of the exosome signal with various immune cell subset markers including CD11b (Macrophages), CD19 (B-cells) CD4 (Helper T-cells), and CD8 (Killer T- cells). CD11b is abundantly expressed on the surface of monocytes and macrophages which are situated within the subcapsular sinus of the lymph node(155). Exosomes co-localized with CD11b+ macrophages in both the dominant and non-dominant lymph nodes but the dominant node had ~4 times greater macrophage-exosome co-localization as compared to the non-dominant node at 2

hours (Figure 17a, b). Exosome localization within macrophages was reduced by more than half in both the dominant and non-dominant nodes from 2 hours to 2 days (Figure 17c, d, i).

CD19 is expressed on B-cells and is present in the B-cell follicles underlying the subcapsular sinus in the node. Exosomes were not co-localized with CD19+ B-cells at 2 hours (Figure 17e, f) but were strongly co-localized at 2 days and the dominant node retained about ~5 times more as compared to the non-dominant node (Figure 17g-i). There was no co-localization with either CD4+ or CD8+ T-cells at either of the time points (data not shown).

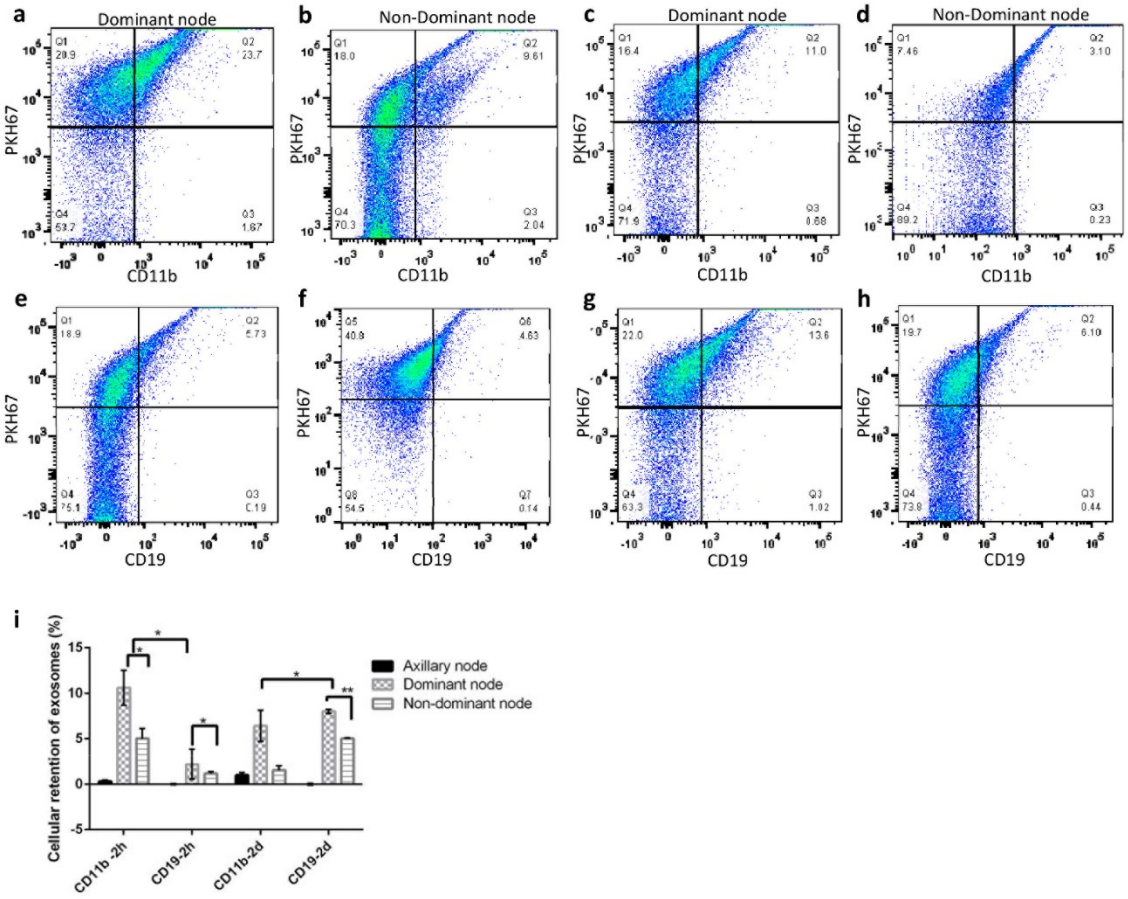

Figure 17: Characterization of exosome uptake by CD11b and CD19 cells in the node by flow cytometry. The dominant node was digested and stained for a) CD11b at 2h, c) CD11b at 2 days, e) CD19 at 2 hours, g) CD19 at 2 days. The non-dominant node was stained for b) CD11b at 2h,

Fig 17 Continued: d) CD11b at 2 days, f) CD19 at 2 hours, h) CD19 at 2 days and i) quantitation of exosome uptake by the dominant and non-dominant nodes at 2 hours and 2 days respectively

Finally, we confirmed the co-localization of exosomes with CD11b macrophages and CD19 B-cells by immunostaining frozen lymph node sections. We observed a strong co-occurrence of PKH (green) signal from the exosomes with CD11b from the macrophages and CD19 from the B-cells (Figure 18 a and c respectively). Additionally, we also checked for CD169 co-localization with exosomes to confirm macrophage mediated exosome capture (Figure 18b). In order to ensure that the PKH signal is still present on intact exosomes, we checked for CD81 expression and found a very high degree of CD81 and PKH co-occurrence indicating that the dye was still associated with the exosomal membrane (Figure 18d).

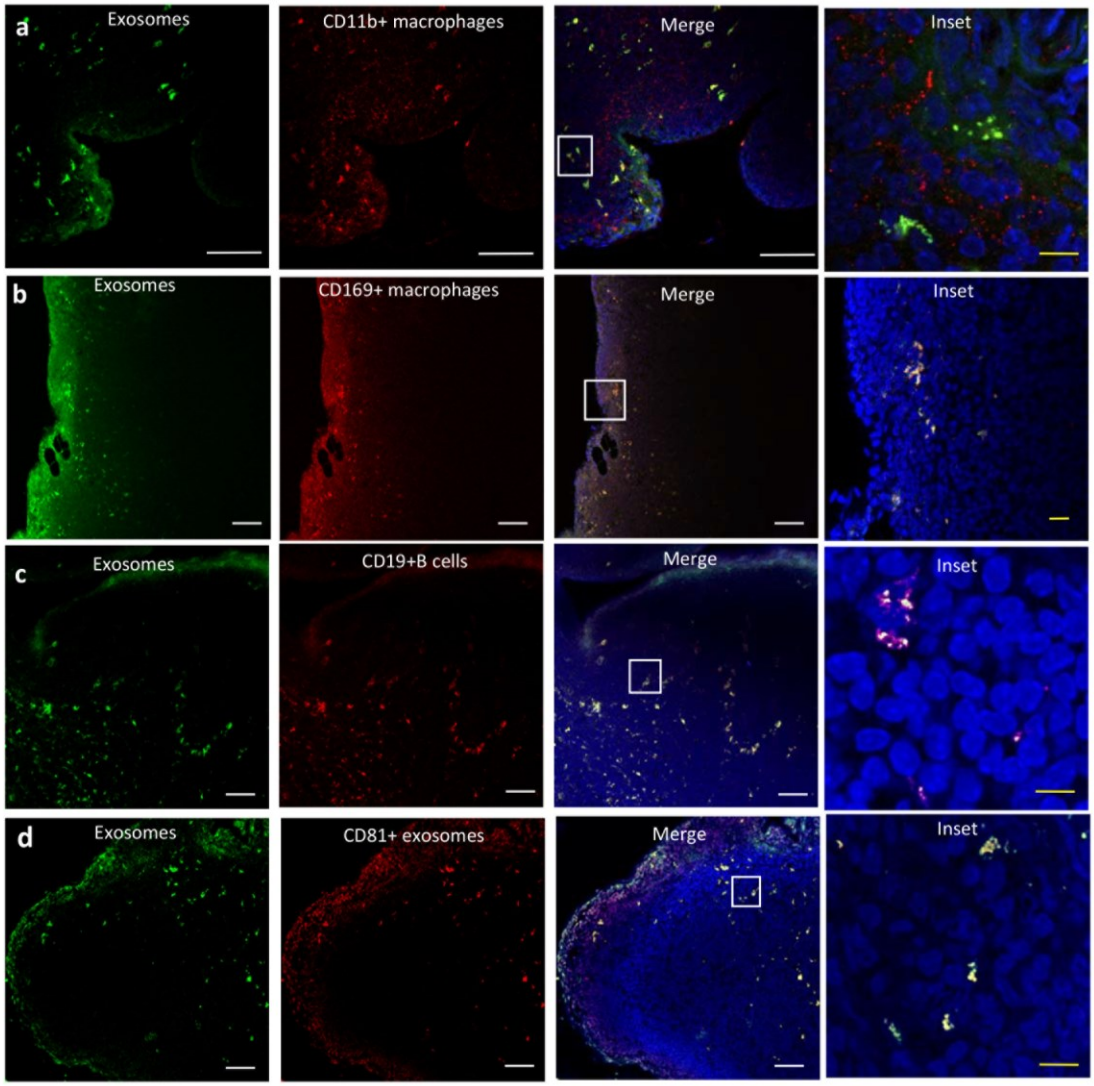

Figure 18: Localization of exosomes within the lymph node. Shown are serial lymph node sections at 2 days following injection of 10ug of exosomes (green). Immune cells were identified as indicated (red) with antibodies against a) CD11b (macrophages), b) CD169 (macrophages), and c) CD19 (B-cells), d) CD81 (red) was used as a secondary localization marker to confirm exosome retention in the node. White scale bar= 50um while yellow scale bar is 5um.

3.5 Discussion

The draining lymph nodes are a stable retention site for exosomes with the quantity of exosomes retained in the nodes steadily increasing in both the dominant and non-dominant nodes from 2 hours to 2 days. Exosomes carry functional mRNA and miRNA which cause changes in gene

expression in recipient cells(156). They have also been shown to carry antigens when released from infected cells resulting in a suppression of inflammatory response *in vivo(157)*. Thus, the speed of exosome transport and retention at the node has important implications in innate immune responses. Antigen presenting cells can acquire antigens in peripheral tissues such as skin, migrate through the lymphatics to the node and activate an immune response(109). Macrophages can release exosomes that carry specific antigens to initiate an immune response at the node: *M.tuberculosis* infected macrophages released exosomes containing mycobacterial lipoproteins which were able to stimulate a pro-inflammatory response in mice(140). Our data suggests that exosomes can reach the lymph node and be taken up by the Cd11b+ macrophages within 5 min and thus offer a faster route for information and antigen transfer from the periphery as compared to dermal antigen presenting cell migration to the lymph node which can take hours. Additionally, this process would allow for some APCs to remain around the peripheral site of infection to survey for further signs of infection, while at the same time preemptively warning the lymph node of the danger with specific information of the nature of the infection encoded within the exosomes. This is supported by the observation that DCs continue to crawl around within the interior of the lymphatic capillary, often in directions opposite to that of lymph flow, even during inflammation(158). Further studies elucidating the time for APC's to package and secrete pertinent antigens and RNA molecules via exosomes are warranted to more fully understand this process. Additionally, the quantity of exosomes required to elicit a response is as yet unknown and will likely contribute the magnitude of the response developed at the node.

While both nodes exhibited stable fluorescence from the time of detection and were brightly fluorescent upon excision (at 2 hours or 2 days), a majority of exosomal uptake in the node was within 10 min post injection. While subtle difference in depths and diameters of the two nodes

within the animal can contribute to this phenomenon, we could not observe a visible difference in the size of the nodes.

Exosomes accumulated the most in the liver, followed by the injection site and the kidney, with the stomach and intestine showing minor exosomal presence. Another study of exosomal biodistribution showed presence of exosomes in the liver and spleen 30 min post injection in the tail vein(159). While we detected a strong signal from the liver, we were unable to detect any exosomes in the spleen until the 2 day time point. It is likely that transport via the blood and lymph will result in different biodistributions of the exosomes within whole animals and intradermal injections result in lymphatic transport with accumulations in the nodes and liver while intravenous injections result in transport by blood and accumulation in the spleen and kidneys. This is an important finding, as the *in vivo* release of exosomes from cells in the interstitium will necessarily concentrate themselves in the lymph nodes via lymphatic transport. Interestingly, in either case, a lymphoid organ is involved in exosome retention along with the liver. This phenomenon is corroborated by Saunderson *et al(124)*, where intravenously injected exosomes accumulate in the spleen and subcutaneous injections lead to an accumulation in the lymph node 60 min post injection. We believe that the exosomes have not entered the circulation in sufficient quantity at 2 hours, due their lymphatic targeting and high levels of retention the node, thus explaining the appearance of exosomes in both the spleen and thymus only at the two day time point.

Lymphatic flow and the resulting immune response are known to be intimately connected(151) and in certain cases of inflammation lymph flow itself can be modulated through the recruitment of immune cells to the contractility of the afferent vessels draining the node (152). While lymphatic transport of exosomes has been implied in several papers(24, 124) they have focused on the downstream retention and effects of exosomes at the lymph node and the role of lymphatic

drainage has been overlooked. Our results suggest that lymphatic flow can transfer exosomes from the periphery to the draining lymph nodes and that the transport capacity of the afferent vessels draining to the lymph node contributes to the distribution of exosomes between the nodes with the dominating collecting vessel transporting a higher payload of exosomes to the dominant node even though both nodes appear to drain the same tissue space. This distribution remains consistent even for up to two days, and is the first study to our knowledge, that shows that the quantity of antigen in the node is correlated to the lymphatic flow in that node. Additionally, the lymphatic uptake kinetics are similar for both human and mouse cell line derived exosomes, which implies that lymphatic transport is a common mode for exosome transport from the periphery to the draining lymph nodes rather than a selective route that depends on the biological state of the cellular source at early time points. Future studies that characterize the lymphatic retention and biodistribution of exosomes from different cell types could help understand the role of the cell of origin in the fate of exosomes *in vivo*.

HEY cells are an ovarian cancer cell line and the strong retention of HEY exosomes in the lymph node is comparable to the retention of melanoma exosomes in the node(127). Given that ovarian cancer has one of the poorest outcomes(160), spreads through the retroperitoneal lymphatics during metastasis(161), and the numerous reports of tumor exosomes modulating immune responses at the node(132, 162), understanding the lymphatic transport of these exosomes will further help in understanding the role of lymphatic transport during cancer progression.

Rapid uptake of exosomes into the node also appears to be facilitated by active transport mechanisms in the initial lymphatic endothelial cells that are selective for exosomes, as the presence of LEC *in vitro* specifically enhanced the transport of exosomes across a permeable membrane, but not size-matched nanoparticles or lower molecular weight dextran. In fact exosome

transport was 10 times higher than that of size-matched beads at 37^{O}C. Reduction of exosome transport at 4^{O}C by 80% reduction implies active cellular transport. This concurs with previous data that indicates that exosome uptake is actin dependent(148) and active(163). The molecular mechanisms that underlie exosome uptake is not well characterized and is a matter of debate. Several mechanisms including clathrin mediated endocytosis(164), pinocytosis, plasma and membrane fusions and phagocytosis(165) have been proposed without much consensus. Once a clearer understanding of uptake mechanisms is achieved, specific inhibitors can tease out the contributions of these pathways in exosome uptake by the lymphatic endothelial cells. Additional work to characterize the intracellular compartments as well as surface receptors that participate in exosomal shuttling will reveal potential transport mechanisms that enable selective uptake and transport. Rapid and active transport of other particles have recently been reported in lymphatic endothelial cells including lipoproteins, antigens, and albumin bound free-fatty acid, suggesting that active lymphatic trafficking, while selective, is not restricted solely to exosomes(150, 166-168)

In vivo, the initial lymphatics have unique button junctions that when combined with anchoring filaments enable fluid uptake and transport from the interstitium into the initial lymphatics(169). Additionally, elevated transmural flow has been shown to alter expression of cell-cell junction proteins in LEC to increase uptake(170). Thus, the injection of an exosome bolus would increase interstitial fluid pressure, lymphatic flow, and thus uptake of exosomes either directly or indirectly through active rearrangement of junctions to alter lymphatic permeability. It is likely that this passive drainage works in concert with active transcytosis to further enhance exosome clearance from the interstitial space.

Lymphatic endothelial cells (LECs) were recently shown to play an active role in scavenging antigens and presenting them to the cognate T-cells(171). Collecting lymphatic permeability was also shown to enhance the sampling of lymphatic antigens by antigen presenting cells within the surrounding adipose tissue(49). Thus, the selective transport of exosomes by LEC's is a further demonstration of their active role in the establishment of immunity as they aid the exposure of the exosomes to immune cells.

The dominant and non-dominant nodes widely differ in exosome uptake by macrophages and B-cells. While this difference could be partially caused by the differing amounts of exosomes received by each node, may not be sufficient to explain the differences observed. Macrophages in the subcapsular sinus can capture and retain antigen from the lymphatics for up to 72 hours and then present them intact to B-cells(172, 173). Additionally, T-cells transferred exosomes to APC's at the immunological synapse through cognate interactions(174). A similar mechanism could be potentially operating in exosome transfer although further studies need to be conducted to understand the kinetics of exosome movement within the node. It will be interesting to further understand the time and location of RNA and protein release from the exosomes at the node and the modulation of the immune cell subsets by this mechanism. Further studies need to be conducted to see if these differences in co-localization could impact the immune response development at each of these nodes in the presence of antigen which could reveal important information about the development of an innate immune response at the lymph node.

3.6 Conclusions

Collectively, our findings highlight the importance of lymphatic permeability and drainage in the transport of exosomes from the periphery to the lymph nodes. It also sheds light on the immune cell subsets involved in exosome retention at the node which was hitherto unknown and can

potentially be exploited in targeting the lymph node. The differential distribution of exosomes between the two draining nodes while unexpected has opened up new questions in distribution of antigens during an immune response and vaccine response suggesting subtle differences between the immune cell niche between the dominant and non-dominant nodes. The combination of rapid lymphatic delivery to the node and the functional consequences of exosomes on downstream cells could be a powerful combination in drug delivery but will need a great deal of further work to unlock the full spectrum of possibilities.

CHAPTER 4: EXOSOMES DERIVED FROM TLR ACTIVATED CELLS SHOW DISTINCT EFFECTOR FUNCTIONS

4.1 Abstract

The innate immune system is vital to rapidly responding to pathogens and Toll-like receptors (TLRs) are a critical component of this response. Nanovesicular exosomes play a role in immunity, but to date their exact contribution to the dissemination of the TLR response is unknown. Here we show that exosomes from TLR stimulated cells (TLR-exosomes) can largely recapitulate TLR activation in distal cells *in vitro*. We can abrogate the action-at-a-distance signaling of exosomes by UV irradiation, demonstrating that RNA is crucial for their effector function. We are the first to show that exosomes derived from poly (I:C) stimulated cells induce *in vivo* macrophage M1-like polarization within murine lymph nodes. These TLR-exosomes demonstrate enhanced trafficking to the node and preferentially recruit neutrophils as compared to control-exosomes. This work definitively establishes the differential effector function for TLR-exosomes in communicating the activation state of the cell of origin.

4.2 Introduction

Detecting microbial pathogens rapidly and containing their spread is a critical function of the innate immune system[1]. Toll-like receptors (TLRs) are an essential arm of innate immunity as they detect highly conserved pathogen associated molecular patterns (PAMPs) and play an important role in host cell defense[2]. The direct response of cells stimulated with TLR agonists locally is well characterized[3,4]. Dendritic cells exposed to the TLR4 agonist lipopolysaccharide (LPS) show a distinct gene expression response as compared with cells exposed to the TLR3 agonist poly I:C (pIC), and these gene expression profiles are known to be pathogen specific[5]. TLR stimulation induces production of a broad range of molecules including cytokines and chemokines[6], which are

essential for host response to infection as well as for the development of an adaptive immune response[7].

While cytokines and chemokines are well studied for their roles in mediating cell-cell communication to establish immunity[8], recently more complex messengers such as extracellular vesicles have been discovered[9]. Exosomes are nanovesicles (30-150 nm in diameter) released by the fusion of large multivesicular endosomes with the host cell membrane[10]. They are produced by most known cell types, and ubiquitously found in biological fluids[11] and carry functional cargo in the form of mRNA, miRNA and proteins to distal recipient cells where the contents can modulate the recipient cell phenotype[12].

Exosomes have many distinct roles in physiology and immunity[13-15] and have known to play dual roles in both immune system activation[16] and immune suppression[17]. Furthermore, we recently showed that exosomes are rapidly trafficked from peripheral tissues by the lymphatics, and retained in the draining lymph node by macrophages in a murine model[18].

While local cellular response to TLR stimulation is well studied both *in vitro* and *in vivo*[19-21], the role of exosomes in the distal dissemination of the TLR response is less well understood. We speculated that exosomes from TLR stimulated cells could potentially transmit information to distal unexposed cells *in vitro.* Moreover, we wanted to understand the impact of stable lymphatic retention of exosomes by macrophages in the development of an immune response *in vivo*.

Here we delineate the differential effector function of TLR-exosomes based on the innate immune activation state (control-, LPS-, pIC-stimulation) of the cell of origin in both *in vitro* and *in vivo* experiments. pIC derived exosomes are rapidly transported to the lymph node and polarize distal macrophages to an M1-like state and recruit neutrophils. We show that exosomes are

reprogrammed to carry a TLR-specific message to distal cells and more work is warranted to understand the implications of this in immunity to pathogens and cancer.

4.3 Materials and Methods

4.3.1 Cell culture and TLR stimulation

Fetal bovine serum (Atlanta Biologicals, Lawrenceville, GA) was centrifuged for 15 hours at 120,000 g, 4^{O}C to remove exosomes and was used to make exosome free cell culture media. HEY cells (Cedarlane Labs, Ontario, Canada) were cultured in RPMI 1640 (Mediatech, Manassas, VA) supplemented with 10% exosome free fetal bovine serum, 2 mM L-glutamine, 10 mM HEPES buffer (both from Mediatech), penicillin (100 U/ml), and streptomycin (100 μg/mL) (Thermo Fisher Scientific, Waltham, MA) for 48 hours and the culture media was used for isolation of exosomes by ultracentrifugation. Ultra-pure *E.coli* K12 LPS and poly(I:C) (Invivogen, San Diego, CA) were used to treat cells at concentrations of 100 ng/mL and 10 μg/mL respectively for most experiments. Fluorescent LPS- Alexa Fluor 594 (Thermo Fisher Scientific) and poly(I:C) Rhodamine (Invivogen) were used at the same concentration to determine exosome mediated carryover.

4.3.2 Exosome isolation and characterization

Conditioned media was collected from HEY cells (with or without TLR agonist treatment) at 90% confluence for exosome isolation. Briefly, the culture media was spun at 300 g, for 10 minutes to remove dead cells followed by a spin at 16,500 g, 20 min. The supernatant was then filtered through 0.22 μm filters and centrifuged at 120,000 g for 120 min. The pellet containing exosomes was re-suspended in a suitable volume of PBS. The size homogeneity of vesicles obtained was checked using a Zetasizer Nano ZS90 (Malvern Instruments Ltd, Worcestershire, UK) and quantified using Pierce BCA Protein assay kit (Thermo Fisher Scientific).

4.3.2.1 Flow Cytometry:

To analyze the expression of exosomal surface markers, 4 μm aldehyde/sulfate latex beads (Thermo Fisher Scientific) were coated with anti-CD9 antibody (BD Biosciences, San Diego, CA; Cat: 555370) overnight and incubated with 30 μg of exosomes. The exosome-beads complexes were probed with human anti-CD81-PE (BD Biosciences; Cat: 555676) or human anti-CD63-PE (BD Biosciences; Cat: 557305) and data was acquired on a LSR II Flow cytometer (BD Biosciences). Data analysis was performed using the FloJo software (FlowJo version 10, Ashland, OR).

4.3.2.2 Confocal microscopy

The exosomes were labeled using PKH67 Green Fluorescent Cell Linker Kit for General Cell Membrane Labeling (Sigma-Aldrich, St. Louis, MO) as per the manufacturer's instructions. Briefly, exosomes in PBS were added to 500 μL of Diluent C and 2 μl of PKH67 dye was added to 500 μL of Diluent C. The two solutions were mixed and incubated for 5 min at room temperature. 1 ml of 1% BSA was added to stop the reaction. The labeled exosomes were centrifuged at 120,000 g for 70 min to remove excess dye. Labeled exosomes were added to $5*10^5$ cell suspension, mixed gently for 2-3 min and seeded in 6-well plates. The cells were imaged after 24 and 48 hours using a Zeiss LSM 700 Image processing and data analysis were performed using the ZEN imaging software (Zeiss, Germany).

4.3.2.3 Scanning electron microscopy

Exosomes were fixed with 3.7% glutaraldehyde (Sigma–Aldrich) on carbon stubs for 15 min. After washing twice with PBS, the fixed exosomes were dehydrated with an ascending sequence of ethanol (40%, 60%, 80%, 96–98%). After evaporation of ethanol, the samples were left to dry at

room temperature for 24 h on a glass substrate, and then analyzed by Hitachi Cold Field Emission SEM SU8200 (Hitachi High-Tec, Tokyo, Japan).

4.3.2.4 UV treatment of exosomes:

Exosomes from control, and TLR agonist stimulated cells were re-suspended in PBS were then subjected to UV-light (254 nm) for 30 mins at 4°C to neutralize RNA carried within similar to previous studies[27].

4.3.2.5 Nucleic acid extraction from exosomes

Exosomal RNA was extracted from exosome samples using the QIAamp viral RNA mini kit (Qiagen), and RNA was eluted with 40 μL buffer AVE, according to the manufacturer's instructions. RNA quality and quantity was analyzed using Nanodrop and Agilent Bioanalyzer chips

4.3.2.6 Western blot

The total protein was extracted from cells and exosomes using modified RIPA buffer (Thermo Fisher Scientific) and cell debris was removed by centrifugation. Equal amounts of protein (15–20 μg) were then separated on polyacrylamide gels, transferred onto PVDF membranes (Bio-Rad, Hercules, CA, USA) and blotted using mouse anti-human CD81 Antibody (BD Biosciences; Cat: 555676). Membranes were developed using SuperSignal™ West Dura Extended Duration Substrate (Thermo Fisher Scientific).

4.3.3 Microarray procedure and data analysis

Total RNA was isolated from control and TLR stimulated parental and recipient cells (grown with exosomes) after 48 hours using RNeasy mini RNA isolation kit (QIAGEN, Valencia, CA). The integrity of the RNA was verified using the Agilent 2100 Bioanalyzer (Agilent Technologies,

Santa Clara, CA). mRNA's were converted to double stranded DNA and amplified using the Applause 3'-Amp System (NuGen, San Carlos, CA). This cDNA was fragmented and biotin labeled using the Encode Biotin Module (NuGen), hybridized to Affymetrix HG U133 Plus 2.0 oligonucleotide arrays and analyzed with a Gene Chip Scanner 3000 (Affymetrix, Santa Clara, CA). Raw data in the form of CEL files were produced by the Affymetrix GeneChip Operating System (GCOS) software.

mRNA microarray data were analyzed using the Expression Console software (Affymetrix) and Bioconductor tools[44] written in the R statistical programming language (www.rproject.org). Pre-processing of raw signal intensities and normalization was performed using GCRMA (R). Linear modelling of the transformed data was determined by using Limma[45] in R with the Benjamini and Hochberg correction. Differentially expressed probesets were identified using a threshold 5% FDR correction and a fold change ≥ 1.4 was applied. The microarray data is publicly accessible in GEO under the accession number GSE81248.

4.3.4 Real-time quantitative PCR (qRT-PCR)

Parental HEY cells were grown with or without LPS or poly(I:C) stimulation and total RNA from the cells was collected at 2h, 6h, 12h , 24h or 48 hours. Similarly, control, LPS or poly(I:C) exosomes were added to recipient cells and total RNA was collected from cells grown with exosomes at 2h, 6h, 12h, 24h and 48 hours respectively. Total RNA from macrophages as well as parental and recipient cells was extracted using an RNeasy plus kit (QIAGEN), and cDNA was generated with SuperScript VILO cDNA Synthesis Kit (Thermo Fisher Scientific). Analysis was done on a Strategene Mx3005P System (Agilent Technologies) with SYBR Green PCR master Mix (Thermo Fisher Scientific). The (intron spanning) primers were used for quantitative real-time PCR are shown Table 3 and Table 4. The fold change was calculated using the $\Delta\Delta$Ct method.

All analyses were run in Prism 6 (GraphPad Software Inc, La Jolla, CA) and all data is presented as mean ± standard deviation.

4.3.5 Proximity Ligation Assay(PLA)

HEY cells were cultured on 12-mm glass cell culture coverslips (Thermo Fisher Scientific). Cells were washed three times with phosphate-buffered saline (PBS) and then fixed for 15 min in PBS with 4% paraformaldehyde. After washing with gentle shaking, cells were permeabilized for 5 min with methanol and washed. The proximal-ligation assay to detect the interaction of p50 with p65, anti- NF-κB p50 (Santa Cruz Biotech, Dallas, TX; Cat: sc-8414) and anti-NF-κB p65 (Santa Cruz; Cat: sc-372) and for p65- SIRT1 interaction, anti-NF-κB p65(Santa Cruz Biotech; Cat: sc-8008) and anti-SIRT1 (Santa Cruz; Cat: sc-15404) were used with a Duolink PLA assay kit (Sigma Aldrich). Images were acquired Zeiss LSM 700 (Zeiss).

4.3.6 Animal study and handling

Exosomes from unstimulated (Control) and poly I:C stimulated HEY cells were dual labeled with PKH67 and near infrared dye using IRDye® 800CW Protein labeling kit (Licor, Lincoln, NE). Control or Poly I:C exosomes (total quantity=10 μg) were injected intradermally into the tail of eight-week-old male Balb/C mice (Charles River Laboratories, Wilmington, MA) as described previously[18] and euthanized on day two(t=48 hours). PBS was mixed with PEGylated IRdye 800CW (Licor) and injected similarly as the experimental control. The LAL Chromogenic Endotoxin Quantitation Kit (Thermo Fisher Scientific) was used per the manufacturer's instruction to measure LPS concentration on all injected exosomes to ensure no endotoxin crossover. All procedures in this study have been approved by the Georgia Institute of Technology IACUC Review Board (Protocol #A15051).

4.3.7 Lymph node extraction and macrophage isolation

The draining (sacral) lymph nodes, and control (axillary) lymph nodes were harvested from Control exosomes [Group 1; n=10], poly I:C exosomes[Group 2; n=10] and PBS control [Group 3; n=8]. Harvested lymph nodes from all groups were digested with collagenase D (Roche Ltd., Mannhein, Germany) and homogenized using 70 μm pore size strainers as previously described[46]. Cells were centrifuged at 300 g, 4^{O}C, 5 mins and the pellet was resuspended in HBSS and used for either whole node sequencing or macrophage isolation. CD11b positive macrophages were pulled down with Anti-mouse CD11b magnetic particles (BD Biosciences; Cat: 558013) according to the manufacturer's protocol. The isolated macrophages were resuspended in Trizol (Thermo Fisher Scientific) and stored at -80^{o}C till further analysis.

4.3.8 Immunohistochemistry of frozen lymph node sections

One set of lymph nodes (both sacral and axillary) from both groups were snap-frozen in Tissue-Tek OCT (VWR, Radnor, PA) and sectioned at the Winship Cancer Institute's Pathology Core. Frozen sections of excised sacral and axillary nodes were blocked in 10% BSA in PBS and incubated with primary antibody overnight, and then secondary antibody for 2 h. Primary antibodies were anti-CD86 (Cat: MA1-10299), anti-iNOS(Cat: PA3-030A), anti-MHCII (Cat: MA5-16913) [all 3 from Thermo Fisher Scientific] and anti-IL12A (Acris Antibodies, San Diego, CA; Cat: AM32704AF-N). These sections were detected using secondary antibodies conjugated with Alexa Fluor 647 or Alexa 680 (Thermo Fisher Scientific) and imaged by confocal microscopy using a Zeiss LSM 700.

4.3.9 RNA Seq: Macrophage and whole node RNA isolation and library prep

RNA was isolated from macrophages or digested whole nodes stored in Trizol (ThermoFisher Scientific) per the manufacturer's instructions. Briefly, macrophages from control exosomes

(n=2), pIC exosomes (n=2) and PBS dye (n=2) were homogenized for 20–30 sec with a rotor-stator homogenizer (Kimble Chase, Vineland, NJ). The sample lysates were then transferred to 2.0 ml Phase Lock Gels – Heavy (Eppendorf, Hamburg, Germany). Choloroform was added to each sample and centrifuged at 12,000 rcf for 10 min, and the upper aqueous layer was transferred to a new tube. The RNA was precipitated in isopropanol and washed in 75% ethanol according to the standard TRIzol protocol. The RNA pellet was then re-suspended in RNase-free water (Ambion, Austin, TX) according to the manufacturer's instructions. RNA quantity and integrity were assessed by examining the relative intensity of 18s and 28s rRNA bands using an Agilent 2100 Bioanalyzer and RNA6000 Pico LabChip Kit (Agilent Technologies).

10 ng of Macrophage RNA was used as input to a Clontech Smart Seq v4 kit (Clontech labs, Mountain View, CA) to generate double stranded cDNA per the manufacturer's instructions. The cDNA was quantified using the Qubit HS DNA kit (Thermo Fisher Scientific) and 1 ng was used to prepare libraries using a Nextera XT DNA library preparation kit (Illumina, San Diego, CA) per the manufacturer's instructions.

250 ng of whole node RNA was used as input in a TruSeq Stranded mRNA library prep kit (Illumina) to generate cDNA libraries. Both libraries were quantified using a Qubit Fluorimeter (Thermo Fisher Scientific) and multiplexed samples were run on a HiSeq 2500 instrument (Illumina). Using 101 bp paired end sequencing we allocated ~40 million reads per library index.

4.3.10 Data analysis

RNA seq analysis for the three conditions, each with two replicates, was performed using raw reads (101bp, paired end) from an Illumina HiSeq 2000 machine. The reads were first aligned to the mouse reference genome (mm10, UCSC), using TopHat with default parameters. The transcripts were assembled from the aligned reads using Cufflinks, and the transcript abundance

was calculated in terms of FPKM (fragments per kilobase of exon per million fragments mapped)[47]. To compare the expression profile of the different samples, we used Cuffdiff, a differential expression analysis tool provided with the Cufflinks package. The results from Cuffdiff were used to plot the gene expression distribution graphs using a custom R script

The pathway analysis was performed using the GAGE RNA Seq workflow for pathway enrichment analysis[48]. The –Log10(P-value) of the pathways of interest was plotted in R. Details of the analysis and the custom R scripts used to generate the figures are publicly available at the Github web site https://github.com/shashidhar22/macrophageRnaSeq. The data is publicly accessible in Sequence read archive (SRA) under the accession numbers: SRP074717 and SRP074576.All graphs were generated on Prism 6 (GraphPad Software Inc, La Jolla, CA) and data is presented as mean ± standard deviation.

4.4 Results

4.4.1 Characterization of exosomes

To understand the effect of stimulation of local cell and the effect of exosomal cargo on distal cell expression, we collected exosomes from local ovarian adenocarcinoma (HEY) cells that were unstimulated (control exosomes), or stimulated with poly I:C (pIC exosomes), or lipopolysaccharide (LPS exosomes) for 48 hours. The three groups of exosomes were added to naïve (distal) cells and the changes in gene expression profiles were compared between local TLR stimulation (for 6 hours) and distal stimulation mediated by exosomes (for 48 hours) on a microarray (Figure 19).

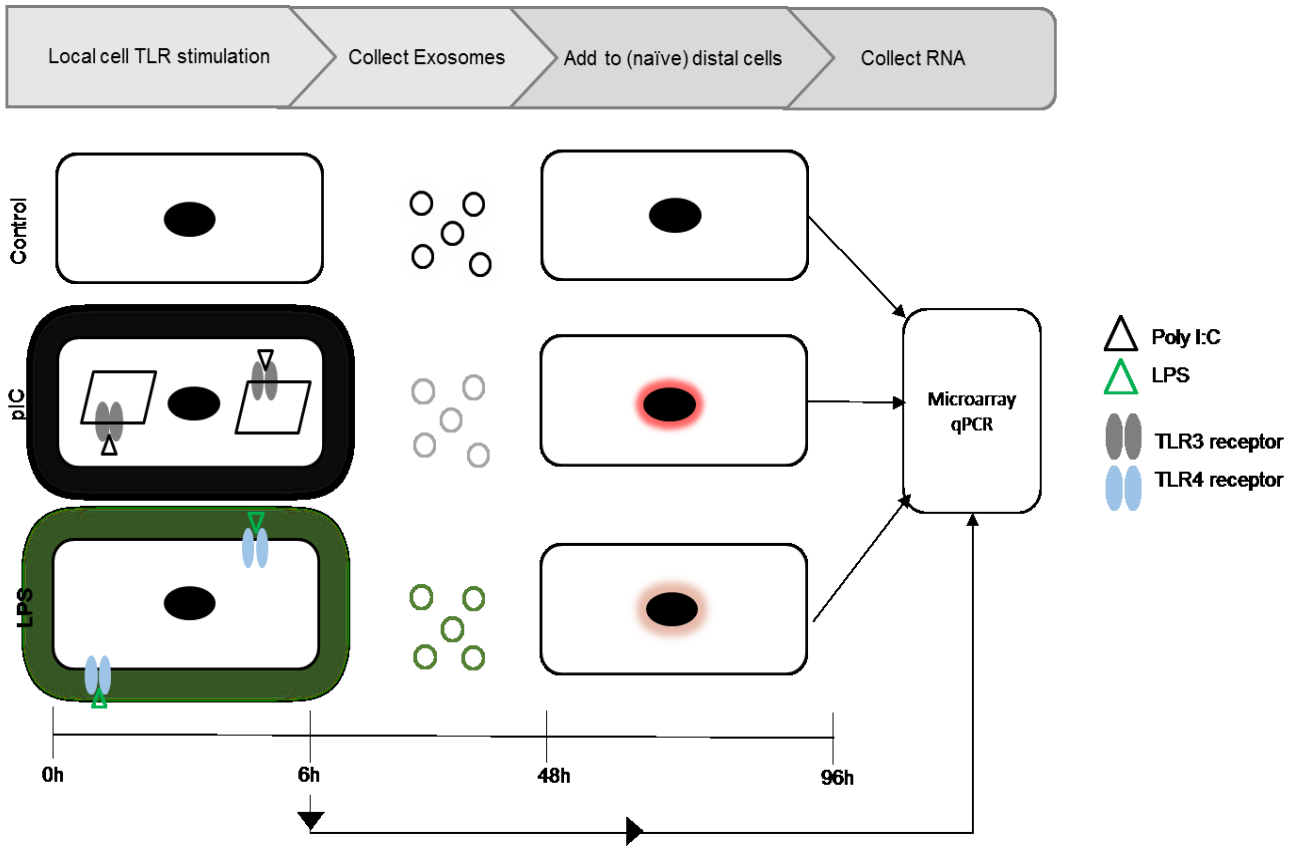

Figure 19: Schematic of experiment to elucidate transmission of TLR response to naïve distal cells.

Surface CD81 protein expression by western blot revealed similar expression (Figure 20c, Figure 37a) and flow cytometry showed comparable levels of expression of CD81 and CD63 on control, pIC and LPS exosomes (Figure 20a, Figure 37 b-c). The size distribution profiles were similar for the three groups (Figure 20b) and the overall shape of control, pIC and LPS exosomes was spherical, as revealed by scanning electron micrographs (Figure 20 d-f respectively). The uptake of control, pIC and LPS exosomes by distal cells was comparable (Figure 20 g-i). Therefore, the three groups of exosomes did not differ in biophysical and biochemical properties or cellular uptake.

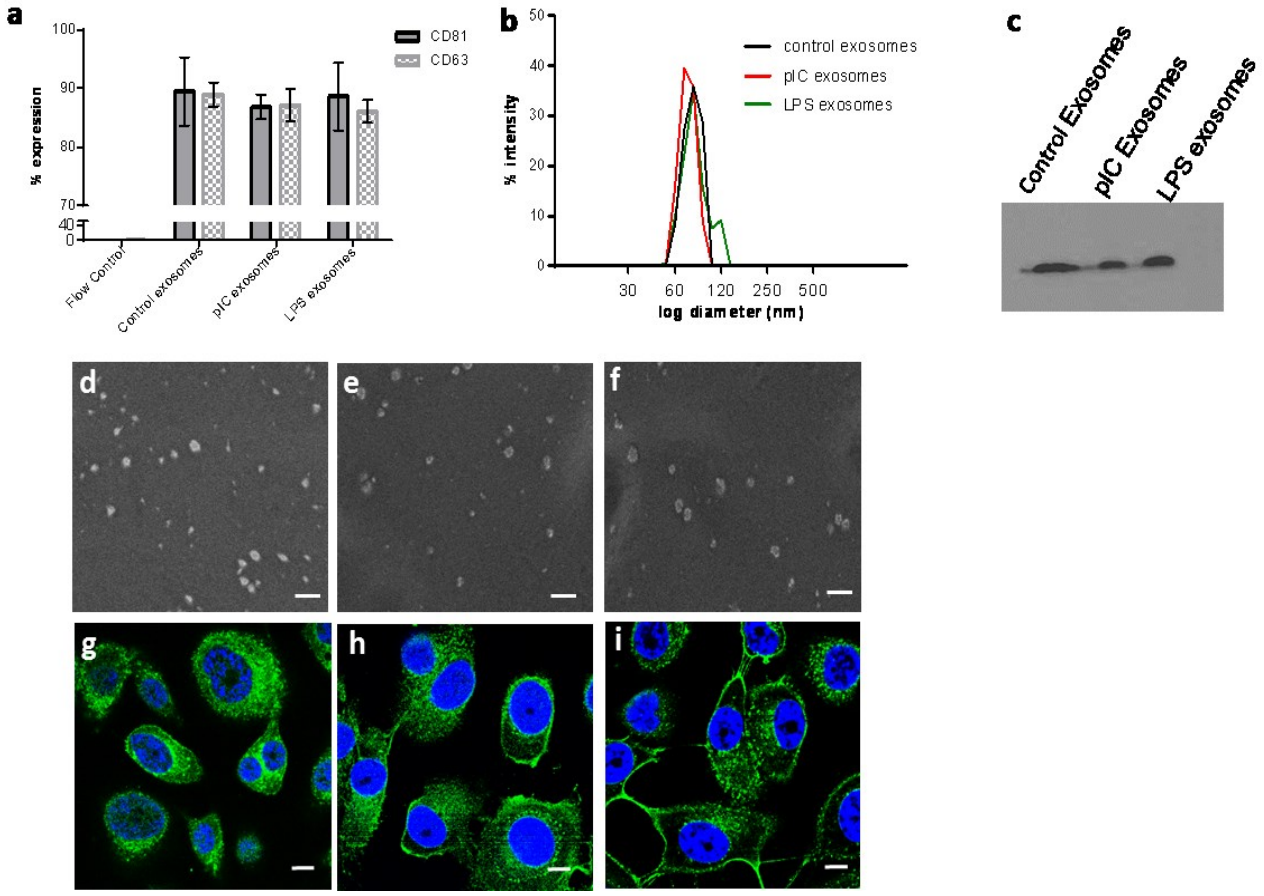

Figure 20: Characterization of exosomes used in the study. (a) Expression of CD81 and CD63 on the surface of Control, pIC and LPS exosomes as quantified by flow cytometry (b) Size distribution profiles of control, pIC and LPS exosomes quantified on a Zetasizer. (c) Western blot of CD81 protein expression on control, pIC and LPS exosomes (d) Scanning electron micrographs of (e) Control exosomes, (f) pIC exosomes and (g) LPS exosomes showing characteristic spherical. shape. Scale bar, 500nm. Confocal images of distal cells showing uptake of pkh67 labeled (h)Control exosomes, (i) pIC exosomes and (j) LPS exosomes. Scale bar, 10µm.

4.4.2 Effect of LPS on local and distal cells

Microarray data was analyzed for genes that were upregulated in both local and distal cells with respect to unstimulated cells. Differentially expressed genes that are involved in initiation of an inflammatory response were compared between local and distal cells. Both local and distal cells stimulated with LPS or LPS exosomes respectively showed an enhanced expression of inflammatory genes (Figure 21a). The classical response to LPS occurs via binding to membrane

bound *TLR4* which results in activation of an inflammatory response with the release of molecules such as TNFA, CCL3 and IL1B. The cell then enters a refractory where it is resistant to any further stimulation with LPS and is characterized by increased expression of *TOLLIP* accompanied by NF-κB inactivation(175) (Figure 21b).

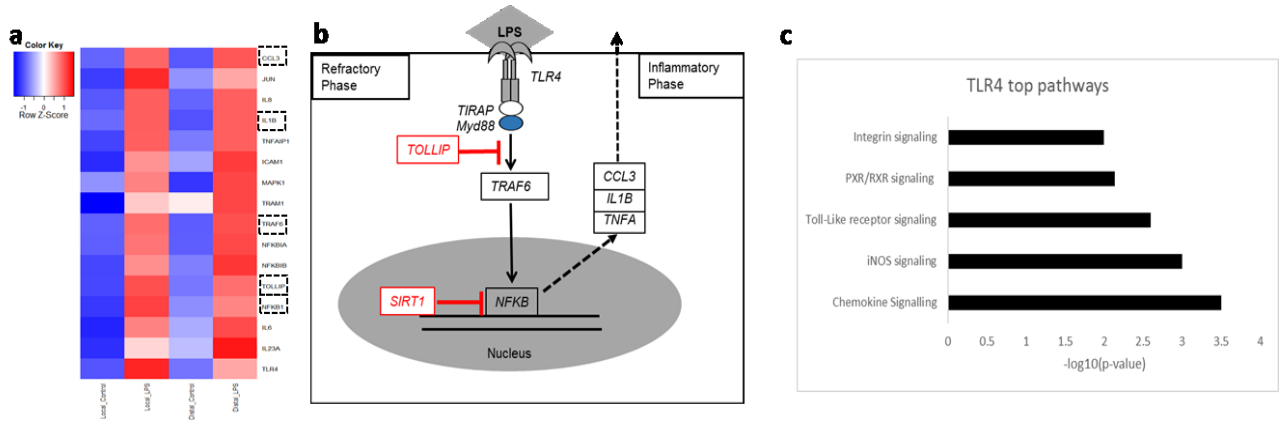

Figure 21: Microarray analysis to compare local and distal LPS response. (a) Heat map of gene expression profiles (b) LPS response pathway showing the key genes and inhibitors that establish the initial inflammatory phase and the subsequent refractory phase (c) Pathways enriched in distal cells stimulated with LPS exosomes.

We examined the pathways enriched in distal cells with LPS exosomes and saw an increase in chemokine signaling as well as TLR pathway activation (Figure 21c). To examine the temporal response of local and distal cells to LPS and LPS exosomes respectively, we evaluated changes in gene expression in local and distal LPS cells with respect to control cells using real-time PCR. We looked at *CCL3*, *TNFA, TIRAP, IL1B, TRAF6* and *TOLLIP* expression over 48 hours and observed that local cells responded strongly to LPS stimulation at 6 hours with *TOLLIP* expression peaking at 12 hours. Conversely, distal cells responded to LPS exosome stimulation strongly at 24 hours. Interestingly, both local and distal cell expression changes were comparable with a shift of ~18h in temporal expression (Figure 22a).

To determine the contribution of exosomal nucleic acid contents to the distal cells gene expression, we exposed exosomes to UV, and the RNA within exosomes was completely degraded upon exposure to UV. (Figure 38 a-c). This UV treatment did not completely abrogate protein expression or inhibit uptake by cells (Figure 39). Interestingly, distal gene expression after exposure to UV treated LPS exosomes was comparable to distal cells treated with control exosomes for all genes except *TNFA,* indicating that the nucleic acid contents of the exosomes were necessary and sufficient in transmitting the effector functions to distal cells (Figure 22b).

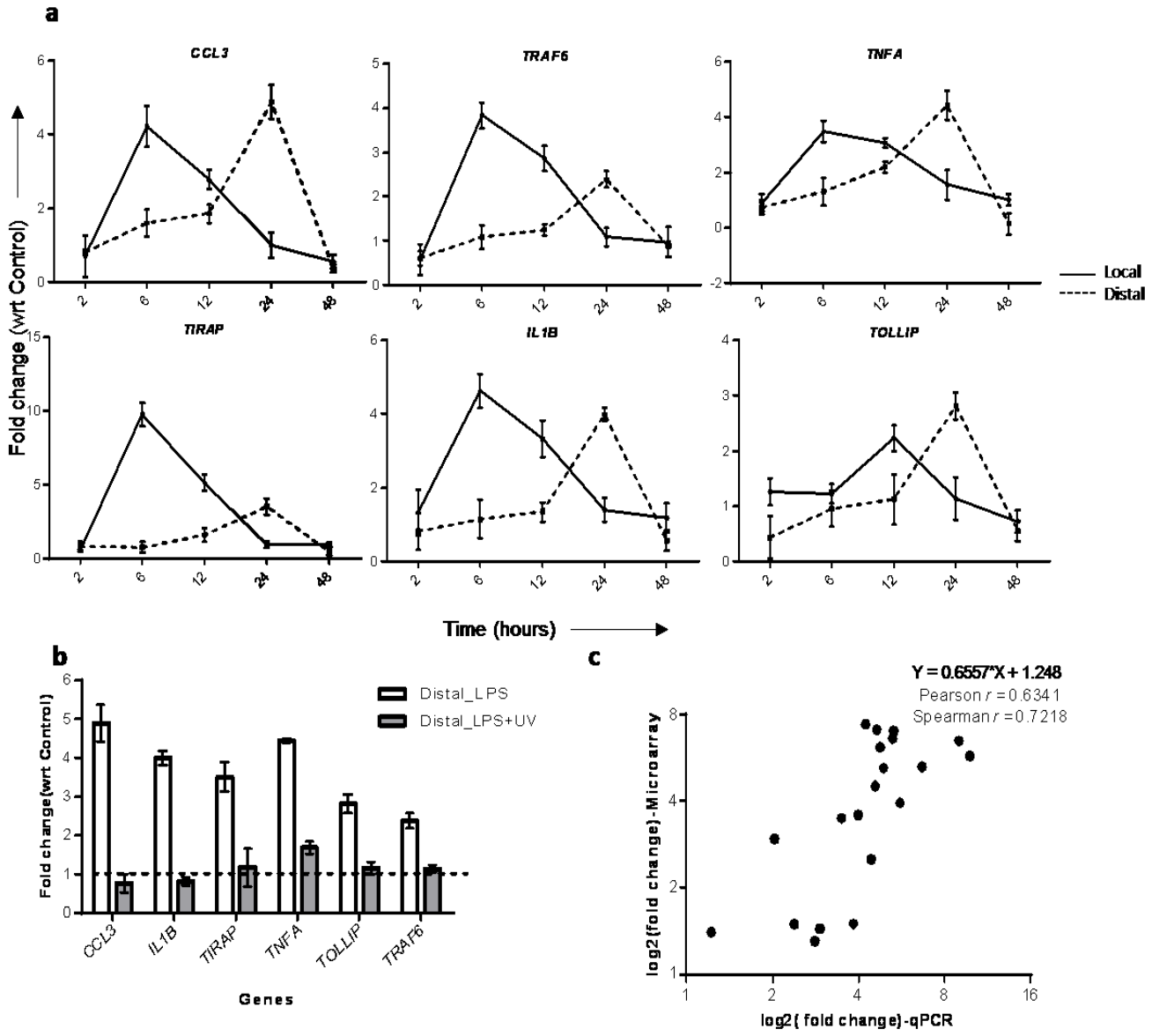

Figure 22: Temporal changes in gene expression in local and distal cells post LPS stimulation. a) Time course of gene expression comparing local cell response to poly I: C (solid lines) against distal cell response to poly I: C exosomes (dotted lines) for the genes shown. (b) Distal cell gene expression after exposure to either LPS exosomes or LPS exosomes after UV treatment (24 hours post exosome addition) (c) Scatter plots showing the correlation between the fold changes detected via qtr. when compared to microarrays

There was very limited carryover of LPS to distal cells (~4%) by exosomes (Figure 23 a-b). The effect of 4% LPS on local cells at various time points (6h, 12h and 24h) was fairly low (Figure

23c) and doesn't contribute significantly to the effect of LPS exosome stimulation on distal cells but might explain *TNFA* levels after addition of UV treated exosomes(Figure 23 d).

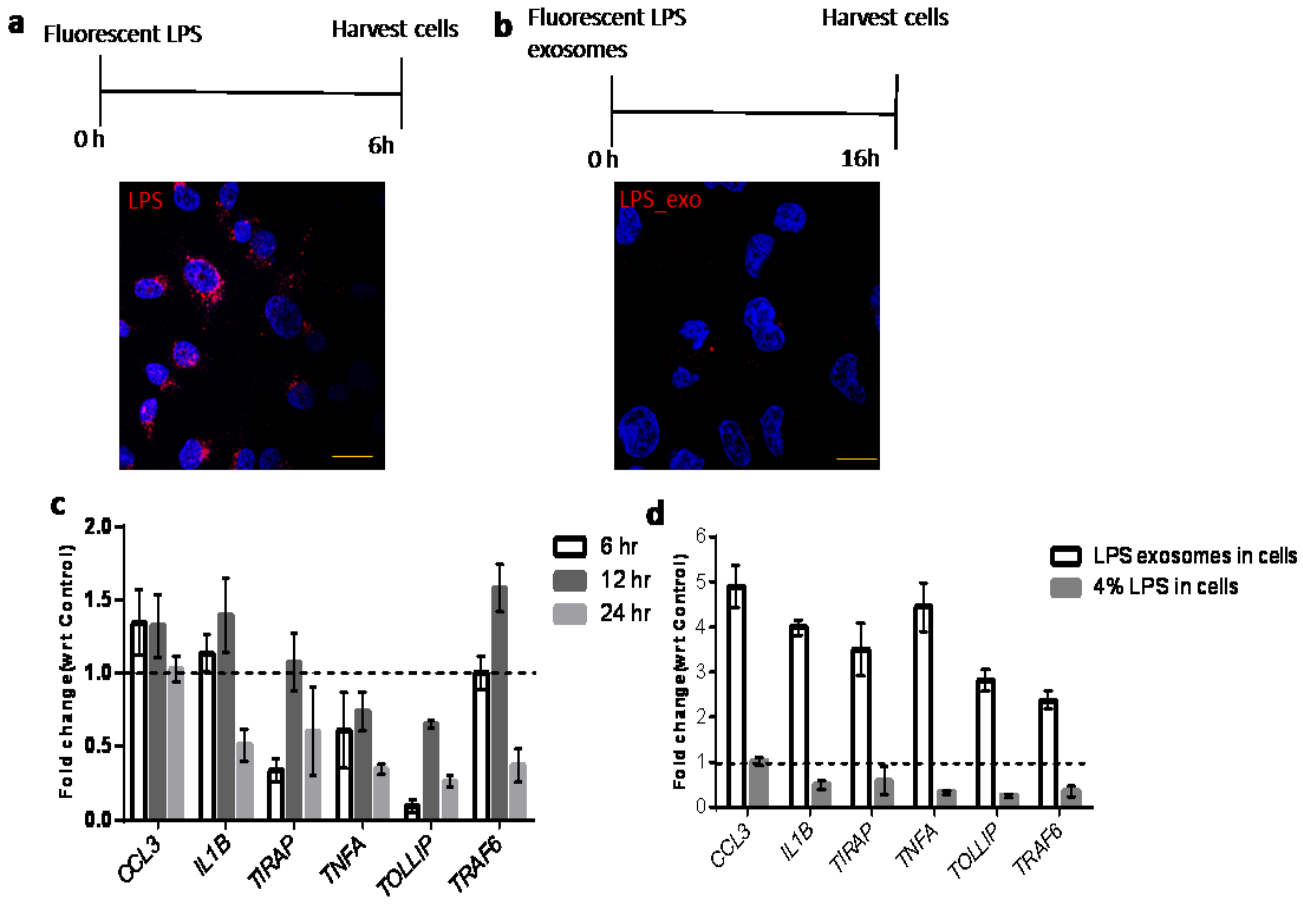

Figure 23: Estimating the carryover of LPS from local cells to distal cells by exosomes. Confocal images showing (a) LPS-AF594 uptake by local cells and (b) exosomes from local cells treated with LPS-AF594 added to distal cells to show 4% LPS carryover. Scale bars, 50 µm. (c) Time course of gene expression in local cells after stimulation with 4% LPS and (d) Comparison of gene expression at 24 hours between local cells stimulated with 4% LPS and distal cells stimulated with LPS exosomes.

A proximity ligation assay (PLA) was used to determine the co-localization of the p50 and p65 subunits of NF-κB to indicate activation. NF-κB activation in local and distal cells exposed to LPS or LPS exosomes respectively was assessed by PLA (Figure 40a). Distal cells treated with LPS exosomes showed co-localization of p50 and p65 subunits indicating that the NF-κB complex was active (Figure 24a).

Endotoxin tolerance is a protective mechanism to prevent overt inflammation in response to LPS and results in a transient unresponsive cellular state, characterized by the epigenetic inactivation of the p65 subunit of NF- κB by SIRT1, a histone deacetylase(176), Local and distal cell response to restimulation with LPS and resulting impact on NF-κB activation and silencing state was analyzed by PLA (Figure 40 b). Distal cells exposed to LPS exosomes when re-stimulated with LPS enter a refractory state similar to endotoxin tolerance accompanied by NF-κB inactivation and p65-SIRT1 co-localization (Figure 24b). Additionally, both NF-κB activation and *SIRT1* mediated inactivation was lost upon pre-incubation of exosomes in UV prior to addition to distal cells (Figure 24c).

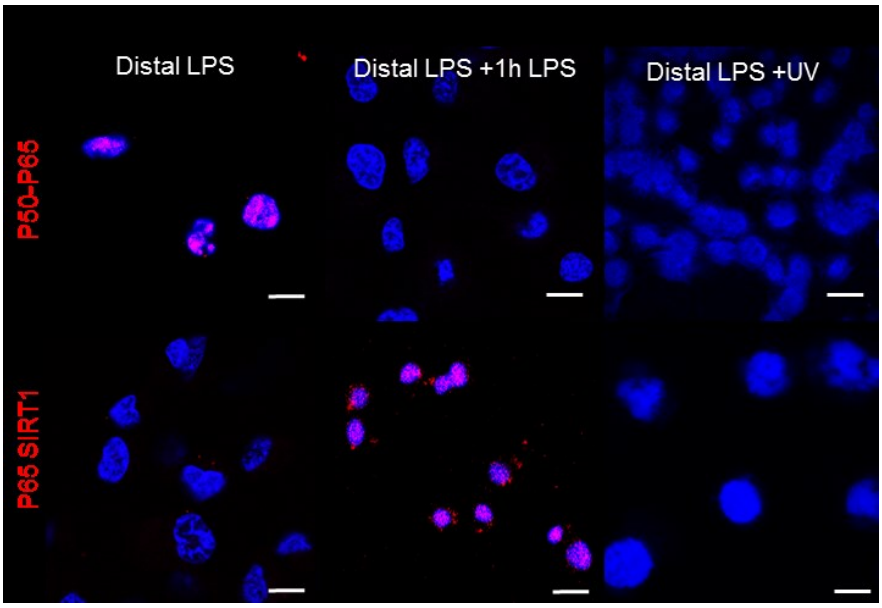

Figure 24: Activation state of NF-κB in local and distal cells with LPS, LPS exosomes or secondary stimulation. (a) NF-κβ activation state in distal cells with LPS exosome stimulation, (b) SIRT1 mediated inactivation of NF-κB after restimulating distal cells with LPS and (c) inactivation of NF-κB by pretreating LPS exosomes with UV by using a proximity ligation assay. Scale bar 20μm.

4.4.3 Effect of pIC on local and distal cells

Microarray data was analyzed for genes that were upregulated in both local and distal cells with respect to unstimulated cells and distal cells with control exosomes. Differentially expressed genes that are involved in antiviral activity were compared between local and distal cells (Figure 25a). The classical pIC response occurs via endosomally bound TLR3 which results in NF-κB and interferon activation. A cytoplasmic pathway of recognition utilizes *MDA5* and mitochondrial protein *MAVS* to activate interferon production(177)(Figure 25b).

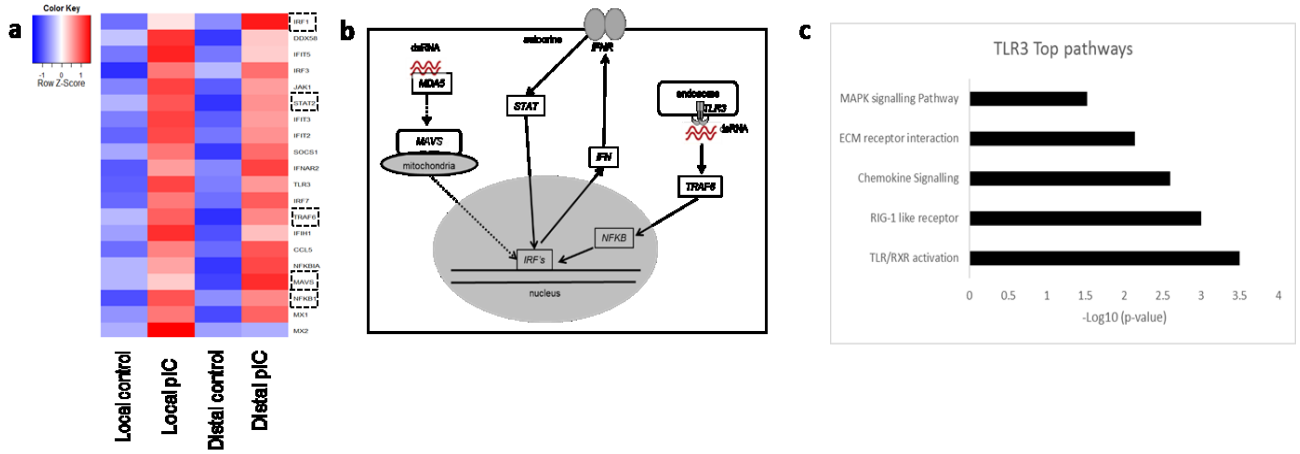

Figure 25: Microarray analysis to compare local and distal pIC response. (a) Heat map of top changed genes between local and distal cells. (b) Pathways of cellular response to pIC. (c) Pathways enriched in distal cells stimulated with pIC exosomes.

We examined the pathways enriched in distal cells with pIC exosomes and saw an increase in both the cytoplasmic RIG-1 like pathways as well as TLR pathway activation (Figure 25c). To examine the temporal response of local and distal cells to pIC and pIC exosomes respectively, we evaluated changes in gene expression in local and distal pIC cells with respect to control cells using quantitative PCR (Figure 26a). We looked at *IRF1*, *MAVS, IFN, STAT1* and *TRAF6* expression over 48 hours and observed that local cells responded strongly to pIC stimulation between 6-12 hours. Conversely, distal cells responded to pIC exosome stimulation strongly between 12-24

hours. Interestingly, both local and distal cell expression changes were comparable with a shift of ~12-18 h in temporal expression. Additionally, the correlation between local and distal cell gene expression as determined by microarrays and validation by PCR was high (Figure 22c).

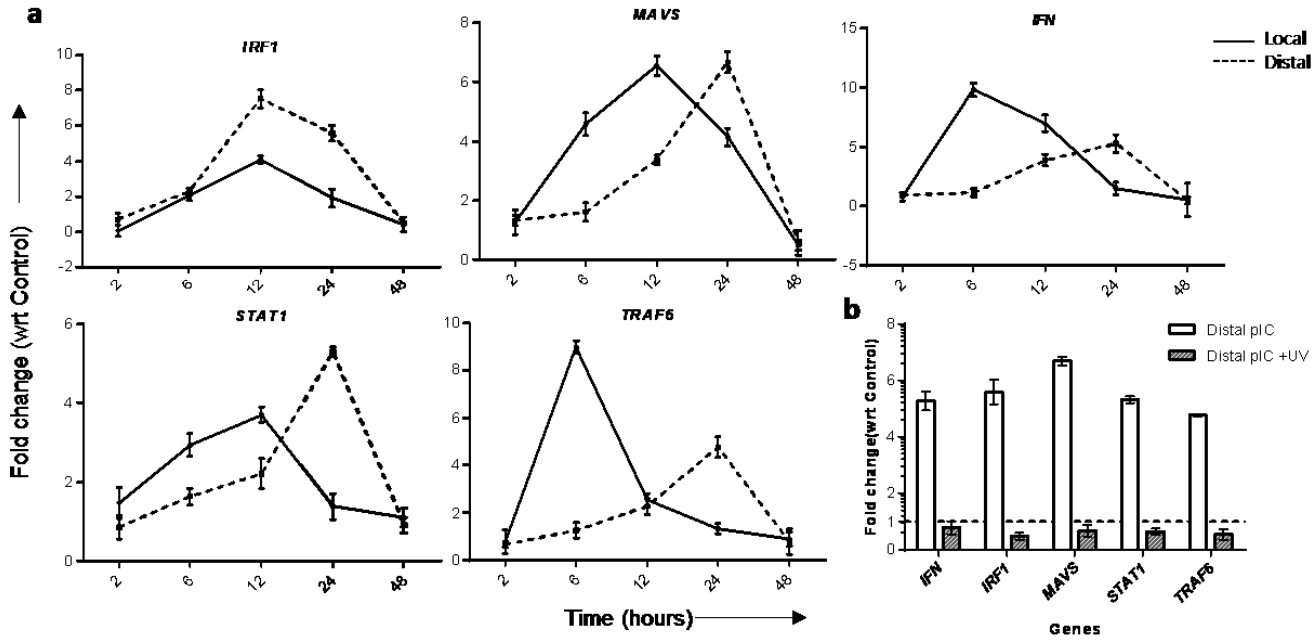

Figure 26: Temporal changes in gene expression in local and distal cells post pIC stimulation. (a) Time course of gene expression comparing local cell response to pIC (solid lines) against distal cell response to pIC exosomes (dotted lines) for the genes shown. (b) Distal cell gene expression after exposure to either pIC exosomes or pIC exosomes + UV treatment (24 hours post exosome addition)

Distal gene expression after exposure to UV treated pIC exosomes showed a complete abrogation of changes in gene expression indicating that the nucleic acid contents of the exosomes were crucial in transmitting the effector functions to distal cells (Figure 26). There was no carryover of pIC to distal cells by exosomes (Figure 27a-b).

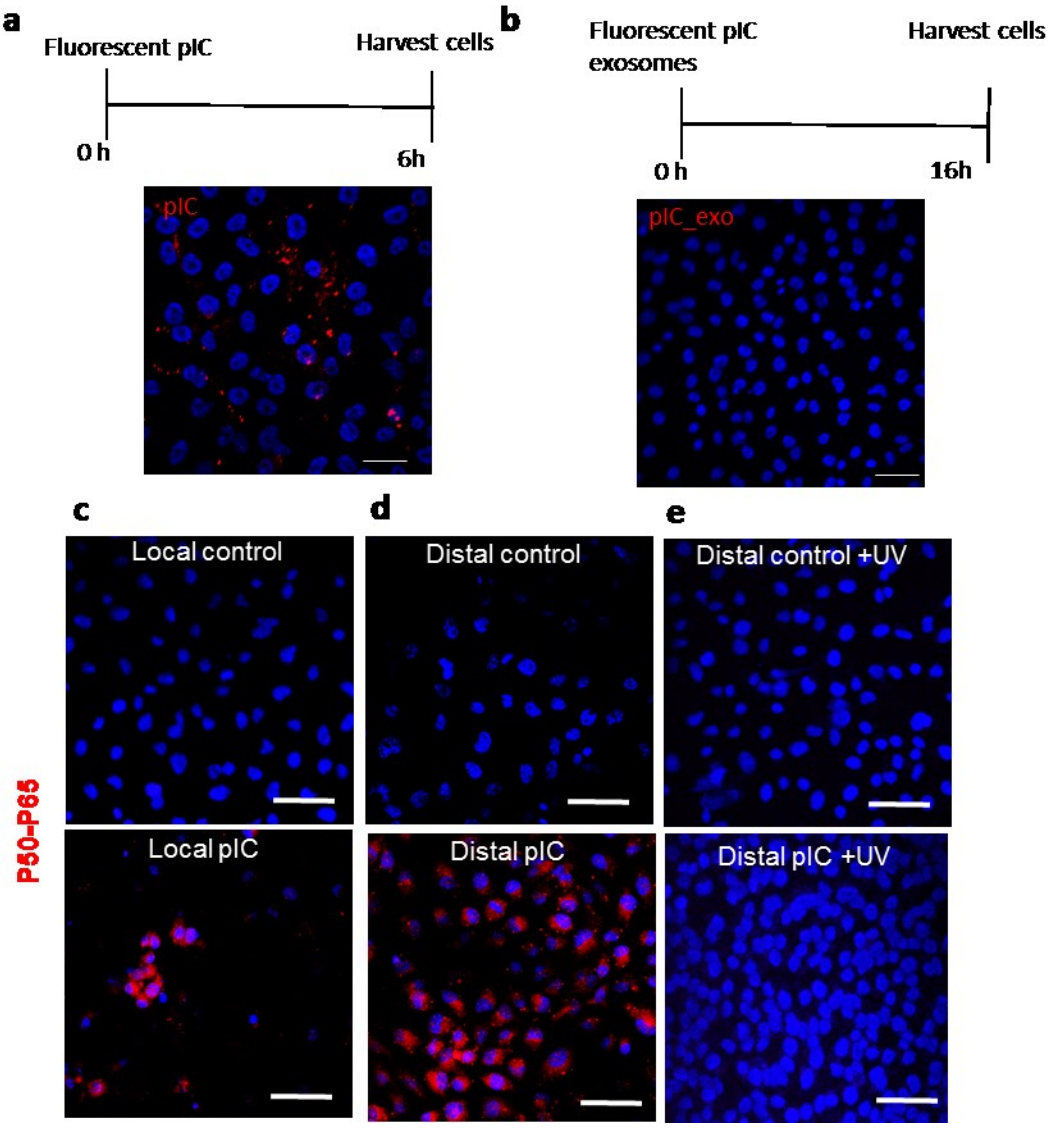

Figure 27: Activation state of NF-κB in local and distal cells with pIC or pIC exosomes. (a) Confirmation of pIC stimulation of local cells using fluorescent pIC, (b) estimation of pIC carryover by exosomes to distal cells. NF-κB activation in (c) local cells with pIC, (d) distal cells with pIC exosomes or (e) distal cells with UV treated pIC exosomes confirming the colocalization of P50-P65 subunits using a proximity ligation assay. Scale bars, 50 μm

The NF-κB activation state in local and distal cells was verified using a proximity ligation assay. Both local and distal cells exposed to pIC or pIC exosomes showed NF-κB activation (Figure 27 c, d respectively). Additionally, this activation was lost upon pre-incubation of UV treated exosomes prior to addition to distal cells (Figure 27e).

4.4.4 Effect of exosome uptake on macrophages

We verified the uptake of both control and pIC exosomes by macrophages (
Figure 28 a, b). To understand the impact of exosome uptake on macrophage function *in vivo, m*ice were injected with either PBS or control or pIC exosomes. The lymph nodes were extracted at 48 hours post injection; CD11b macrophages were pulled down analyzed by RNA-Seq. Whole lymph nodes were sectioned to verify protein expression in sections by immunohistochemistry (
Figure 28c).

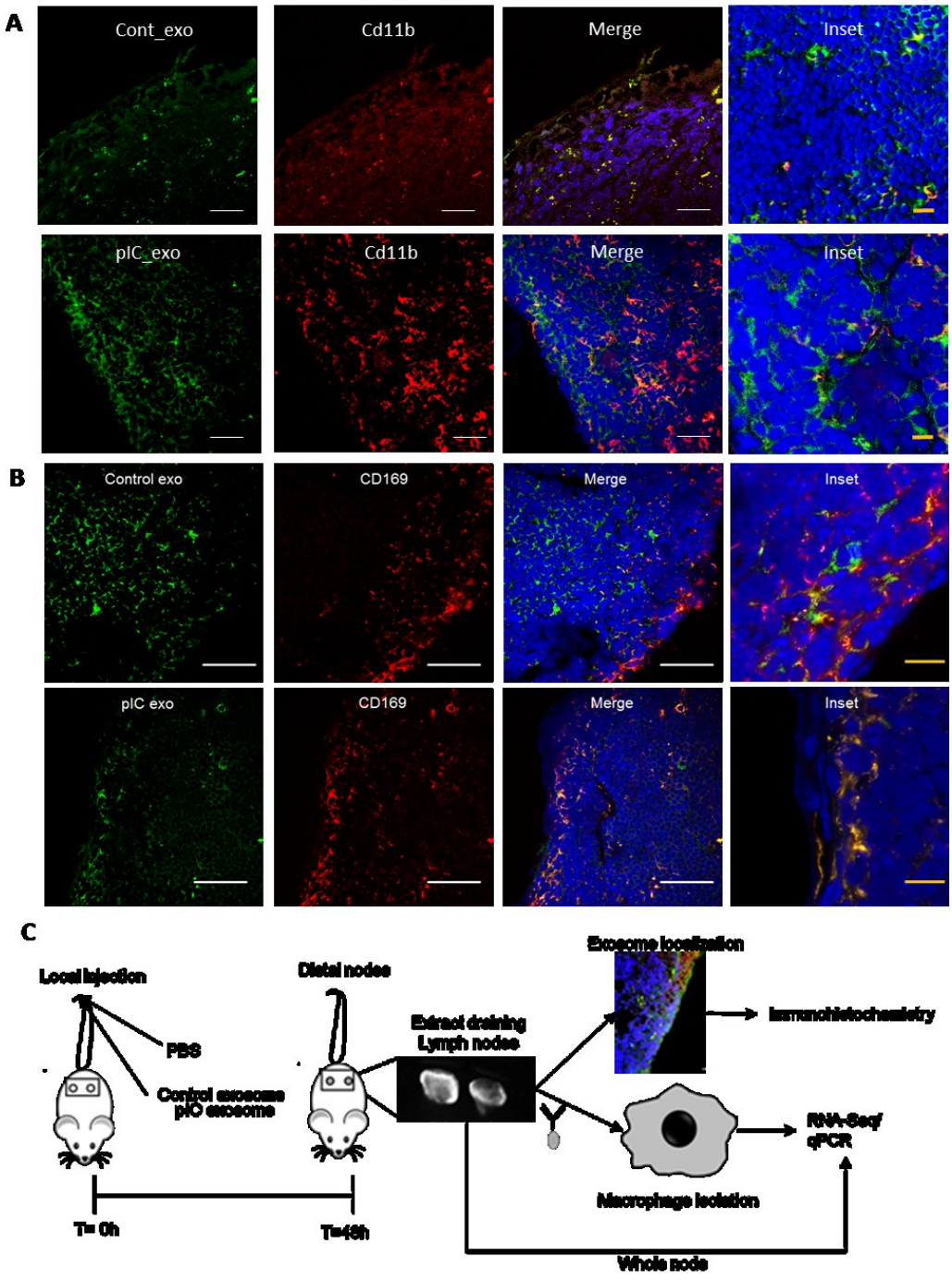

Figure 28: Macrophages retain both control and pIC exosomes. (a) CD11b+ macrophages and (b) CD169+ macrophages retain control and pIC exosomes. (c) Schematic showing mouse study

Figure 28 continued: with injection of either PBS or exosomes (control or pIC) locally followed by excision of distal draining lymph nodes, isolation of macrophages and analysis of gene expression by next generation sequencing.

The relative gene expression of macrophages with PBS, control and pIC exosomes is depicted for selected genes. Control exosomes show an intermediate phenotype with an increased expression of most M1 genes while pIC exosomes strongly polarize the macrophages to an 'M1 like' state with a significant shift in gene expression. The housekeeping gene expression is the same across the samples (Figure 29a). The pathways enriched in macrophages with pIC exosomes are all pro-inflammatory and show the activation of the TLR response *in vivo* (Figure 29b). A complete list of genes enriched in pIC exosomes with respect to PBS and control exosomes is provided (Table 5 and

Table 6).

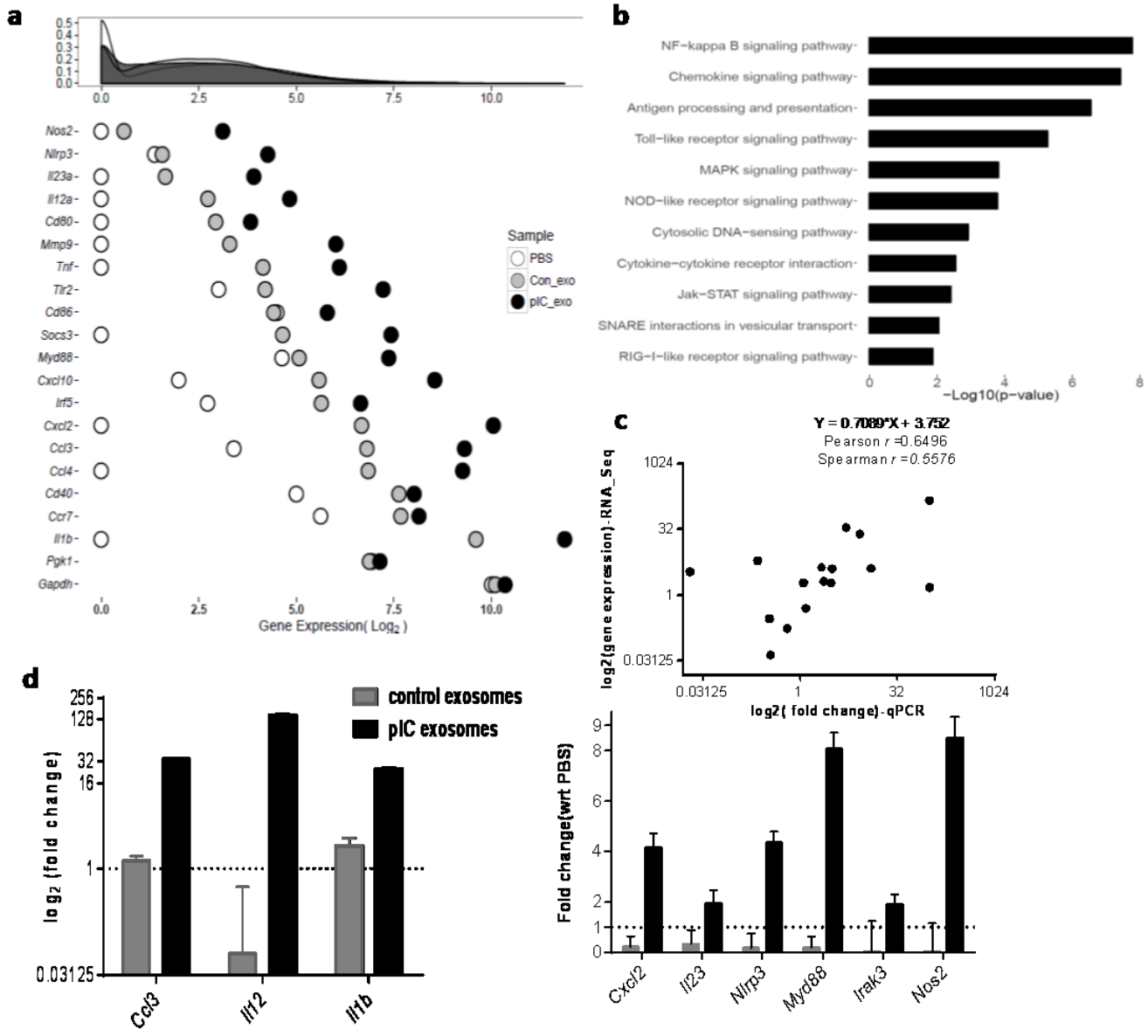

Figure 29: Impact of pIC and control exosome uptake by CD11b+ macrophages in mice at the RNA level. (a) Relative expression of key M1 and housekeeping genes in macrophages after exposure to PBS, control or pIC exosomes. (b) Pathways enriched in distal macrophages with pIC exosomes as compared to PBS. (c) Scatter plots showing the correlation between the fold change detected via qPCR when compared to RNA-Seq. (d)Validation of key M1 genes in macrophages with control or pIC exosomes as compared to PBS by qPCR.

The expression of M1 markers was validated in both control and pIC exosomes with respect to PBS macrophages by qPCR. pIC exosomes had a higher expression of all the selected M1 markers when compared to control exosomes (Figure 29d). The correlation between macrophage gene

expression with PBS, control or pIC exosomes determined by RNA-Seq and validation by quantitative PCR was high (Figure 29c). Whole lymph node sections with pIC exosomes showed high expression of Il12, Nos2, Cd86, and MhcII (Figure 31), while sections with control exosomes showed low to no expression of the same markers (Figure 32).

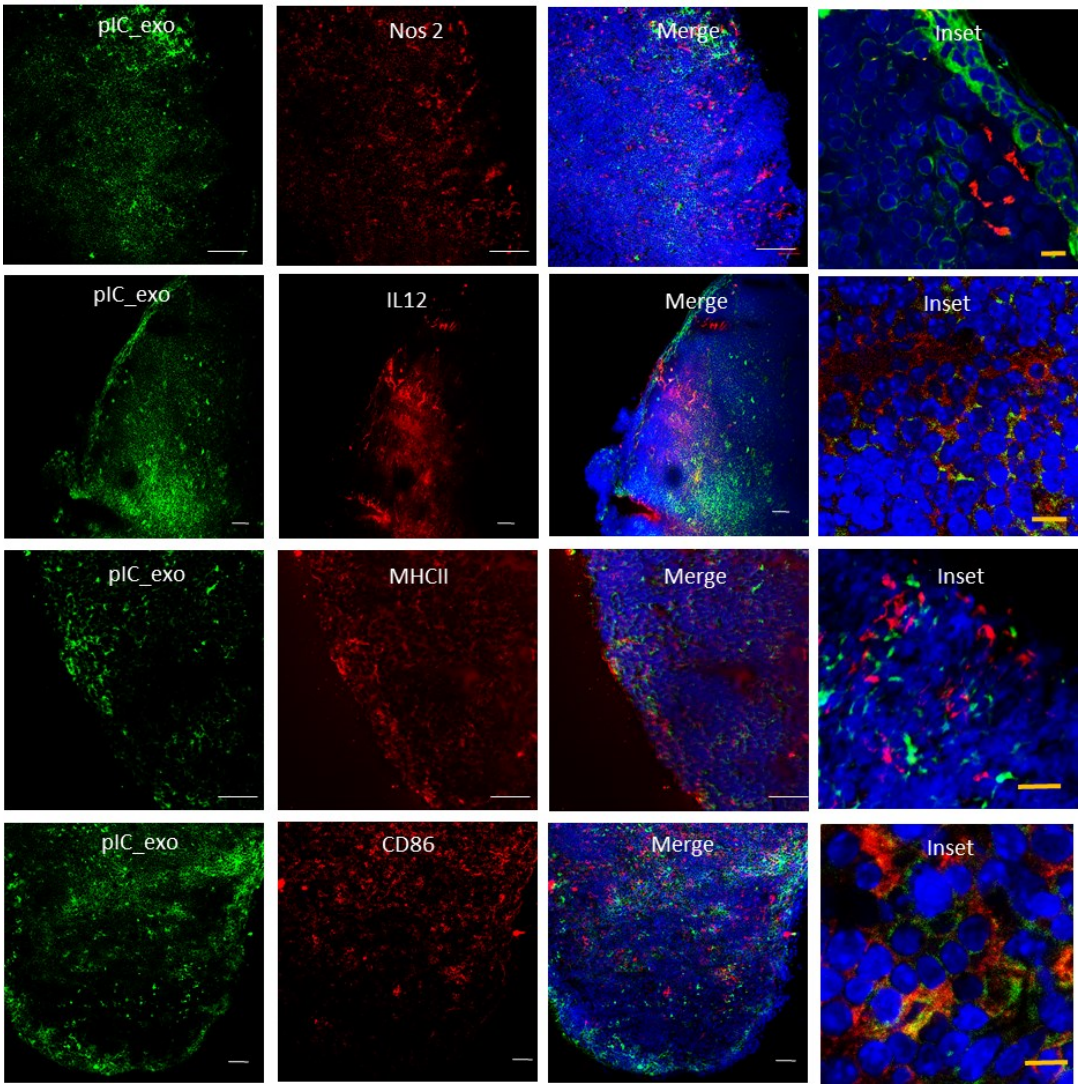

Figure 30: Validation of key M1 markers in whole lymph node sections with pIC exosomes. Immunohistochemistry of sections showing high expression of Nos2, Il12, Mhc-II and Cd86

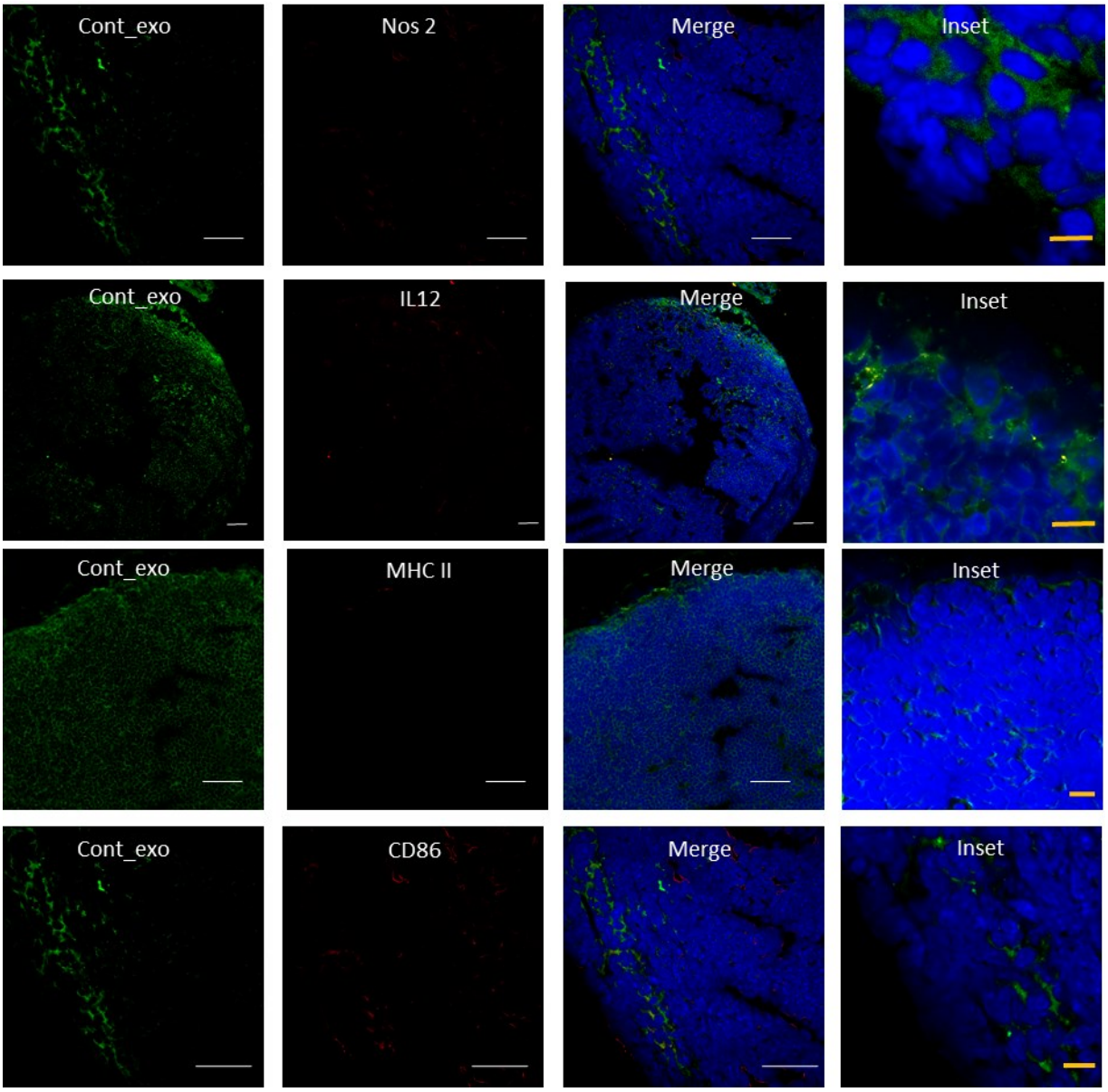

Figure 31: Validation of key M1 markers in whole lymph node sections with control exosomes. Immunohistochemistry of sections showing little to no expression of *Nos2, Il12, Mhc-II* and *Cd86*

4.4.5 Impact of lymphatic trafficking of exosomes on draining lymph node retention

To investigate differences in lymphatic transport of control and pIC exosomes, mice tails were imaged using the NIR system described previously(178). We observed that the kinetics of transport of pIC exosomes in both the dominant and non-dominant vessel was considerably higher than that of control exosomes in either lymphatic vessel (Figure 32 a-i). Similarly, pIC exosomes were

retained to a much higher extent in the draining lymph nodes as compared to control exosomes (Figure 33a-e). We showed that the transport times of the control and pIC exosomes were not significantly different in the vessels or lymph nodes (Figure 32j). The packet frequency of control and pIC exosomes at the collecting vessels and nodes are shown in (Figure 33g)

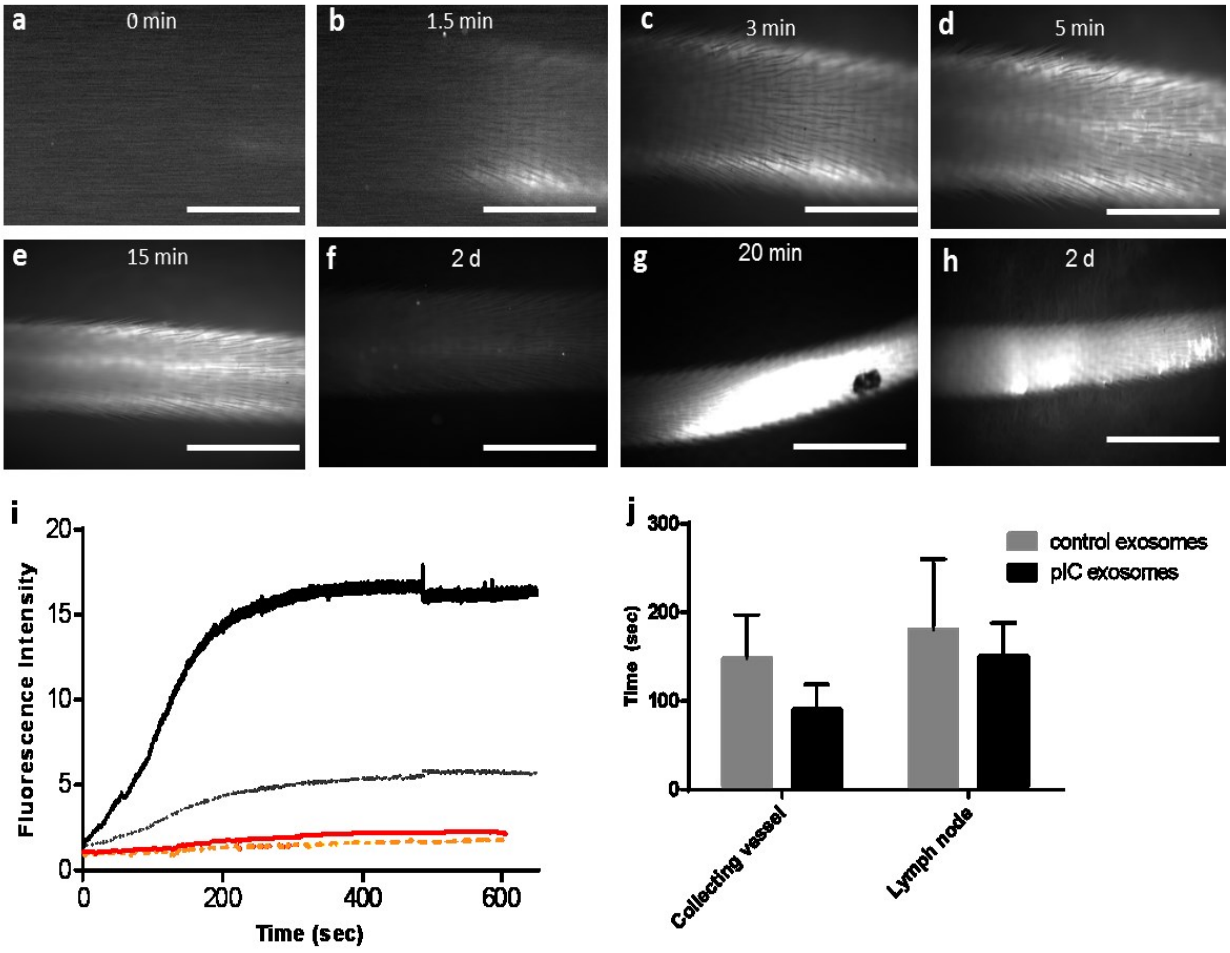

Figure 32: Lymphatic transport and retention of exosomes. pIC exosomes are seen in the lymphatic collecting vessels at (a) 0 mins, (b) 1.5 mins, (c) 3 mins, (d) 5mins , (e) 15 mins and (f) 2 days. The injection site is shown at (g) 20 mins and (h) 2 days.(i) Kinetics of lymphatic vessel transport showing control and pIC exosome trafficking in the dominant and non-dominant vessels (j) Arrival time of detectable levels of fluorescence for pIC and control exosomes in collecting lymphatic vessels and draining lymph nodes

The total packet transport is significantly higher for pIC exosomes than control exosomes (Figure 33f) Taken together, this data suggests that initial lymphatic uptake between the exosome

populations is similar, but that mechanisms involved in exosome capture and retention at the lymph node are significantly enhanced in exosomes released from pIC stimulated cells.

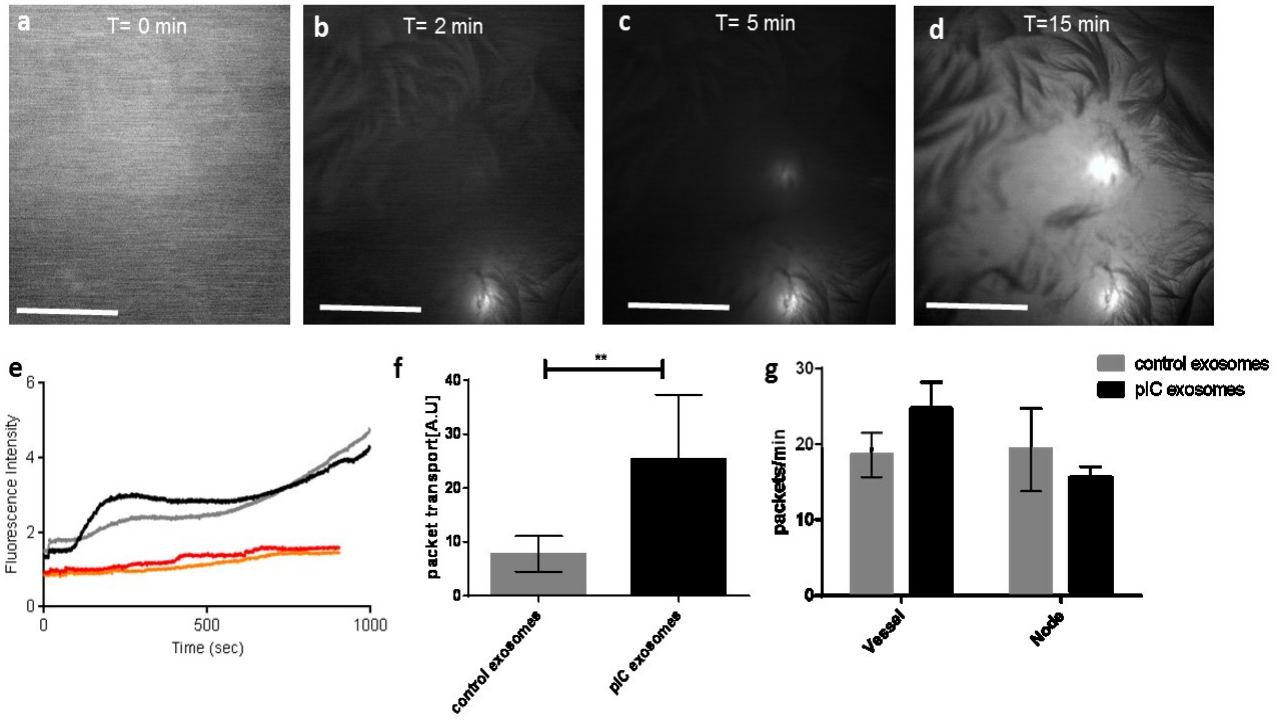

Figure 33: Lymphatic retention of exosomes. pIC exosomes are detected in the draining lymph node at (a) 0 mins, (b) 2mins, (c) 5 mins and (d) 15 mins. (e) Kinetics of draining lymph node retention of control and pIC exosomes in dominant and non-dominant nodes. (f) Lymphatic packet transport of control and pIC exosomes (g) Packet frequency of control and pIC exosomes in the collecting lymphatic vessels and nodes.

To understand the impact of exosome retention on the lymph node *in vivo,* the lymph nodes were extracted at 48 hours post exosome injection and analyzed by RNA-Seq (Figure 34a). We extracted the gene expression of the 546 genes utilized to estimate the abundance of 22 immune subsets based on the CIBERSORT algorithm, extending the algorithm to utilize our RNA-Seq data[24]. Using this analysis we found evidence of neutrophil, mast cell and monocyte recruitment in the pIC-exosomes group as compared to the PBS and control-exosome groups (Figure 41). The relative gene expression of whole nodes with PBS, control and pIC exosomes for selected neutrophil markers shows that control and pIC exosomes increase neutrophil recruitment and activation markers with pIC exosomes having a stronger effect (Figure 34b). The pathways

enriched in whole nodes with pIC exosomes with respect to PBS is shown in Figure 34c. A complete list of genes enriched in whole nodes with pIC exosomes with respect to control exosomes in given in Table 7. The expression of pro-inflammatory genes and neutrophil recruitment markers were validated in whole node with control or pIC exosomes with respect to PBS nodes by qPCR. pIC exosomes had a higher expression of all the selected genes when compared to control (Figure 34d)

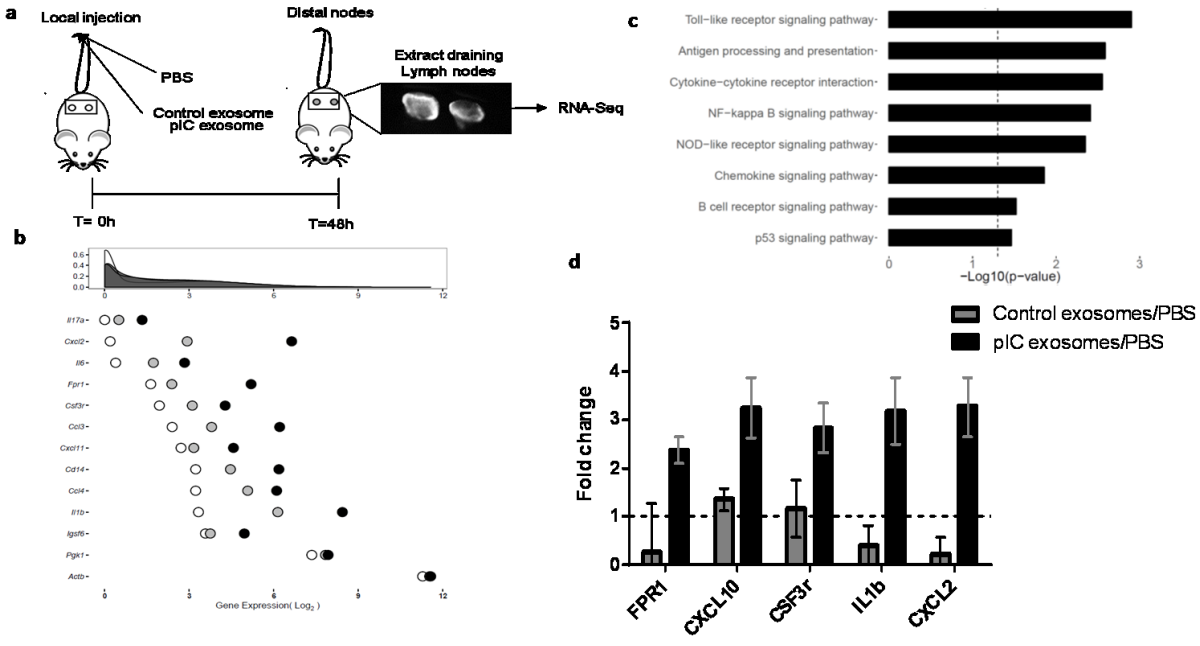

Figure 34: Impact of exosomes retention on whole lymph nodes. (a) Schematic of experiment showing PBS, control or pIC exosomes in mouse tail, followed by lymph node extraction at 48 hours and RNA-Seq. (b) Relative expression of key neutrophil markers in whole lymph nodes after exposure to PBS, control or pIC exosomes and (c) Pathway analysis showing pathways enriched in pIC exosomes in whole nodes with respect to PBS. d) Validation of expression level key transcripts identified in RNA-Seq by qRT-PCR.

Neutrophil recruitment to the node was also verified by imaging markers GR1 and Ly6g in the whole nodes. pIC exosomes induced a stronger presence of neutrophils in the whole node as compared to control exosomes (Figure 35)

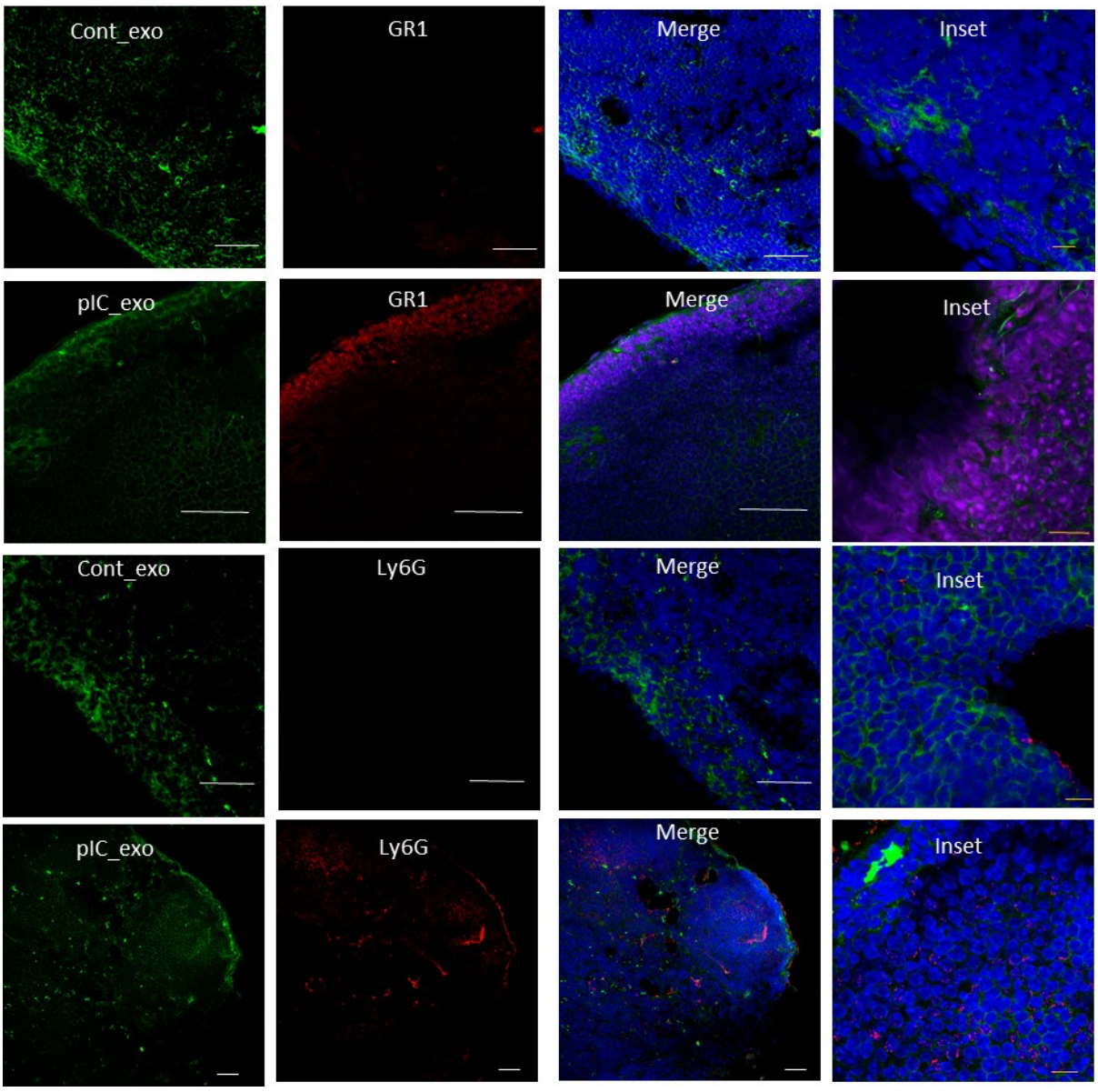

Figure 35: Validation of key neutrophil recruitment markers in whole lymph node sections with control and pIC exosomes. Immunohistochemistry of sections showing little to no expression of *GR1* and *Ly6G* in control sections but high expression in pIC sections.

Finally, our model for exosome mediated cell-cell communication in the dissemination of the TLR response is shown. We have shown that both LPS and pIC exosomes elicit a pro-inflammatory or antiviral gene response *in vitro* that is characterized by the activation and localization of NF-κB in the nucleus. Furthermore, exosomes are taken up by macrophages and polarized to a 'M1-like'

pro-inflammatory state characterized by the increased expression of *Il12* and *Nos2* while the node is reprogrammed to recruit neutrophils and shows increased inflammation (Figure 36).

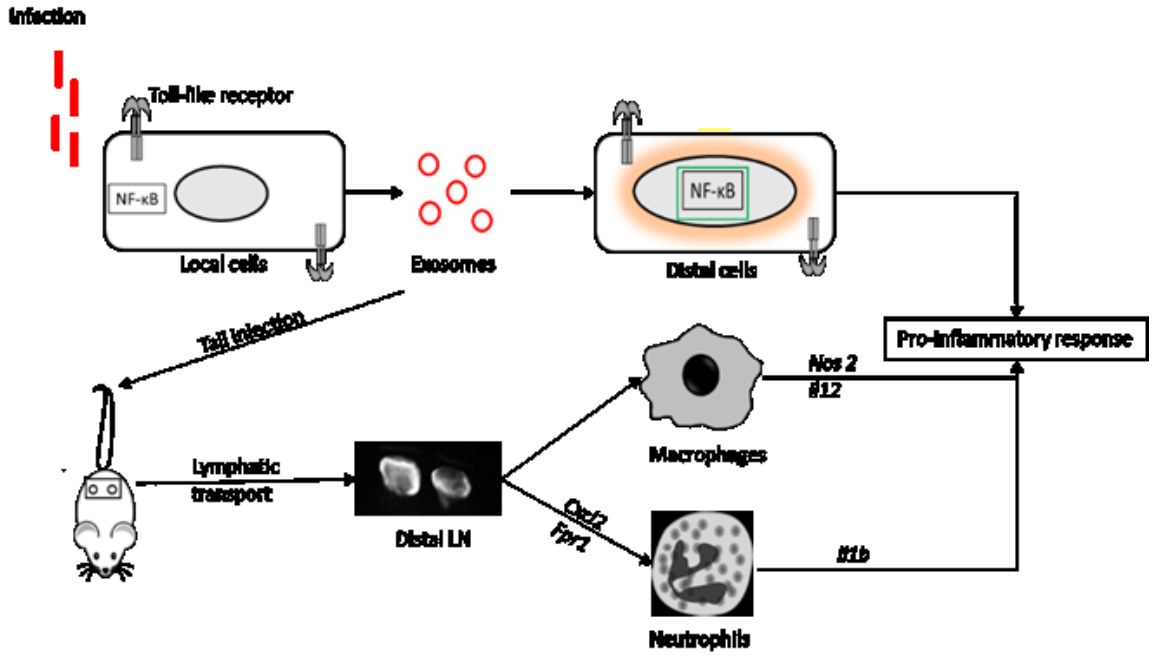

Figure 36: Model of exosome action showing transmittance of local cell TLR activation to distal cells resulting in a pro-inflammatory response both *in vitro* and *in vivo*

4.5 Discussion

The ability of the immune system to recognize and respond to foreign organisms is essential to survival and TLR's play a central role in this response(179). While the local response of cells directly exposed to pathogens via Toll-like receptor activation is well characterized(15, 135, 180), the transmission of this response to distal cells is understudied.

Exosomes have many distinct roles that vary depending on their cell of origin, from modulating the immune response(181), to cancer progression and immune evasion(182). Here, for the first time we can compare the responses at distal target cells to the local cell response in the context of TLR response and understand the transmittance of information from the cell of origin. Our findings

show that distal cells are primed to respond to imminent pathogen attack via TLR mediated NF-κB activation and the resulting secretion of pro-inflammatory cytokines.

Our experiments demonstrate reproducible perturbations of distal cells without little to no agonist carryover demonstrating the importance of immune state of the cell of origin. pIC exosomes induced the activation of both the cytoplasmic and endosomal RNA recognition pathways to produce an antiviral response while LPS exosomes show activation of the *TLR4* response resulting in an inflammatory response in distal cells. We observed that no pIC and very low quantities of LPS (<5%) were carried in exosomes, indicating that the distal response was not due to agonist carryover. Nevertheless, the expression of *TIRAP* in distal LPS cells and *TRAF6* and *MAVS* in distal pIC cells indicates that most, if not all, of the components downstream of TLR activation are being activated.

We delineated the temporal kinetics of exosome impact on distal cell phenotype to discover ~12-18 hours shift in distal cell response which we believe is required for sufficient exosome uptake, unpacking and release of contained biomolecules for the response in distal cells, similar to luciferase mRNA delivery by glioblastoma derived vesicles(122). Both exosomal RNA contents and the distal cell response are completely abrogated by UV treatment (Supp fig 3) and we believe that the RNA is the key contributor to the effects observed.

We also show an epigenetic reprogramming of distal cells to be resistant to any subsequent LPS stimulation, a well characterized outcome of endotoxin tolerance(183); absence of the ability to enter endotoxin tolerance would lead to an uncontrolled cytokine storm and inflammation(184). While the TLR response and endotoxin tolerance is well characterized in immune cells, it is less understood in non-immune cells(185). This is the first study to demonstrate that exosomes from non-immune cells prime distal cells for both epigenetic change and for increased defense against

pathogens without the distal cells ever being exposed to the antigens responsible for the change. Further studies are needed to understand the contribution of exosomes from non-immune cells to the innate and adaptive immune response.

Human selection at the *TLR1* locus on *4p14* has been reported, with a functional non-synonymous variant in the transmembrane domain associated with susceptibility to *Mycobacterium leprae* infection(186). A nonsynonymous mutation in *TLR5* led to altered NF-κB signaling in response to stimulation with bacterial flagellin(187). Additionally, families with fully penetrant mutations within key TLR genes are susceptible to a wide variety of pathogens(188), demonstrating the global importance of TLR signaling in immunity.

SCS macrophages were shown to play roles in suppressing the spread of melanoma thus enhancing immunity(189). We have previously shown that SCS macrophages played an important role in exosomes retention(178) which we expand to demonstrate that ovarian cancer-derived exosomes are capable of inducing an inflammatory response via *Il12 and Nos2* in macrophages *in vivo*. *Nos2* results in nitric oxide (NO) production by macrophages aids in cytotoxic activity against viruses and bacteria(190), reduced lymphatic contractions(46) and inhibits ovarian cancer growth(191). Future work will elucidate the impact of macrophage uptake pIC exosomes and the subsequent immune response.

The biological importance of exosomes in the cancer – immune cell crosstalk is a growing area of research. Ovarian cancer is associated with one of the highest mortalities(192) and survival statistics have not improved significantly over the past three decades(193), highlighting the need for better understanding the tumor microenvironment. Inflammation in the tumor microenvironment results in cancer survival, proliferation and migration(194) and increases lymphatic permeability(48). Given that TLR activation of immune cells negatively impacts tumor

outomes(195-197), and actively contributes to inflammation, tumor derived exosomes play a vital role in cancer fate. Administration of poly I:C in mouse models of melanoma, lung cancer and colon cancer elicited robust anti-tumor immune responses*(198)*. Future work in understanding both the mechanism of anti-tumor response by pIC and the role of exosomes in this process will provide key insights in the use of TLR agonists for cancer immunotherapy.

We expand upon the impact of lymphatic transport and macrophage mediated retention of exosomes(178) to demonstrate that ovarian cancer-derived exosomes are capable of inducing an inflammatory response in macrophages *in vivo*. Interestingly, pIC exosomes had a much stronger impact on the macrophage response resulting in their polarization to a 'M1-like' state, as characterized by production of *Il1b*, *Il12*, *Nos2* and *Cxcl2*(199). *Nos2* results in nitric oxide (NO) production by macrophages and helps in cytotoxic activity against viruses and bacteria(190) and also results in reduced lymphatic contractions(46).

Conversely, trafficking of pIC exosomes by the lymphatic system was enhanced within the first 20 mins post intradermal exosome injection. The ability of pIC exosomes to rapidly modulate lymphatic function to increase transport and nodal retention coupled with NO secretion 48 hours later makes the kinetics of pIC exosome movement in the lymphatics very interesting. Given the reliance of exosomes and immune cell trafficking on lymphatic transport, the impact of NO secretion by macrophages on the subsequent immune response should be studied.

The pathways enriched in macrophages with pIC exosomes are all indicative of a TLR response resulting in the production of a pro-inflammatory state demonstrating the ability of exosomes to functionally transmit the TLR activation state of the cell of origin *in vivo*. Future studies wherein the injection of control or pIC exosomes is followed with a microbial challenge will help us elucidate the contribution of exosomes in establishing an immune response *in vivo.*

We saw an enrichment of neutrophil recruitment signals including FPR1 and CXCR2(200) in the whole node accompanied with an increase in pro-inflammatory cytokines, such as IL1B. Neutrophils release cytokines and chemokines to coordinate the innate and adaptive immune responses and play active roles in antigen presentation(201). Thus, the lymph node microenvironment is being reprogrammed by exosomes to respond to the signals sent by the parent cells

The ability of exosomes to carry siRNA, drugs, proteins and other molecules makes them ideal therapeutic vehicles(202). This is the first study to show that UV irradiation 'resets' the exosomes effect on distal cells, and this approach can be used to neutralize exosomal cargo prior to loading of the therapeutic molecules. Furthermore, our *in vitro* model may be appropriate to verify the intended effects of exosomes prior to therapeutic use and eliminate any TLR agonist response thereby overcoming technical challenges to maximize the clinical potential to provide viable therapeutic options.

This study demonstrates that exosomes play a key role in informing the immune system of the presence of foreign organisms initiating a pro-inflammatory response both *in vitro* and *in vivo.* Furthermore, based on the differences in distal cell response with LPS and pIC exosomes, we show that the function and contents of exosomes vary with the biological state of the cell of origin and the result in reprogramming the target (distal) cells to elicit an inflammatory response.

4.6 Conclusions

We demonstrate that exosomes from cells stimulated with TLR ligands locally are able to transmit an antiviral and inflammatory response in distal cells which is specific to the biological state of the cell of origin *in vitro*. We were also able to reset the distal response by UV irradiating the exosomes prior to distal cell exposure. Additionally, we showed that exosomes from pIC

stimulated cells polarize distal macrophages in the draining lymph node towards a pro-inflammatory "M1-like" phenotype accompanied by saw enhanced lymphatic transport and retention of pIC exosomes which was hitherto unknown. Furthermore, we characterize the lymph node milieu by showing a pro-inflammatory remodeling and neutrophil recruitment at the node. This study helps dissect the role of exosomes in cell-cell communication and expand upon current knowledge of their role in modulating the gene expression profile of distal cells in the context of Toll-like receptor biology.

CHAPTER 5: CONCLUSIONS AND FUTURE DIRECTIONS

In this thesis, I have established a role for exosomes as rapid and complex messenger that aid and modulate the innate immune system. Specifically, I have demonstrated the ability of exosomes to use the lymphatic system to rapidly travel from the periphery with information related to biological state of the cell of origin and transport it to the draining lymph node, a hub for information processing and immune response initiation. Using the tools developed in the Dixon lab for quantifying lymphatic transport, I have definitively shown, for the first time that lymphatics play a crucial role in the transport of exosomes both *in vitro* and *in vivo*. Further drawing on the expertise of the Vannberg lab in the genomics of infectious diseases, I have shown that the TLR activation state of the cell of origin is largely recapitulated by exosomes in distal cells both *in vitro* and *in vivo.*

I have detailed my main findings and future work that will help further the paradigm of exosome mediated activation of innate immunity below:

a) I have developed a transwell model to show that lymphatic endothelial cells actively and selectively transport exosomes *in vitro* by transcytosis. This *in vitro* model can be further used to test compounds for their efficacy in either increasing or suppressing cellular transport of exosomes which can help uncover the mechanisms underlying exosome uptake and secretion.
b) I have successfully labeled exosomes with two labels: a near infrared fluorophore conjugated to the N-terminal of exosomal membrane proteins and a second fluorophore was in the lipid bilayer of the exosomes to enable ex-vivo, multi scale analysis of cellular exosome uptake and transport. This can be further expanded in the future by using NIR fluorophores with different spectra and imaging exosomes from different sources simultaneously. While I have data to show that pIC exosomes are transported and retained in the lymphatics to a higher extent than control exosomes, this will enable parallel tracking of control and pIC exosomes to understand the transport kinetics further.

c) While the differential transport of exosomes by collecting vessels has been previously demonstrated, the surprising finding of differential exosome retention in the lymph nodes was novel. Future studies need to be conducted to see if these differences in co-localization could impact the immune response at each of these nodes in the presence of antigen which could reveal important information about the development of an innate immune response at the lymph node.

d) I determined the primary immune subsets within the lymph nodes that were responsible for exosomes uptake and retention. Cd11b+ macrophages were a stable target for exosomes within the lymph node and were found to contain exosomes at very early time points (2 hours) as well as 2 days. I also showed that B-cells were found to contain exosomes at 2 days but not 2 hours, implying that the macrophages played a role in exosome processing and transfer to B-cells. Future work using confocal and multiphoton microscopy will be useful to understand the intraorgan capture and kinetics of exosome transfer within the node.

e) Since innate immunity is fast acting, the time points in my in vitro and in vivo work have been limited to 2 days and has been focused at the uptake and retention of exosomes at the cellular level. The functional consequences of exosomes are as a result of the complex biomolecular cargo contained within them, future work on the release of exosomal RNA and protein within the target cells both in vitro and in vivo will help elucidate the principal mechanisms of innate immune modulation by exosomes that result in pro-inflammatory responses in the target cell.

f) I have used confocal microscopy to demonstrate uptake of extraneously labeled exosomes by cells in vitro. Future work using genetically marked exosomes (such as CD63-RFP) will enable us to monitor in real time the kinetics of exosome uptake and release by cells.

g) I have shown the ability of exosomes from TLR stimulated cells to largely recapitulate the TLR activation state in the cell of origin. While many studies have demonstrated that exosomes are capable of modifying the phenotype of the distal cells, the phenotype of the cell of origin has never been compared to the exosome induced phenotype distally. This unique study design enables us to compare and contrast the ability to exosomes to activate the various facets of

TLR activation and response in distal cells in the context of local cells. Future work can be done on further characterizing other TLR agonists to verify that the dissemination of the TLR response is not limited to some TLR's.

h) This study points to a crucial role for exosomal RNA in the dissemination of the TLR response as UV irradiation of exosomes prior to distal cells results in complete abrogation of the distal cell response. While other studies in the field have used UV light to abrogate exosome effects, such extensive characterization enables us to depict the importance of exosomal cargo in its functionality. Future studies in understanding the uptake and impact of UV treated exosomes will further delineate the role of exosomal RNA. Comparing the in vivo trafficking of UV exosomes in the lymphatic rodent tail model with control and pIC exosomes will allow us to further dissect the difference in lymphatic transport and retention of exosomes. Additionally, the contribution of exosomal proteins to the distal response can be studied using proteomics which may explain the differences in expression of exosomal surface proteins that might contribute to differential exosome trafficking.

i) The kinetics of exosome mediated changes in distal cell gene expression has been clearly characterized with respect to local cell response and helps understand the temporal kinetics involved in exosome uptake, cargo release and transcriptional modulation. This will be useful to design future studies using exosomes to deliver therapeutic RNA molecules.

j) This is the first study to show that exosomes can prime distal target cells for epigenetic modification. Further work with SIRT1 knock out cells can help define the contribution of other epigenetic players in the TLR activation by exosomes. Since we used a cancer cell model for the demonstration of exosome effector function, comparing the methylation status of the target cells before and after exosome exposure would reveal the impact of tumor derived exosomes in distal cell remodeling.

k) The data shown here is the first evidence that exosomes could directly be involved in modulating flow to the lymph node. This is a significant finding since enhanced lymphatic function also leads to enhanced uptake of the exosomes within the cells of the draining lymph

node. Given the reliance of exosomes and immune cell trafficking on lymphatic transport, the impact of exosome-mediated flow modulation, either through NO secretion by macrophages or some other unidentified mechanism, on the subsequent immune response warrants further study. Furthermore, the total lymphatic pump flow is significantly higher for pIC-exosomes than control exosomes implying the ability of pIC exosomes enhance lymphatic flow. Future work with isolated collecting vessels can help quantify the modulation of lymphatic flow by exosomes.

l) The expression of Nos2 by macrophages with pIC exosomes is very interesting since NO signaling results in the reduction of lymphatic trafficking. Future work where the injection of PIC exosomes is followed by the injection of a NIR tracer will help us quantitate the change in lymphatic trafficking as modulated by exosomes.

m) I have shown that the lymph node shows markers of neutrophil recruitment and activation which implies the initiation of the innate immune response in the node. Future work with a challenge model where the mouse is exposed to exosomes followed by a pathogen will help outline the ability of exosomes to prepare the organism for imminent pathogen attack

n) This work comprehensively dissects the impact of exosome uptake and retention by the draining lymph node. I expanded on the exosome mediated macrophage reprogramming to show that macrophages undergo M1 polarization via *Il12* and *Nos2 in vivo*. I have also profiled the impact of the whole lymph node after exosome uptake to show remodeling of the node milieu to a pro-inflammatory state through the expression of *Il1b*. Future work in understanding the impact of lymph node reprogramming will help understand the physiological roles played by exosomes in the development of the innate immune response

APPENDIX

A.1. Supplementary information for Aim 1

A.1.1. Supplementary figures

Supplementary figure: Characterization of exosomes used in the study

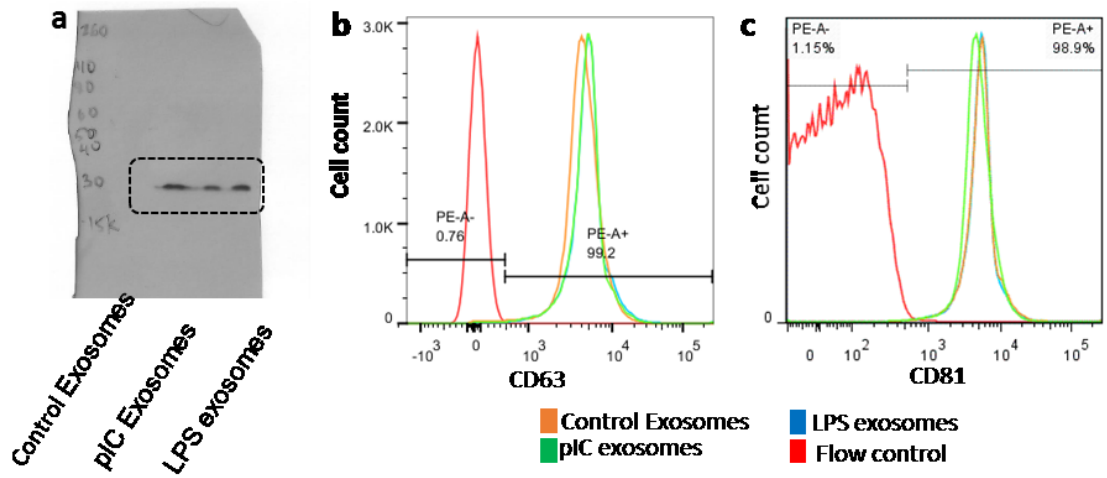

Figure 37: Characterization of exosomes used in the study. (a) Complete western blot of CD81 with control, pIC and LPS exosomes. Flow cytometry showing (b) CD63 and (c) CD81 levels on the exosomes.

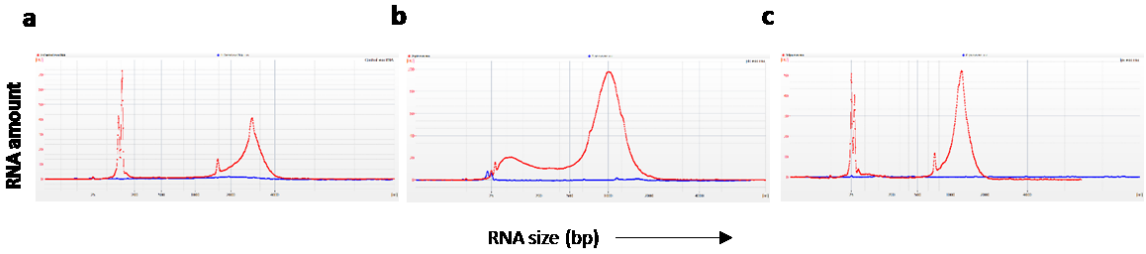

Figure 38: Effect of UV on nucleic acid content of exosomes. RNA size distribution profiles obtained on a Bioanalyzer pico RNA chip of (a) Control exosomes , (b) pIC exosomes, and (c) LPS exosomes ; before (red lines) and after UV treatment (blue Line)

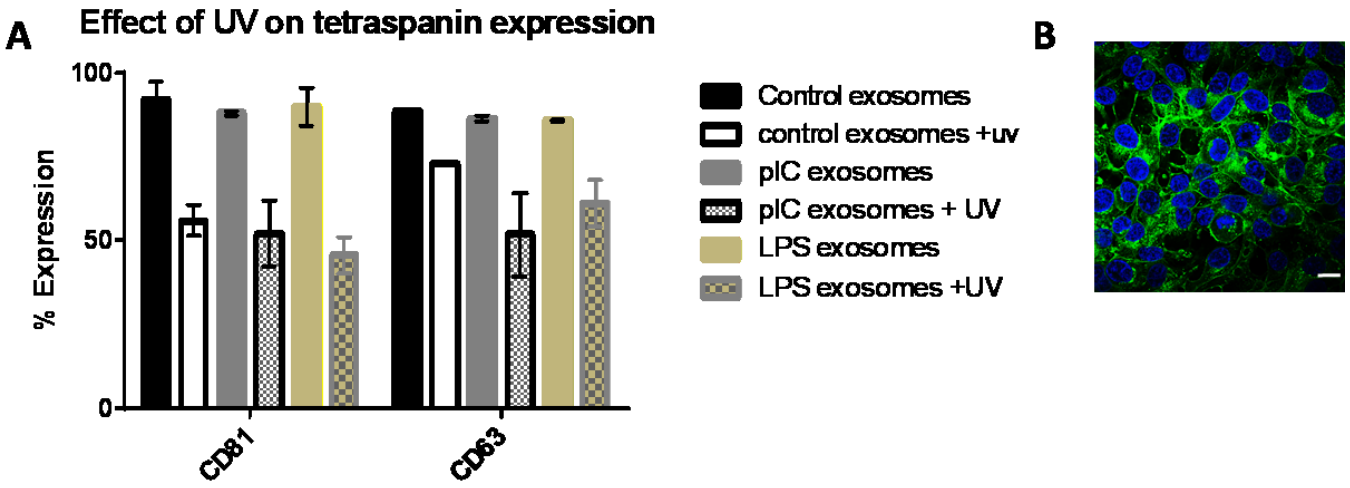

Figure 39: Impact of UV on protein expression and cellular uptake. A) Changes in tetraspanin expression on exosome surface before and after exposure to UV light, and B) UV treated exosomes are taken up by cells

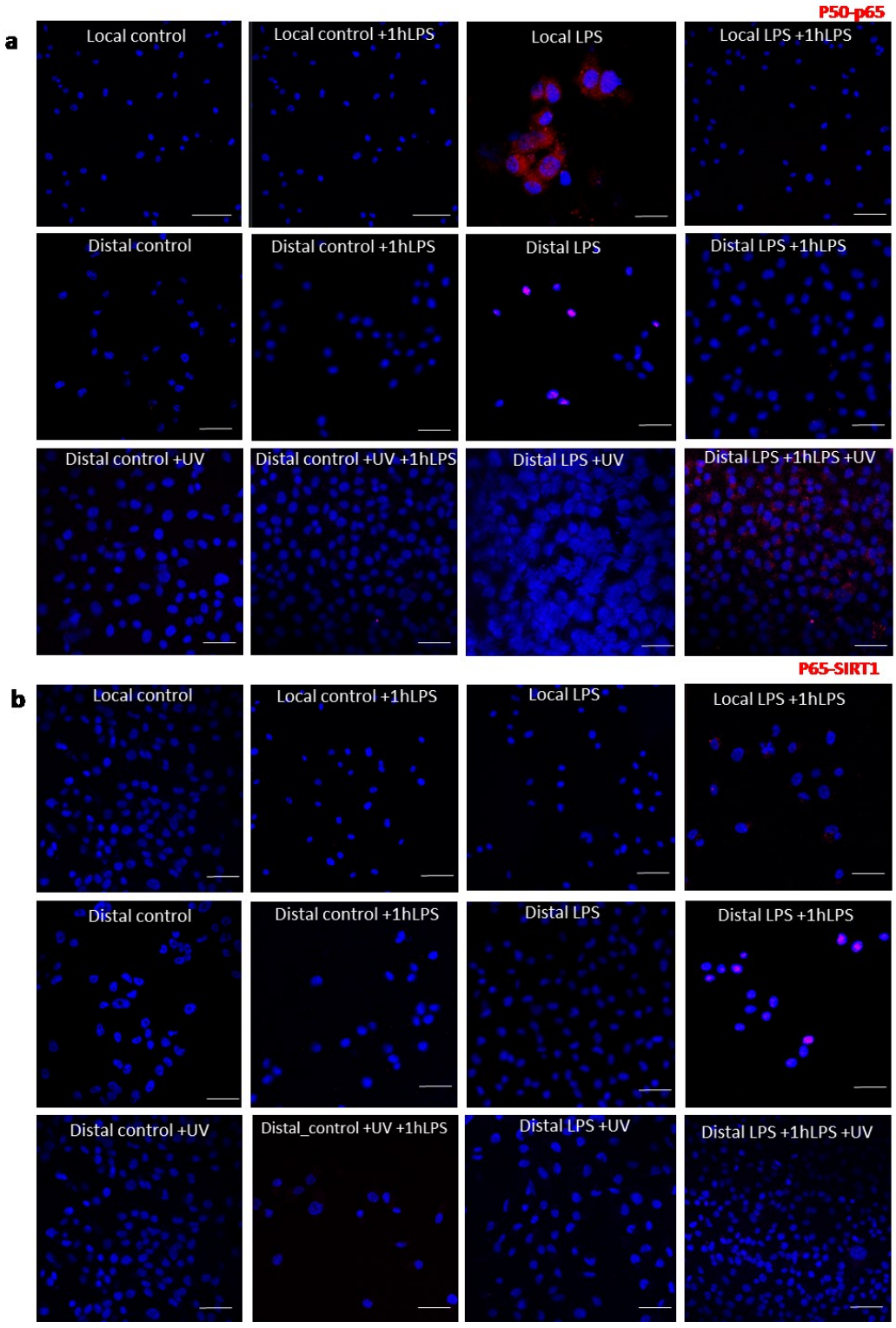

Figure 40: The LPS response in local and distal cells. Proximity ligation assay showing (a) the P50-P65 co-localization and (b) P65-SIRT1 in the cells indicated

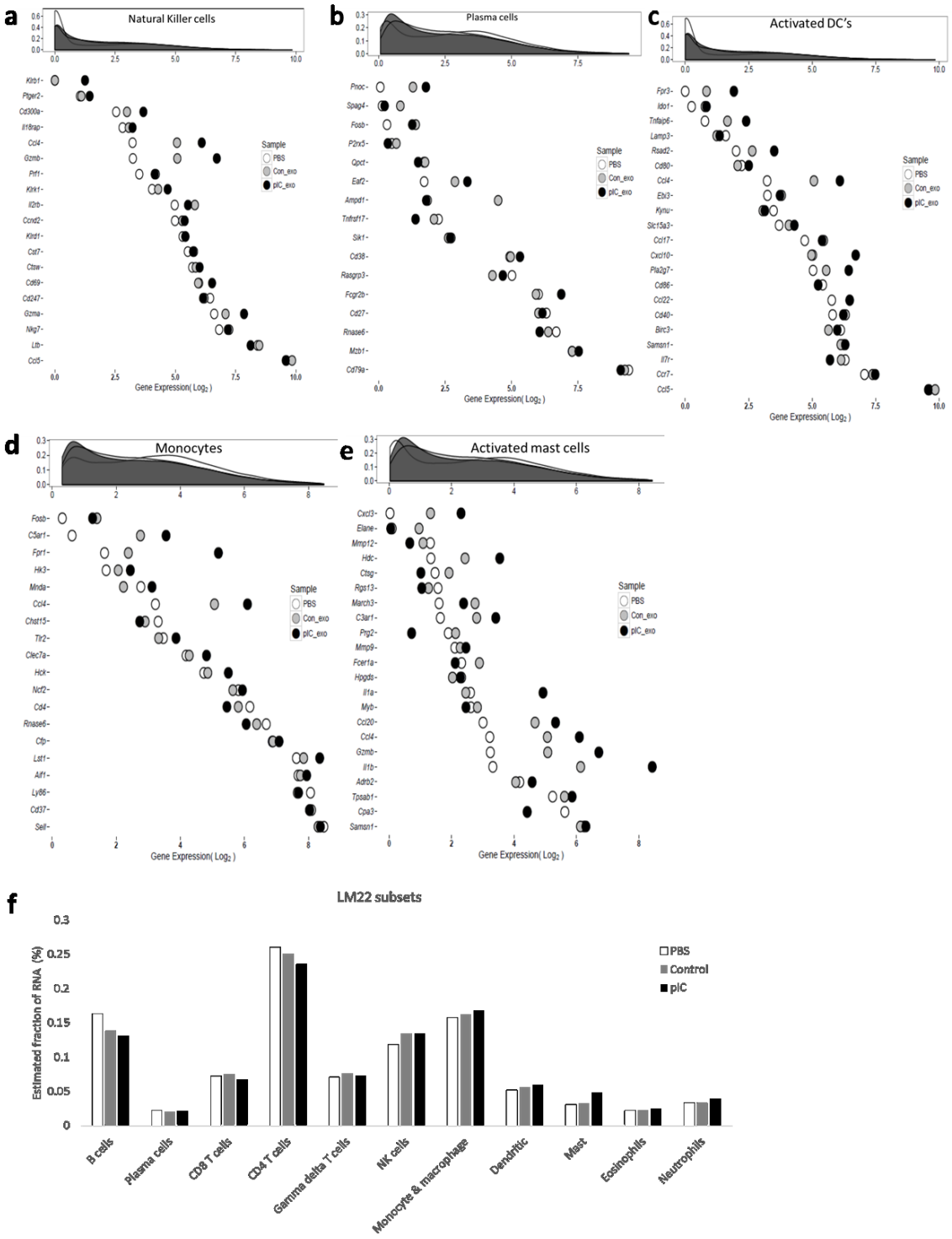

Figure 41: Relative gene expression of PBS, control exosomes and pIC exosomes depicted in a) natural killer cells, b) plasma cells c)activated dendritic cells, d) monocytes, e) activated mast

Figure 41 continued cells. F) Relative fraction of PBS, control exosomes and pIC exosomes gene expression in the 10 main immune subsets

A.1.2. Supplementary Tables

Table 3: List of human primers used in the study

Gene Symbol	mRNA NCBI Accession	Forward Primer (5'-3')	Reverse Primer (5'-3')
IRF1	NM_002198.2	CTCTGAAGCTACAACAGATGAG	GTAGACTCAGCCCAATATCCC
MAVS	NM_001206491.1	CAGGAGCAGGACACAGAAC	AGGAGACAGATGGAGACACAG
TRAF6	NM_004620.3	GAGTCGTGCGGTTGGTG	GCTGGATCCACAGCTGTTTT
IFNA1	NM_024013.2	GAGTGTGGAGACCATCAAGGA	GTATTGCTTTGCGTTGGACA
STAT1	NM_007315.3	TTCAGGAAGACCCAATCCAG	TGCTCTGAATATTCCCCGAC
TNF	NM_000594.3	GAGGCCAAGCCCTGGTATG	CGGGCCGATTGATCTCAGC
CCL3	NM_002983.2	TGCAACCAGTTCTCTGCATC	TGGCTGCTCGTCTCAAAGTA
IL1B	NM_000576.2	AGCTGATGGCCCTAAACAGA	CCTGAAGCCCTTGCTGTAGT
TOLLIP	NM_019009.3	CATGTCTGGTGTTTGTGGTTC	TGTGGGCATTCTCTTTCTGTC
TIRAP	NM_001039661.1	TTAAGGCTGAAAGAGTGTCCG	CTGTTCTCTGCTCCACCTG
Reference Gene			
GAPDH	NM_001256799.2	ACATCGCTCAGACACCATG	TGTAGTTGAGGTCAATGAAGGG

Table 4: List of mouse primers used in the study

Gene Symbol	mRNA NCBI Accession	Forward Primer (5'-3')	Reverse Primer (5'-3')
Cxcl2	NM_009140.2	CCAACCACCAGGCTACAGG	GCGTCACACTCAAGCTCTG
IL12a	NM_001159424.2	CAATCACGCTACCTCCTCTTTT	AGCAGTGCAGGAATAATGTTTC
IL23a	NM_031252.2	AACAACAGCTCGGATTTGGTAT	ATGACCAGGACATTCAGCAGT
Nos2	NM_001313922	GTTCTCAGCCCAACAATACAAGA	GTGGACGGGTCGATGTCAC
Irak3	NM_028679.3	GTTCTACTCCTGTTCCGTCACC	GTCCCGTTGCTCATATAGGGATA
Myd88	NM_010851.2	GACCGTGAGGATATACTGAAGGA	GGCCACCTGTAAAGGCTTCTC
CCL3	NM_011337.2	TGTACCATGACACTCTGCAAC	CAACGATGAATTGGCGTGGAA
IL1B	NM_008361.4	GAAATGCCACCTTTTGACAGTG	TGGATGCTCTCATCAGGACAG
NLRP3	NM_145827.3	ATTACCCGCCCGAGAAAGG	CATGAGTGTGGCTAGATCCAAG
Reference Gene			
ActB	NM_007393.5	GGCTGTATTCCCCTCCATCG	CCAGTTGGTAACAATGCCATGT

Table 5: Genes enriched in pIC macrophages w.r.t PBS macrophages

Gene	Locus	Value PBS	Value pIC	log2(fold_change)	p-value	q-value
8030451O07Rik	chr16:72226382-72234327	42.9639	0	-inf	5.00E-05	0.0534667
Vmn1r228	chr17:20776058-20777501	39.518	0	-inf?	5.00E-05	0.0534667
Kcna4	chr2:107290588-107298504	19.3042	0	-inf?	5.00E-05	0.0534667
Icmt	chr4:152297213-152318625	0	20.9953	inf	5.00E-05	0.0534667
Saa3	chr7:46711997-46715676	0	602.841	inf	5.00E-05	0.0534667
Suv39h1	chrX:8061170-8074760	0	19.632	inf	5.00E-05	0.0534667
Rfk	chr19:17394042-17401349	27.3396	0	-inf?	0.0001	0.06416
Atg13	chr2:91674611-91710592	0	26.4579	inf	0.0001	0.06416
Neurog3	chr10:62133089-62134763	57.8144	0	-inf?	0.00015	0.06416
4921533I20Rik	chr18:17234482-17235482	88.7925	0	-inf?	0.00015	0.06416
Npl	chr1:153503015-153549714	42.6803	0	-inf?	0.0002	0.06416
Olfr1356	chr10:78846950-78847913	40.8647	0	-inf?	0.0002	0.06416

Table 5 continued

Wimp	chr13:32802029-32822610	0	63.451	inf	0.0002	0.06416
1700037C18Rik	chr16:3905797-3908689	0	56.9555	inf	0.0002	0.06416
Olfr167	chr16:19514695-19515634	0	37.286	inf	0.0002	0.06416
Tas2r134	chr2:51627510-51628407	0	52.0894	inf	0.0002	0.06416
Olfr1264	chr2:90021137-90022064	0	48.2576	inf	0.0002	0.06416
Agap3	chr5:24452176-24502047	0	27.5255	inf	0.0002	0.06416
Inmt	chr6:55170626-55174990	54.0105	0	-inf?	0.0002	0.06416
Art4	chr6:136848450-136857600	0	19.5346	inf	0.0002	0.06416
Htr5b	chr1:121509772-121528465	36.8468	0	-inf?	0.00025	0.06416
Cbr2	chr11:120729484-120732021	74.9733	0	-inf?	0.00025	0.06416
Nrn1	chr13:36725621-36734477	45.8621	0	-inf?	0.00025	0.06416
Rsrp1	chr4:134923624-134927370	80.7523	0	-inf?	0.00025	0.06416
Themis2	chr4:132782356-132796364	0	25.6782	inf	0.00025	0.06416
Mvk	chr5:114444268-114460590	0	54.993	inf	0.0003	0.0712889
Cirh1a	chr8:106893639-106923094	0	29.4662	inf	0.0003	0.0712889
Olfr827	chr10:130210159-130211128	45.6499	0	-inf?	0.00035	0.0802
Gpbar1	chr1:74278599-74279589	0	76.9662	inf	0.0004	0.0802
Vmn1r202	chr13:22501336-22502245	0	56.2155	inf	0.0004	0.0802
Sec61a2	chr2:5870986-5895353	0	24.2966	inf	0.0004	0.0802
Tspan7	chrX:10485115-10596604	0	24.7349	inf	0.0004	0.0802
Teddm1a	chr1:153891645-153893060	0	30.9105	inf	0.00045	0.0824914
Rab11fip4os1	chr11:79591211-79694012	0	23.9915	inf	0.00045	0.0824914
Socs3	chr11:117966086-117969366	0	35.0248	inf	0.00045	0.0824914
Cited2	chr10:17723227-17725674	0	42.4857	inf	0.0005	0.083687
Appbp2	chr11:85191309-85235120	20.2115	0	-inf?	0.00055	0.083687
Olfr1445	chr19:12883882-12884827	0	35.2985	inf	0.00055	0.083687
Ifnb1	chr4:88522024-88522794	0	72.7145	inf	0.00055	0.083687

Table 5 continued

Mgst1	chr6:138140536-138156752		64.4402	0	-inf?	0.00055	0.083687
Klrb1b	chr6:128813705-128826315		0	33.7584	inf	0.00055	0.083687
Ntpcr	chr8:125734202-125748235		54.633	0	-inf?	0.00055	0.083687
Spryd3	chr15:102116527-102136215		0	23.229	inf	0.0006	0.083687
Olfr1087	chr2:86690031-86690973	0		41.9582	inf	0.0006	0.083687
Svop	chr5:114026912-114091380		0	20.7093	inf	0.0006	0.083687
Cldn34b4	chrX:76393349-76397979		0	40.1605	inf	0.0006	0.083687
Camk1	chr6:113326975-113343922		34.6672	0	-inf?	0.00065	0.0887319
Olfr741	chr14:50473056-50486395		0	45.0443	inf	0.0007	0.089824
Chmp2b	chr16:65539132-65562697		34.072	0	-inf?	0.0007	0.089824
Stard7	chr2:127270228-127298934		19.2474	0	-inf?	0.0007	0.089824
Pold2	chr11:5861865-5878256		0	35.1219	inf	0.0008	0.0991564
Ginm1	chr10:7767946-7780917		41.3771	0	-inf?	0.00085	0.0991564
Ptgs1	chr2:36230425-36252271		20.0208	0	-inf?	0.00085	0.0991564
Vmn1r15	chr6:57258148-57259048		53.9254	0	-inf?	0.00085	0.0991564
Elovl4	chr9:83778691-83806305		19.5133	0	-inf?	0.00085	0.0991564
Slc25a22	chr7:141429748-141437874		0	19.066	inf	0.00105	0.1203
P4ha2	chr11:54100923-54131667		0	20.0854	inf	0.0011	0.121683
Mrpl55	chr11:59202485-59206135		0	61.4094	inf	0.0011	0.121683
Insl3,Jak3	chr8:71676382-71690577		0	22.4754	inf	0.00195	0.212054
Cd1d2	chr3:86986585-86989532		0	40.8373	inf	0.0025	0.267333
Elovl1	chr4:118428092-118437343		19.6743	0	-inf?	0.00295	0.310282
Tssc4	chr7:143069367-143071087		22.825	0	-inf?	0.004	0.323885
Ppt2	chr17:34616661-34628279		0	19.4096	inf	0.0042	0.323885
Spata3	chr1:86021941-86029958		22.7755	0	-inf?	0.0049	0.323885
Susd3	chr13:49230830-49248706		29.1898	0	-inf?	0.0052	0.323885
Slc50a1	chr3:89268245-89270570		50.0845	0	-inf?	0.0053	0.323885

Table 5 continued

Ift22	chr5:136908149-136913244	76.9089	0	-inf?	0.0053	0.323885
C1qtnf7	chr5:43515568-43616586	19.1167	0	-inf?	0.0054	0.323885
Ybx3	chr6:131364857-131388450	34.7044	0	-inf?	0.00565	0.323885
Dhrs11	chr11:84820727-84829003	0	31.138	inf	0.0057	0.323885
Mptx2	chr1:173274460-173277756	0	65.5094	inf	0.00585	0.323885
Vmn1r200	chr13:22395028-22395967	0	40.6515	inf	0.00585	0.323885
Ppm1g	chr5:31202667-31220545	0	23.3792	inf	0.00585	0.323885
Olfr224	chr11:58566398-58567343	0	33.7066	inf	0.00625	0.323885
2810032G03Rik	chr12:5376501-5416132	0	28.8057	inf	0.00625	0.323885
Angptl4	chr17:33774899-33781575	0	25.8577	inf	0.00625	0.323885
Olfr1341	chr4:118709408-118710347	0	29.2462	inf	0.00625	0.323885
Olfr483	chr7:108103310-108104258	0	37.5952	inf	0.00625	0.323885
Olfr862	chr9:19883382-19884303	0	29.7759	inf	0.00625	0.323885
4933412E12Rik	chr10:116950561-116963279	21.3103	0	-inf?	0.0065	0.323885
Tspan17	chr13:54789404-54796775	0	30.9838	inf	0.0066	0.323885
Olfr1272	chr2:90281646-90282573	0	38.1952	inf	0.0066	0.323885
Mmp23	chr4:155650654-155653384	0	37.5151	inf	0.0066	0.323885
Wdr91	chr6:34880425-34910831	0	18.8525	inf	0.0066	0.323885
Asna1	chr8:85017930-85025278	0	42.6107	inf	0.0066	0.323885
Ear6,Ear7	chr14:51853767-51854642	38.0098	0	-inf?	0.00665	0.323885
4930579F01Rik	chr3:138164134-138186713	24.7816	0	-inf?	0.00675	0.323885
Slc25a33	chr4:149744035-149774267	0	20.6883	inf	0.0068	0.323885
Olfr237-ps1	chr6:43153306-43154239	0	24.7116	inf	0.0068	0.323885
R3hcc1	chr14:69697303-69714809	23.5724	0	-inf?	0.0069	0.323885
Ccnb1ip1	chr14:50789248-50795728	0	22.8899	inf	0.007	0.323885
Ccdc134	chr15:82127921-82142202	0	18.8391	inf	0.007	0.323885
Actl10	chr2:154544404-154558853	0	28.282	inf	0.00705	0.323885

Table 5 continued

Cdkn2c	chr4:109660875-109666756	25.8656	0	-inf?	0.00705	0.323885
Ccl20	chr1:83116765-83119167	0	29.6737	inf	0.00725	0.323885
Spaca1	chr4:34024871-34050067	30.0177	0	-inf?	0.00725	0.323885
Kdf1	chr4:133518962-133530790	0	25.3996	inf	0.0073	0.323885
Tac2	chr10:127724477-127731768	54.988	0	-inf?	0.0074	0.323885
Taar1	chr10:23920405-23921404	0	30.7256	inf	0.00745	0.323885
Gm5111	chr6:48589444-48590584	0	42.7986	inf	0.00745	0.323885
Fah	chr7:84585158-84605942	0	23.2363	inf	0.00745	0.323885
Nrbf2	chr10:67266688-67285281	24.0699	0	-inf?	0.0076	0.323885
Wdr46	chr17:33940722-33949695	22.1773	0	-inf?	0.0076	0.323885
Rrp36	chr17:46667452-46674255	46.9523	0	-inf?	0.0076	0.323885
Aldh3b1	chr19:3913490-3929716	23.1654	0	-inf?	0.0076	0.323885
Msrb2	chr2:19371635-19394971	33.3518	0	-inf?	0.0076	0.323885
Olfr1305	chr2:111872914-111873853	28.9292	0	-inf?	0.0076	0.323885
Wnt10a	chr1:74792018-74804175	0	20.5375	inf	0.00775	0.323885
Gstt4	chr10:75814943-75822543	0	32.5337	inf	0.00775	0.323885
Hddc3	chr7:80343136-80346097	0	37.3227	inf	0.00775	0.323885
Exosc6	chr8:111056338-111057664	0	46.0969	inf	0.00775	0.323885
9930111H07Rik	chr1:85775270-85784694	0	21.2558	inf	0.0078	0.323885
Ntmt1	chr2:30807976-30823014	0	28.7616	inf	0.0078	0.323885
Ggh	chr4:20042051-20066111	0	20.8744	inf	0.0078	0.323885
Vmn1r25	chr6:57978393-57979302	0	26.9174	inf	0.0078	0.323885
Cml1	chr6:85910153-85915677	0	30.3489	inf	0.0078	0.323885
Fgf3	chr7:144838611-144843348	0	38.6524	inf	0.0078	0.323885
Sprr3	chr3:92456501-92458720	22.6371	0	-inf?	0.0079	0.323885
Tnfrsf18	chr4:156026341-156028891	22.4939	0	-inf?	0.0082	0.323885
Olfr785	chr10:129409367-129410306	20.4505	0	-inf?	0.00825	0.323885

Table 5 continued

B230217C12Rik	chr11:97840779-97843043		20.1123	0	-inf?	0.00825	0.323885
Fam195b	chr11:120542887-120549727		25.9445	0	-inf?	0.00825	0.323885
Tmem14c	chr13:41016249-41022582		32.0683	0	-inf?	0.00825	0.323885
Cbr1	chr16:93607836-93610349		43.6206	0	-inf?	0.00825	0.323885
Ctsw	chr19:5465239-5468498		26.2031	0	-inf?	0.00825	0.323885
Tm2d1	chr4:98355369-98383265		26.309	0	-inf?	0.00825	0.323885
Urod	chr4:116990216-116994375		27.3033	0	-inf?	0.00825	0.323885
Ier2	chr8:84661330-84662852		35.3164	0	-inf?	0.00825	0.323885
Rrad	chr8:104628065-104631321		25.2089	0	-inf?	0.00825	0.323885
Gm6936	chr16:49980459-49997475		19.8891	0	-inf?	0.0084	0.323885
Ivd	chr2:118861999-118881357		20.4369	0	-inf?	0.0084	0.323885
Glmp	chr3:88325022-88328631		28.0218	0	-inf?	0.0084	0.323885
Olfr512	chr7:108713354-108714335		27.2798	0	-inf?	0.0084	0.323885
Olfr807	chr10:129754512-129755448		0	23.3018	inf	0.0085	0.323885
Jmjd6	chr11:116837431-116843449		0	20.1006	inf	0.0085	0.323885
Dynlt1b	chr17:6430111-6436295		0	38.7014	inf	0.0085	0.323885
Olfr1234	chr2:89362482-89363427	0		23.5992	inf	0.0085	0.323885
1700009N14Rik	chr4:39450292-39451778		0	21.383	inf	0.0085	0.323885
Snhg5	chr9:88521052-88522897		0	26.0158	inf	0.0085	0.323885
Ifi27l2b	chr12:103450897-103457223		0	28.0971	inf	0.0086	0.323885
E330017A01Rik	chr16:58635261-58638403		0	42.2717	inf	0.0086	0.323885
Snrnp35	chr5:124483154-124491122		0	26.1556	inf	0.0086	0.323885
4632427E13Rik	chr7:92740705-92741459		0	51.7959	inf	0.0086	0.323885
Olfr49	chr14:54281895-54282925		22.0851	0	-inf?	0.00865	0.323885
Cma1	chr14:55941450-55944661		25.9075	0	-inf?	0.00865	0.323885
Vmn1r224	chr17:20419162-20420059		20.3149	0	-inf?	0.00865	0.323885
Nubp2	chr17:24882610-24886350		20.5085	0	-inf?	0.00865	0.323885

Table 5 continued

Olfr1145	chr2:87809821-87810799	23.3217	0	-inf?	0.00865	0.323885
Svs2	chr2:164235928-164238341	20.0852	0	-inf?	0.00865	0.323885
Fam213b	chr4:154896429-154899043	53.3879	0	-inf?	0.00865	0.323885
Vmn1r60	chr7:5544196-5545099	24.8937	0	-inf?	0.00865	0.323885
1700026D08Rik	chr7:83775616-83794839	23.893	0	-inf?	0.00865	0.323885
Bst2	chr8:71534261-71537437	60.0248	0	-inf?	0.00865	0.323885
Olfr980	chr9:40005993-40007029	18.9121	0	-inf?	0.00865	0.323885
Clec4d	chr6:123262106-123275268	0	19.4164	inf	0.00875	0.323885
5430425K12Rik	chr13:80940402-80948597	20.0775	0	-inf?	0.00895	0.323885
1110007C09Rik	chr13:49202950-49216026	54.1188	0	-inf?	0.00895	0.323885
Amdhd2	chr17:24155832-24163733	26.0834	0	-inf?	0.00895	0.323885
Olfr1448	chr19:12919362-12920307	23.2755	0	-inf?	0.00895	0.323885
Olfr1024	chr2:85904068-85905052	23.8723	0	-inf?	0.00895	0.323885
Pithd1	chr4:135975601-135987244	31.7372	0	-inf?	0.00895	0.323885
4930513D17Rik	chr5:39461748-39603574	30.172	0	-inf?	0.00895	0.323885
Tas2r118	chr6:23969160-23970060	28.0034	0	-inf?	0.00895	0.323885
Vmn1r123	chr7:21162184-21163108	25.181	0	-inf?	0.00895	0.323885
Olfr944	chr9:39217358-39218294	22.1162	0	-inf?	0.00895	0.323885
Mrgprb1	chr7:48444112-48456342	8.69978	56.4743	2.69854	0.0092	0.323885
Uck2	chr1:167226083-167285127	0	45.9198	inf	0.00925	0.323885
Hist1h3f	chr13:23544051-23544954	0	63.0315	inf	0.00925	0.323885
Vmn1r210	chr13:22827193-22828114	0	22.5534	inf	0.00925	0.323885
Tacstd2	chr6:67534058-67535822	0	31.3957	inf	0.00925	0.323885
Mrpl44	chr1:79776017-79781445	22.668	0	-inf?	0.00985	0.323885
Dcxr	chr11:120725372-120727281	30.438	0	-inf?	0.00985	0.323885
Tubb2a-ps2	chr12:11882195-11882899	20.6329	0	-inf?	0.00985	0.323885
Tpsb2	chr17:25366332-25368092	19.7134	0	-inf?	0.00985	0.323885

Table 5 continued

Ptgds	chr2:25466711-25469749	26.0146	0	-inf?	0.00985	0.323885
Cdkn2b	chr4:89306288-89311032	25.8236	0	-inf?	0.00985	0.323885
Pop5	chr5:115235850-115240970	44.762	0	-inf?	0.00985	0.323885
Ptov1	chr7:44863067-44869788	20.5055	0	-inf?	0.00985	0.323885
Ruvbl2	chr7:45421897-45434464	20.6705	0	-inf?	0.00985	0.323885
Upf3a	chr8:13785614-13798537	29.2402	0	-inf?	0.00985	0.323885
Cdr1	chrX:61183245-61185558	19.6273	0	-inf?	0.00985	0.323885
Prdx4	chrX:155323919-155338454	26.5092	0	-inf?	0.00985	0.323885
Ddt	chr10:75771232-75773374	0	63.5472	inf	0.01	0.323885
Hist3h2a	chr11:58954684-58955192	0	98.6378	inf	0.01	0.323885
Olfr750	chr14:51070310-51071442	0	19.9333	inf	0.01	0.323885
Nudt22	chr19:6993018-6996037	0	23.3294	inf	0.01	0.323885
Xpa	chr4:46175221-46196311	0	30.771	inf	0.01	0.323885
Icam2	chr11:106377655-106382641	19.5837	0	-inf?	0.01025	0.323885
Cd7	chr11:121036748-121039478	22.625	0	-inf?	0.01025	0.323885
Rpl10l	chr12:66283378-66284401	27.2673	0	-inf?	0.01025	0.323885
Gm10823	chr16:27849929-27926128	25.8352	0	-inf?	0.01025	0.323885
Bex6	chr16:32179799-32186944	26.4758	0	-inf?	0.01025	0.323885
Psmg1	chr16:95979934-95990903	19.5249	0	-inf?	0.01025	0.323885
Mad2l1bp	chr17:46147384-46153551	19.3716	0	-inf?	0.01025	0.323885
Mydgf	chr17:56176540-56183920	23.2706	0	-inf?	0.01025	0.323885
1700030N03Rik	chr19:3153798-3197703	79.6032	0	-inf?	0.01025	0.323885
Gm826	chr2:160311400-160327494	23.1694	0	-inf?	0.01025	0.323885
Wfdc3	chr2:164731225-164743267	26.9721	0	-inf?	0.01025	0.323885
Psmg3	chr5:139823593-139826843	36.7331	0	-inf?	0.01025	0.323885
Timm50	chr7:28305825-28312046	21.3216	0	-inf?	0.01025	0.323885
5830454E08Rik	chr9:120577330-120578073	40.7484	0	-inf?	0.01025	0.323885

Table 5 continued

A930006K02Rik	chr16:91465103-91470123	0	43.618	inf	0.0105	0.323885
Grxcr2	chr18:41986200-41999049	0	29.5598	inf	0.0105	0.323885
Dfnb59	chr2:76650272-76658554	0	25.0701	inf	0.0105	0.323885
Penk	chr4:4133535-4138445	0	26.6919	inf	0.0105	0.323885
Olfr68	chr7:103777395-103778343	0	20.9962	inf	0.0105	0.323885
Arv1	chr8:124722138-124734123	0	23.1182	inf	0.0105	0.323885
Camta2,Spag7	chr11:70663768-70688105	57.3321	2.50407	-4.517	0.011	0.337684
Nt5dc2	chr14:31134852-31168641	21.0978	0	-inf?	0.01355	0.413985
Ccl19	chr4:42754524-42756518	130.83	1096.71	3.06741	0.01465	0.445471
Fam60a	chr6:148921058-148946432	149.931	33.6692	-2.1548	0.01565	0.473634
Pde6g	chr11:120447606-120453500	23.3889	0	-inf?	0.01625	0.489484
Pnrc2	chr4:135870925-135873846	17.4832	125.979	2.84915	0.01745	0.523174
Msr1	chr8:39467447-40227787	14.1845	72.1555	2.34679	0.0179	0.534169
Chchd7	chr4:3938887-3951382	139.618	6.43323	-4.4398	0.01815	0.539122
Acy3	chr19:3986569-3990005	0	18.9047	inf	0.01835	0.542551
Prr27	chr5:87825696-87846386	0	19.2469	inf	0.0187	0.550363
Gucy1a2	chr9:3532348-3905787	4.88846	21.0582	2.10693	0.0188	0.55078
Capza1	chr3:104822784-104864505	23.954	95.9779	2.00243	0.02025	0.590564
Cox18	chr5:90214724-90223996	0	20.408	inf	0.0228	0.661922
Pgap1	chr1:54472999-54557684	12.6214	39.5624	1.64826	0.02415	0.697957
Zap70	chr1:36761797-36782820	21.8591	0	-inf?	0.02545	0.73223
Sox11	chr12:27334267-27342718	70.0018	17.981	-1.96092	0.02595	0.739543
A730020M07Rik	chr3:121634935-121646453	19.6322	0	-inf?	0.02595	0.739543
Cxcl13	chr5:95956938-95961068	372.854	1100.85	1.56193	0.02605	0.739543
Myl1	chr1:66924295-66945056	27.9507	0	-inf?	0.04945	0.862506
Tbx1	chr16:18581703-18590671	0	19.628	inf	0.02635	0.744765
Casc5	chr2:119047118-119104121	6.7173	41.4277	2.62464	0.0271	0.762604
BC037032	chr15:4020110-4155344	12.6229	65.5151	2.37579	0.0284	0.795696

Table 5 continued

Btbd18	chr2:84659078-84668781	11.7068	64.8968	2.4708	0.02875	0.798528
Tktl2	chr8:66511739-66519199	13.1168	48.9789	1.90075	0.02875	0.798528
Cyhr1	chr15:76643394-76660208	6.46585	81.1985	3.65054	0.0294	0.807484
Myo9a	chr9:59751173-59928866	9.49742	32.0823	1.75617	0.0294	0.807484
Sdcbp	chr4:6365679-6396122	39.9372	134.138	1.74792	0.02945	0.807484
Ttc14	chr3:33800182-33844310	11.4942	43.675	1.9259	0.0307	0.838175
Prlr	chr15:10177237-10349180	21.2528	61.3362	1.52908	0.0317	0.86181
Cacnb4	chr2:52428319-52676609	7.96714	32.9625	2.04869	0.03185	0.862235
Rfx7	chr9:72532239-72622949	6.41744	37.7751	2.55737	0.0327	0.862506
Cnot7	chr8:40492537-40634792	17.9681	84.2284	2.22887	0.0328	0.862506
Gm13546	chr2:58163973-58177063	33.6367	0	-inf?	0.03295	0.862506
Cfb	chr17:34856373-34862514	59.1975	219.062	1.88773	0.0333	0.862506
Gm13157	chr4:147753973-147809788	60.0194	199.302	1.73146	0.03345	0.862506
1500011B03Rik	chr5:114808195-114813976	69.772	0	-inf?	0.03355	0.862506
Ccr6	chr17:8236042-8257129	96.1231	18.006	-2.4164	0.03365	0.862506
Rc3h2	chr2:37370070-37422903	30.2586	83.7996	1.4696	0.03445	0.862506
Itgal	chr7:127296259-127335137	3.74952	31.8574	3.08685	0.03645	0.862506
S100a6	chr3:90612893-90614414	657.262	127.69	-2.36383	0.0368	0.862506
Trim30b	chr7:104355397-104358646	6.06866	61.1817	3.33365	0.03685	0.862506
Unc5d	chr8:28646716-29219636	38.3182	10.8762	-1.81685	0.0371	0.862506
Gpcpd1	chr2:132529081-132578248	7.20012	39.9156	2.47086	0.03725	0.862506
Cml2	chr6:85865421-85869137	3.24936	32.2051	3.30906	0.038	0.862506
1700025M24Rik	chr5:73268579-73284184	31.6883	0	-inf?	0.0381	0.862506
Jazf1	chr6:52768067-53068624	49.7855	5.2142	-3.25521	0.03815	0.862506
Bod1l	chr5:41787539-41844315	11.7008	40.1507	1.77882	0.0382	0.862506
Usp49	chr17:47630689-47684067	2.68761	25.9879	3.27344	0.03825	0.862506
1810026B05Rik,Chd2	chr7:73426651-73558395	28.7033	89.8281	1.64595	0.0384	0.862506

Table 5 continued

1600020E01Rik	chr6:86527329-86564449		31.1869	0	-inf?	0.03865	0.862506
Rbm25	chr12:83632233-83683123		22.3807	75.5445	1.75507	0.0389	0.862506
Fut8	chr12:77238103-77475996		595.664	241.652	-1.30156	0.04015	0.862506
Cpne1,Rbm12	chr2:156071840-156111965		8.06345	57.0215	2.82204	0.0403	0.862506
Bgn	chrX:73483634-73495936		15.3881	77.4481	2.33142	0.0403	0.862506
9430037G07Rik	chr9:88595324-88599243		41.3365	4.61762	-3.16219	0.0405	0.862506
Il33	chr19:29925113-29960715		27.3317	107.872	1.98068	0.0422	0.862506
Tia1	chr6:86404218-86433405	34.067		5.10782	-2.7376	0.0424	0.862506
Crebzf	chr7:90442780-90448043		20.8962	3.24773	-2.68574	0.04265	0.862506
Mdc1	chr17:35841497-35859670		86.5403	31.2146	-1.47115	0.04305	0.862506
Zfp81	chr17:33333727-33358878		131.596	39.749	-1.72713	0.04315	0.862506
L2hgdh	chr12:69690435-69724874		26.4937	2.95839	-3.16277	0.0432	0.862506
Garem	chr18:21127341-21300139		32.3837	3.66879	-3.14189	0.0433	0.862506
Foxa1	chr12:57540631-57546121		6.09907	52.6068	3.10859	0.04335	0.862506
Mkrn1	chr6:39397820-39420369		49.9685	5.6803	-3.13698	0.0434	0.862506
Zfp945	chr17:22846696-22867134		2.31459	20.8215	3.16924	0.0436	0.862506
Vmn2r113	chr17:22943183-22958814		5.64039	49.1333	3.12283	0.044	0.862506
Eif4h	chr5:134619875-134639328		11.8327	104.486	3.14246	0.04405	0.862506
Cd79a	chr7:24897510-24902197		100.165	12.003	-3.06091	0.045	0.862506
Tsr3	chr17:25240169-25256364		27.2416	0	-inf?	0.04545	0.862506
Fxyd5	chr7:31032722-31042331		305.512	37.4639	-3.02766	0.0458	0.862506
Il15ra	chr2:11705292-11733985		8.75868	76.654	3.12958	0.0459	0.862506
Kctd4	chr14:75896936-76010865		185.96	60.5274	-1.61933	0.04595	0.862506
Lxn	chr3:67430114-67475068		35.5344	226.991	2.67534	0.046	0.862506
Ube2d3	chr3:135438758-135467178		46.6531	5.7338	-3.02441	0.0464	0.862506
Ero1l	chr14:45283086-45318572		52.9749	13.7084	-1.95025	0.04675	0.862506
Dcn	chr10:97479499-97518162		52.4608	198.39	1.91903	0.04745	0.862506

Table 5 continued

Serpina3f, 3g	chr12:104214543-104241934	39.9176	142.501	1.83587	0.0475	0.862506
Tiparp	chr3:65527484-65555518	16.9349	64.5231	1.92982	0.0478	0.862506
Pxylp1	chr9:96823342-96889474	13.7749	59.3614	2.10748	0.04825	0.862506
Car3	chr3:14863537-14872373	190.934	22.5028	-3.0849	0.04835	0.862506
Cep57	chr9:13807787-13827107	6.94431	58.624	3.07759	0.0485	0.862506
Serpini1	chr3:75557532-75642523	4.77499	41.5677	3.1219	0.04875	0.862506
Mir7678,Slpi	chr2:164354069-164356507	0	18.8406	inf	0.0493	0.862506
Rmnd5a	chr6:71388633-71440637	14.5115	46.2264	1.67153	0.04935	0.862506

Table 6: Genes enriched in pIC macrophages w.r.t control macrophages

Gene	locus	Value Control	Value pIC	log2(fold_change)	p_value	q_value
Serp2	chr14:76532811-76556889	17.6265	0	-inf	0.0002	0.969383
Gbp9	chr5:105078393-105110292	8.87728	90.6153	3.35157	0.0003	0.969383
Defb48	chr14:62977523-62984510	19.3185	0	-inf	0.00075	0.969383
Hist1h1a	chr13:23763667-23764412	17.6532	0	-inf	0.00105	0.969383
Saa3	chr7:46711997-46715676	249.744	1760.41	2.81739	0.00115	0.969383
Pmp22	chr11:62951192-63386069	8.55896	87.6998	3.35706	0.0015	0.969383
Pik3ap1	chr19:41274217-41385070	8.68499	64.4607	2.89182	0.0022	0.969383
Bst1	chr5:43818892-43843468	4.22605	27.643	2.70953	0.003	0.969383
Gm15056	chr8:20900605-20901973	124.877	1229.32	3.29928	0.0032	0.969383
Mrgpra2b	chr7:47463806-47489582	6.13454	82.8145	3.75486	0.00365	0.969383
Serping1	chr2:84765359-84775429	20.8867	111.605	2.41775	0.004	0.969383
Abce1	chr8:79683441-79711740	3.8509	21.3887	2.47358	0.00495	0.969383
Tlr13	chrX:106143274-106160493	2.68866	28.2885	3.39525	0.00565	0.969383
Alpk1	chr3:127670309-127780527	3.84433	31.1979	3.02064	0.00595	0.969383
Nlrp3	chr11:59542685-59566956	1.95406	18.3023	3.22748	0.007	0.969383

Table 6 continued

Il33	chr19:29925113-29960715	11.1252	58.6499		2.3983	0.00835	0.969383
1810053B23Rik	chr16:93343715-93359543	58.8752	8.46191		-2.7986	0.0095	0.969383
Gm20098	chr17:51882726-51965257	15.4046	3.82278		-2.01066	0.00955	0.969383
Ccl19	chr4:42754524-42756518	193.965	805.785		2.0546	0.00965	0.969383
Bgn	chrX:73483634-73495936	2.25069	37.0296		4.04024	0.01025	0.969383
Tmbim7	chr5:3657003-3679544	14.4757	1.93174		-2.90566	0.01055	0.969383
Dnajb9	chr12:44205896-44210068	2.76637	24.2897		3.13428	0.01165	0.969383
Pstpip2	chr18:77794549-77882879	6.38511	30.772		2.26884	0.01305	0.969383
Rab8b	chr9:66843663-66919705	22.7716	98.2803		2.10967	0.0134	0.969383
Gpr141	chr13:19749681-19824257	3.81407	21.6848		2.50728	0.01375	0.969383
Themis2	chr4:132782356-132796364	17.8501	78.2911		2.13292	0.0154	0.969383
Stx12	chr4:132854063-132884458	6.06862	23.3462		1.94375	0.01545	0.969383
Gstm2	chr3:107981701-107986436	21.3883	90.57		2.08221	0.01555	0.969383
Pfkfb4	chr9:108991901-109032225	4.15233	18.1514		2.12809	0.0158	0.969383
Il18	chr9:50565367-50581837	25.3719	110.691		2.12523	0.0161	0.969383
Olfr695	chr7:106713731-106716345	26.3833	5.09584		-2.37224	0.01645	0.969383
Olfr138	chr17:38274772-38275711	36.0129	7.99548		-2.17126	0.017	0.969383
B230323A14Rik	chr9:69761145-69830199	25.7765	6.02477		-2.09708	0.017	0.969383
Usp8	chr2:126707327-126759314	6.21788	27.0666		2.12202	0.01715	0.969383
Olfr530	chr7:140372684-140373608	24.2926	3.72725		-2.70433	0.0176	0.969383
LOC100504703	chr10:127070480-127071101	18.6478	0	-inf		0.0182	0.969383
Rap2c	chrX:51003913-51018018	3.39226	25.3182		2.89986	0.01855	0.969383
Ggh	chr4:20042051-20066111	6.92689	54.5174		2.97644	0.0189	0.969383
Dcn	chr10:97479499-97518162	31.3259	164.207		2.39009	0.01965	0.969383
Odf2	chr2:29889719-29931746	4.51633	21.6132		2.25869	0.0198	0.969383
Cfb	chr17:34856373-34862514	55.4999	265.978		2.26075	0.02015	0.969383
Cul1	chr6:47454323-47526139	11.6158	41.2845		1.82952	0.02075	0.969383

Table 6 continued

Gna12	chr5:140759943-140830431	7.27527	34.4999		2.24552	0.0208	0.969383
Col3a1	chr1:45311537-45349706	4.05122	16.9559		2.06536	0.021	0.969383
Ccr1	chr9:123962125-123968692	29.4293	111.494		1.92164	0.0216	0.969383
Capn7	chr14:31336723-31371983	3.92507	13.8964		1.82392	0.02185	0.969383
Lcp2	chr11:34047200-34092280	29.6742	114.009		1.94187	0.02205	0.969383
Ier3	chr17:35821712-35822911	30.7313	157.412		2.35677	0.02325	0.969383
Rassf3	chr10:121410350-121476250	15.1804	52.3153		1.78503	0.02335	0.969383
Ap3b1	chr13:94358959-94566316	10.0849	35.4552		1.8138	0.0237	0.969383
Gm7168	chr17:13948372-13950678	20.3774	4.73129		-2.10667	0.02375	0.969383
Olfr1199	chr2:88755740-88756673	42.7385	11.6768		-1.87189	0.02405	0.969383
Sorl1	chr9:41968488-42124289	4.72918	14.1702		1.58319	0.02455	0.969383
Gm5416	chr16:36210402-36217788	0	65.9932	inf		0.0249	0.969383
Nploc4	chr11:120379797-120437700	4.68015	16.0672		1.77949	0.0252	0.969383
Grk6	chr13:55445071-55460927	11.7563	39.1847		1.73685	0.0258	0.969383
Trip13	chr13:73912461-73937767	2.95142	15.0055		2.34601	0.02605	0.969383
Cnn3	chr3:121426540-121458205	19.6022	78.302		1.99803	0.02665	0.969383
Otx2	chr14:48657676-48667644	19.0547	4.89226		-1.96158	0.02685	0.969383
Ripk1	chr13:34002873-34035170	3.16639	19.8561		2.64867	0.0269	0.969383
Tfg	chr16:56690328-56717450	13.3403	48.5655		1.86414	0.02745	0.969383
Il13ra1	chrX:36112107-36171261	8.07564	50.871		2.65519	0.0278	0.969383
Sucnr1	chr3:60081868-60087566	14.0674	1.58376		-3.15092	0.02845	0.969383
Olfr1453	chr19:13027403-13028327	29.1004	7.11782		-2.03153	0.0285	0.969383
Susd6	chr12:80790531-80880833	6.40361	25.5734		1.99769	0.02865	0.969383
Lrrc25	chr8:70616843-70620850	6.79908	83.7823		3.62323	0.0292	0.969383
Dgat2	chr7:99153662-99182713	8.49625	40.4722		2.25203	0.0296	0.969383
Dync1i2	chr2:71211705-71263302	5.98245	22.6304		1.91946	0.0297	0.969383
Tgtp1	chr11:48985328-48992246	3.51893	22.339		2.66636	0.03015	0.969383

Table 6 continued

Bcl2l11	chr2:128126037-128162547	7.5487	28.4769	1.91549	0.0305	0.969383
Zc3h7a	chr16:11136593-11176393	7.25499	38.4446	2.40573	0.0313	0.969383
Tmed7	chr18:46585927-46597535	6.84337	21.2619	1.63549	0.03185	0.969383
Ssr3	chr3:65379656-65392553	9.2873	31.5132	1.76262	0.03195	0.969383
Il18bp	chr7:102015076-102018155	12.3129	65.4335	2.40986	0.03205	0.969383
Il12a	chr3:68690643-68698550	5.66534	27.4637	2.27729	0.0321	0.969383
Wfikkn1	chr17:25877627-25880858	15.164	3.91737	-1.9527	0.03225	0.969383
Gfpt2	chr11:49794154-49838620	3.40338	14.233	2.0642	0.03245	0.969383
Pomgnt1	chr4:116150517-116159844	4.45256	20.1317	2.17676	0.0326	0.969383
Spg21	chr9:65460936-65488470	15.5932	50.2179	1.68728	0.0328	0.969383
Mmp3	chr9:7445821-7455974	10.5736	40.4484	1.93562	0.03305	0.969383
Pdha1	chrX:159988432-160138336	8.34522	30.6502	1.87687	0.0331	0.969383
1110038B12Rik	chr17:34950235-34952471	39.2008	6.78782	-2.52986	0.03315	0.969383
Dclre1a	chr19:56529160-56548222	3.74849	14.3543	1.9371	0.0337	0.969383
Taf9b	chrX:106206873-106221158	4.22182	15.8915	1.91232	0.0344	0.969383
Iigp1	chr18:60376028-60392629	11.4405	39.4112	1.78445	0.03445	0.969383
Garem	chr18:21127341-21300139	14.9744	4.29596	-1.80145	0.03515	0.969383
Ctsl	chr13:64363213-64370306	13.3655	56.6817	2.08437	0.03525	0.969383
Panx3	chr9:37659901-37669222	19.5486	5.92478	-1.72223	0.03545	0.969383
S100a16	chr3:90541222-90543151	2.53632	26.0895	3.36266	0.0357	0.969383
Gm6815	chr16:36194479-36197886	24.9113	8.43998	-1.56149	0.0362	0.969383
B3gnt2	chr11:22834738-22860336	7.95788	26.5961	1.74076	0.0363	0.969383
Clec4a2	chr6:123122689-123143999	10.0645	34.1235	1.7615	0.0365	0.969383
Olfr972	chr9:39873276-39874221	25.1732	6.11923	-2.04047	0.0373	0.969383
Adrb2	chr18:62177712-62179981	10.7379	52.897	2.30047	0.03745	0.969383
Nod1	chr6:54923941-54972612	11.0242	38.0176	1.78599	0.03775	0.969383
Ccne1	chr7:38097983-38107490	1.34643	20.1578	3.90413	0.0378	0.969383

Table 6 continued

Stfa2l1	chr16:36156810-36161948	14.4151	247.498	4.10177	0.038	0.969383
Il10ra	chr9:45253838-45269146	10.3221	45.3276	2.13465	0.0385	0.969383
Mrgpra2a	chr7:47426328-47452139	4.55683	33.7555	2.88902	0.03855	0.969383
Rasa3	chr8:13567217-13677587	8.6855	26.5971	1.61459	0.0386	0.969383
Mptx2	chr1:173274460-173277756	6.61052	31.0838	2.23333	0.0392	0.969383
Xpo6	chr7:126101718-126200408	5.32846	17.0367	1.67686	0.0392	0.969383
Igbp1b	chr6:138657091-138658444	25.3977	5.63629	-2.17188	0.04005	0.969383
Smpdl3b	chr4:132732965-132757171	7.4168	34.7624	2.22866	0.04045	0.969383
Ergic1	chr17:26561511-26656933	6.1747	25.9574	2.0717	0.0409	0.969383
Fabp3	chr4:130308777-130315463	157.49	47.103	-1.74136	0.04155	0.969383
St3gal6	chr16:58470540-58523312	10.3782	37.7726	1.86379	0.04175	0.969383
F630028O10Rik,Mir223	chrX:96239925-96243642	2.02573	20.8035	3.36031	0.04185	0.969383
Pgm1	chr5:64092949-64128158	3.39193	19.537	2.52603	0.04245	0.969383
Peg12	chr7:62461870-62464510	23.1475	6.68513	-1.79183	0.0426	0.969383
Slc40a1	chr1:45908069-45925594	6.40735	25.1718	1.97401	0.04295	0.969383
Olfr1352	chr10:78981049-78984721	14.7438	4.10328	-1.84526	0.0431	0.969383
Plekho2	chr9:65552576-65580087	9.25148	41.9962	2.1825	0.04315	0.969383
Tmem106a	chr11:101582241-101591785	15.149	45.1067	1.57412	0.0432	0.969383
Ctnnb1	chr9:120933399-120960507	14.3199	50.1776	1.80903	0.04325	0.969383
Ngp	chr9:110419807-110423012	15.6557	2.24798	-2.79999	0.0433	0.969383
Mad2l1bp	chr17:46147384-46153551	3.90298	21.6959	2.47478	0.0435	0.969383
Vmn1r64	chr7:5883579-5884542	19.7987	2.61821	-2.91875	0.0437	0.969383
Antxr2	chr5:97884687-98030962	5.37033	24.3591	2.18138	0.04455	0.969383
Micu2	chr14:57916279-57999262	13.0973	40.7597	1.63787	0.04475	0.969383
Marcks	chr10:37133242-37138926	70.029	235.873	1.75198	0.04495	0.969383
Wdr91	chr6:34880425-34910831	2.87002	17.7808	2.63119	0.04545	0.969383
Zmat4	chr8:23669660-24063116	24.9034	8.46755	-1.55633	0.04555	0.969383

Table 6 continued

Plscr1	chr9:92250193-92272561	12.0372	54.291	2.17322	0.0457	0.969383
Riok1	chr13:38036988-38061433	8.22511	22.9243	1.47877	0.046	0.969383
Fpr-rs6	chr17:20182077-20183097	17.6381	2.91847	-2.59542	0.046	0.969383
3110062M04Rik	chr6:34863145-34878065	3.65715	17.9972	2.29898	0.04665	0.969383
Hdhd1a	chr18:50567655-50568699	16.527	3.76865	-2.13271	0.04705	0.969383
Ifitm1	chr7:140967428-140969827	123.178	837.384	2.76514	0.0473	0.969383
Ubd	chr17:37193891-37196101	13.4089	45.77	1.77121	0.0474	0.969383
Tgm2	chr2:158116404-158146392	16.575	60.5639	1.86945	0.0474	0.969383
Ndufs3	chr2:90894635-90904721	35.9538	111.418	1.63177	0.0477	0.969383
Gm10696	chr3:94174411-94178193	28.7039	9.76069	-1.55619	0.04825	0.969383
Alkbh3	chr2:93980033-94010730	7.72873	42.1056	2.44571	0.04845	0.969383
1700037C18Rik	chr16:3905797-3908689	5.99782	31.8476	2.40868	0.04855	0.969383
Tas2r139	chr6:42140935-42141895	19.7514	4.14162	-2.25369	0.04855	0.969383
Gm5483	chr16:36184211-36188110	19.759	243.888	3.62564	0.04905	0.969383
Hspa9	chr18:34937414-34954351	14.3436	48.5239	1.75828	0.04905	0.969383
Adora2b	chr11:62248983-62266452	4.84157	20.2761	2.06623	0.0491	0.969383
Gbp7	chr3:142530335-142550151	11.2838	52.4492	2.21667	0.04915	0.969383
Tdrd7	chr4:45965334-46034765	8.23057	27.4524	1.73787	0.0492	0.969383
Acly	chr11:100476351-100528000	6.00419	26.0092	2.11498	0.0496	0.969383
Arid5a	chr1:36307732-36324029	4.98337	25.2747	2.3425	0.0497	0.969383
Olfr1170	chr2:88224079-88225030	18.7949	4.9625	-1.9212	0.0499	0.969383

Table 7: Genes enriched in pic exosomes vs control exosomes in whole node

gene	locus	Value Control	Value pIC	log2(fold_change)	p_value	q_value
Ankrd23	chr1:36530533-36535729	29.4488	2.37552	-3.6319	5.00E-05	0.098713
Eno3	chr11:70657175-70662513	235.397	24.2773	-3.27742	5.00E-05	0.098713
Ostn	chr16:27307640-27351209	5.16117	0	-inf	5.00E-05	0.098713
S100a9	chr3:90692629-90695721	107.816	417.682	1.95384	5.00E-05	0.098713
Cxcl2	chr5:90903898-90905938	6.58271	98.3162	3.90068	5.00E-05	0.098713
Mylpf	chr7:127211607-127214287	1147.89	6.98374	-7.36077	5.00E-05	0.098713
Tnni2	chr7:142442467-142444405	781.582	9.72325	-6.32882	5.00E-05	0.098713
Cd209b	chr8:3917654-3926841	152.165	33.9096	-2.16588	5.00E-05	0.098713
Ryr1	chr7:29003339-29125151	4.49056	0.285644	-3.9746	0.0001	0.175489
Gzmb	chr14:56258857-56262260	32.9068	104.551	1.66775	0.0002	0.287164
Mmp3	chr9:7445821-7455974	24.8705	79.572	1.67783	0.0002	0.287164
Des	chr1:75360291-75375015	48.0906	14.1908	-1.7608	0.0004	0.451257
Slfn4	chr11:83175185-83190216	7.14325	31.1404	2.12414	0.0004	0.451257
Hp	chr8:109575127-109579172	14.7777	64.7729	2.13197	0.0004	0.451257
Tpm1	chr9:67022592-67049213	966.641	50.4312	-4.26059	0.00075	0.7897
Ldb3	chr14:34526698-34588681	29.3273	0.530055	-5.78996	0.00105	0.999803
Ampd1	chr3:103074013-103099720	21.6483	2.46273	-3.13593	0.0012	0.999803
Lilrb4a	chr10:51490897-51496611	30.0346	85.211	1.50441	0.0013	0.999803
Fpr1	chr17:17876470-17883939	4.20963	35.4804	3.07526	0.00135	0.999803
Ttn	chr2:76703983-76982547	3.73804	0.760293	-2.29765	0.00145	0.999803
Il1b	chr2:129364579-129375733	69.4498	343.866	2.30781	0.0015	0.999803
Tpm2	chr4:43513725-43523554	32.1027	6.47248	-2.31031	0.0016	0.999803
Saa3	chr7:46711997-46715676	352.848	1457.15	2.04603	0.0016	0.999803
Timd4	chr11:46810798-46844333	61.6385	24.103	-1.35462	0.00185	0.999803
Slpi	chr2:164354069-164356507	33.5373	159.756	2.25203	0.0019	0.999803
Fpr2	chr17:17887823-17893952	19.7425	83.0948	2.07345	0.0021	0.999803
Il1rn	chr2:24336859-24351491	17.9351	54.5878	1.6058	0.0023	0.999803
Lcn2	chr2:32384636-32387739	12.512	155.6	3.63645	0.00275	0.999803
Cd14	chr18:36725063-36726815	21.0166	71.4616	1.76564	0.0028	0.999803

Table 7 continued

Cxcl10	chr5:92331840-92414627	30.5607	104.488	1.77359	0.003	0.999803
Neb	chr2:52136646-52338798	5.50376	0.43294	-3.66818	0.00305	0.999803
Clec4e	chr6:123281788-123289871	13.1437	39.1196	1.57352	0.00305	0.999803
Adssl1	chr12:112620046-112641355	27.5228	7.00345	-1.97449	0.00345	0.999803
Wfdc17	chr11:83704055-83706269	115.753	289.719	1.3236	0.004	0.999803
Ccrl2	chr9:111054833-111057518	14.7406	63.5777	2.10873	0.00505	0.999803
Zfpm2	chr15:40655041-41104592	4.43507	0.807652	-2.45715	0.00525	0.999803
Cmya5	chr13:93040714-93144724	6.80668	1.03786	-2.71335	0.0061	0.999803
S100a8	chr3:90669070-90670034	113.347	380.594	1.74751	0.00625	0.999803
Ndrg2	chr14:51905270-51913488	24.1288	5.69835	-2.08214	0.00645	0.999803
Fabp5	chr3:10012584-10016610	107.207	222.109	1.05087	0.0065	0.999803
Hba-a2	chr11:32283674-32284493	158.546	49.9862	-1.6653	0.00665	0.999803
Gm15056	chr8:20900605-20901973	145.143	466.358	1.68396	0.00665	0.999803
Gpd1	chr15:99717592-99725007	10.0203	1.97938	-2.33981	0.0077	0.999803
Irg1	chr14:103047011-103056573	3.91781	37.2071	3.24746	0.0082	0.999803
Ms4a6d	chr19:11586605-11604804	66.4276	132.309	0.994054	0.00885	0.999803
Ank1	chr8:22974835-23150497	1.6122	0.139862	-3.52695	0.0099	0.999803
Xirp2	chr2:67446001-67526606	5.14729	0.600057	-3.10064	0.01215	0.999803
Pde4dip	chr3:97689828-97888707	18.3557	8.01331	-1.19576	0.0122	0.999803
Ccl3	chr11:83647842-83649378	12.8508	72.8743	2.50355	0.0134	0.999803
Sod2	chr17:13007838-13018119	19.5943	36.4829	0.896784	0.01465	0.999803
Clec4a3	chr6:122952514-122969878	25.6426	62.8052	1.29234	0.0148	0.999803
Cacna1s	chr1:136052900-136119822	4.59417	0.970726	-2.24267	0.0156	0.999803
Fcgr4	chr1:171018925-171029761	11.1161	34.6176	1.63886	0.0156	0.999803
Agl	chr3:116739998-116808166	7.68035	3.4872	-1.1391	0.01665	0.999803
Tnfaip2	chr12:111442660-111455018	13.5523	26.9958	0.994198	0.01785	0.999803
4930480M12Rik	chr12:26211266-26240707	2.54168	0	-inf	0.01945	0.999803
1700019M22Rik	chr12:96046620-96047222	2.17313	0	-inf	0.01945	0.999803
1700024P04Rik	chr13:98984089-98984565	3.33114	0	-inf	0.01945	0.999803

Table 7 continued

4930529K09Rik	chr14:86245969-86262042	2.05765	0	-inf	0.01945	0.999803
4930572O13Rik	chr14:25139794-25143241	1.46238	0	-inf	0.01945	0.999803
C1ql4	chr15:99084753-99087728	1.64093	0	-inf	0.01945	0.999803
Krtap22-2	chr16:89010379-89010759	5.39221	0	-inf	0.01945	0.999803
Dcpp2	chr17:23898721-23900787	2.11965	0	-inf	0.01945	0.999803
Defb23	chr2:152459054-152464620	2.04676	0	-inf	0.01945	0.999803
Defb45	chr2:152593190-152596485	5.13912	0	-inf	0.01945	0.999803
Sprr2b	chr3:92316704-92318085	1.70662	0	-inf	0.01945	0.999803
Lce6a	chr3:92620084-92621660	1.41635	0	-inf	0.01945	0.999803
Lce1k	chr3:92806290-92807891	1.85484	0	-inf	0.01945	0.999803
Ifna5	chr4:88835524-88836094	2.38652	0	-inf	0.01945	0.999803
A930016O22Rik	chr7:19411093-19421583	39.3451	1.13871	-5.11071	0.01945	0.999803
4932443I19Rik	chr8:13705888-13743066	1.44307	0	-inf	0.01945	0.999803
Gm2837	chrX:33056285-33057063	1.45128	0	-inf	0.01945	0.999803
Rhox2b	chrX:37412104-37416806	1.49963	0	-inf	0.01945	0.999803
Cd274	chr19:29367437-29388094	24.1427	44.3672	0.877909	0.02035	0.999803
Fcer1g	chr1:171229571-171234349	181.342	343.517	0.921666	0.02065	0.999803
Pfkm	chr15:98038743-98132447	49.1548	3.74335	-3.71493	0.02095	0.999803
Fcgr2b	chr1:170960558-170976071	59.7975	116.465	0.961737	0.0213	0.999803
4930404H11Rik	chr12:71540606-71556133	1.502	0	-inf	0.0221	0.999803
Hbb-bs	chr7:103826522-103827928	175.284	81.4734	-1.10529	0.0224	0.999803
4930578N18Rik	chr16:76122612-76156086	0	2.01623	inf	0.02245	0.999803
S100a2	chr3:90590246-90591508	0	5.34607	inf	0.02245	0.999803
Klrb1	chr6:128706507-128723046	0	1.3904	inf	0.02245	0.999803
Gm17252	chr9:35685078-35687371	0	3.35151	inf	0.02245	0.999803
Gm10823	chr16:27849929-27926128	0	1.32746	inf	0.0225	0.999803
Krtap21-1	chr16:89403026-89403774	0	1.49489	inf	0.0225	0.999803
4933406D12Rik	chr2:146542930-146546108	0	1.52649	inf	0.0225	0.999803
4930593C16Rik	chr9:120924454-120930802	0	2.19614	inf	0.02255	0.999803

Table 7 continued

Olfr768	chr10:129093033-129093972	1.66741	0	-inf		0.02295	0.999803
Olfr777	chr10:129268385-129269321	1.67472	0	-inf		0.02295	0.999803
Olfr314	chr11:58786138-58787269	1.30356	0	-inf		0.02295	0.999803
1810007C17Rik	chr12:49476992-49480862	2.50971	0	-inf		0.02295	0.999803
Vmn1r197	chr13:22327910-22328807	1.77584	0	-inf		0.02295	0.999803
Vmn1r215	chr13:23075791-23076694	1.7595	0	-inf		0.02295	0.999803
Olfr1466	chr19:13341759-13342692	1.68208	0	-inf		0.02295	0.999803
Olfr1265	chr2:90036920-90037850	1.68952	0	-inf		0.02295	0.999803
Olfr1179	chr2:88402008-88402932	1.70458	0	-inf		0.02295	0.999803
Olfr1225	chr2:89170218-89171245	1.47829	0	-inf		0.02295	0.999803
1700012A03Rik	chr6:32050287-32058915	1.72769	0	-inf		0.02295	0.999803
Vmn1r47	chr6:90021887-90022820	1.68208	0	-inf		0.02295	0.999803
Vmn1r168	chr7:23540719-23541649	1.68952	0	-inf		0.02295	0.999803
Klk1b24	chr7:44188262-44192451	1.92486	0	-inf		0.02295	0.999803
Olfr53	chr7:140646451-140652919	1.25919	0	-inf		0.02295	0.999803
Vmn1r117	chr7:20883197-20884121	1.70458	0	-inf		0.02295	0.999803
Olfr667	chr7:104916313-104917294	1.57146	0	-inf		0.02295	0.999803
Olfr250	chr9:38367547-38368543	1.53981	0	-inf		0.02295	0.999803
1110036E04Rik	chr9:64049828-64054100	2.18106	0	-inf		0.02295	0.999803
Cldn34b1	chrX:154886802-154890267	1.3821	0	-inf		0.02295	0.999803
E330017A01Rik	chr16:58635261-58638403	0	1.74503	inf		0.02325	0.999803
Agr3	chr12:35925620-35949730	1.39877	0	-inf		0.02355	0.999803
Hcar2	chr5:123863569-123865516	8.67602	28.469		1.71429	0.0237	0.999803
Gtsf1l	chr2:163087030-163089601	0	1.49668	inf		0.02405	0.999803
Olfr29-ps1	chr4:43781364-43782327	0	1.33019	inf		0.02405	0.999803
Reg1	chr6:78425982-78428666	0	1.79756	inf		0.02405	0.999803
Vmn1r52	chr6:90178715-90179645	0	1.39174	inf		0.02405	0.999803
Olfr213	chr6:116540454-116541438	0	1.29377	inf		0.02405	0.999803
Vmn1r178	chr7:23893528-23894443	0	1.42164	inf		0.02405	0.999803
Olfr628	chr7:103731927-103732878	0	1.35193	inf		0.02405	0.999803
Tcf21	chr10:22817274-22820128	0	1.17905	inf		0.026	0.999803

Table 7 continued

Rfpl4b	chr10:38820540-38821779	0	1.42271	inf	0.026	0.999803
Vmn1r222	chr13:23232114-23233041	0	1.67715	inf	0.026	0.999803
Olfr1163	chr2:88070364-88071407	0	1.44165	inf	0.026	0.999803
Olfr1230	chr2:89296350-89297268	0	1.69867	inf	0.026	0.999803
4930519H02Rik	chr5:15863927-15883766	0	1.5856	inf	0.026	0.999803
Vmn1r174	chr7:23753910-23754852	0	1.64245	inf	0.026	0.999803
Mybpc2	chr7:44501698-44524669	61.4543	1.09595	-5.80926	0.026	0.999803
1700057G04Rik	chr9:92309376-92357876	0	1.42612	inf	0.026	0.999803
Cldn34c4	chrX:127721175-127736554	0	1.97468	inf	0.026	0.999803
Ifitm2	chr7:140954838-140955961	231.253	417.29	0.851577	0.02745	0.999803
Mir466k	chr3:85467376-85467498	96.9582	0	-inf	0.0278	0.999803
Klk1b7-ps	chr7:43945011-43945927	1.88132	0	-inf	0.0278	0.999803
Vmn2r-ps60	chr7:42430104-42430369	7.07224	0	-inf	0.0278	0.999803
Defa-ps12	chr8:19210461-19212760	32.1317	0	-inf	0.0278	0.999803
1700072B07Rik	chr9:58370503-58374183	1.90752	0	-inf	0.0278	0.999803
Mir471	chrX:66792594-66792661	863.81	0	-inf	0.0278	0.999803
1700113B09Rik	chr10:71201744-71204488	0	1.83358	inf	0.02855	0.999803
1700023F02Rik	chr10:66120608-66124064	0	2.88793	inf	0.02855	0.999803
Gm10104	chr8:21065037-21066001	0	2.08044	inf	0.02855	0.999803
Csf3r	chr4:126024658-126044975	7.61702	18.3529	1.26871	0.0287	0.999803
Igfbp5	chr1:72858064-72874865	14.743	7.082	-1.0578	0.029	0.999803
Prss40	chr1:34552330-34560943	0	1.28166	inf	0.0296	0.999803
Taar7a	chr10:23992404-23993481	0	1.61544	inf	0.0296	0.999803
Olfr736	chr14:50392757-50393696	0	1.92415	inf	0.0296	0.999803
1700109G14Rik	chr14:61292982-61305334	0	2.39101	inf	0.0296	0.999803
Gm4719	chr17:89379240-89384993	0	2.37873	inf	0.0296	0.999803
Scp2d1	chr2:144823665-144824415	0	2.60625	inf	0.0296	0.999803
Olfr1213	chr2:88972953-88980267	0	1.28641	inf	0.0296	0.999803
Olfr1245	chr2:89574711-89575773	0	1.64411	inf	0.0296	0.999803
Olfr8	chr10:78955206-78956139	2.24278	0	-inf	0.03005	0.999803
Vmn1r216	chr13:23099148-23100045	2.36779	0	-inf	0.03005	0.999803

Table 7 continued

Gm904	chr13:50643227-50645838	3.83907	0	-inf	0.03005	0.999803
Olfr186	chr16:59026975-59027905	2.25269	0	-inf	0.03005	0.999803
Olfr117	chr17:37659377-37660331	2.17577	0	-inf	0.03005	0.999803
Olfr1445	chr19:12883882-12884827	2.20399	0	-inf	0.03005	0.999803
Olfr1448	chr19:12919362-12920307	2.20399	0	-inf	0.03005	0.999803
Olfr1013	chr2:85769802-85770720	2.29323	0	-inf	0.03005	0.999803
Olfr1161	chr2:88024701-88025713	2.00991	0	-inf	0.03005	0.999803
Cabs1	chr5:87979450-87981541	1.23441	0	-inf	0.03005	0.999803
Olfr535	chr7:140492639-140493578	2.22322	0	-inf	0.03005	0.999803
Olfr480	chr7:108065767-108066796	1.96599	0	-inf	0.03005	0.999803
Spata45	chr1:191036821-191042941	0	1.89715	inf	0.0303	0.999803
Fcgr3	chr1:171051168-171059403	31.122	60.1566	0.950789	0.0303	0.999803
Smco2	chr6:146850109-146871404	1.51336	0	-inf	0.03035	0.999803
Pdlim7	chr13:55497486-55513446	27.6814	9.26722	-1.57871	0.0308	0.999803
Olfr455	chr6:42538066-42539020	0	2.15429	inf	0.03275	0.999803
Olfr556	chr7:102669900-102670923	0	1.96989	inf	0.03275	0.999803
Vmn1r124	chr7:21259693-21260617	0	2.24568	inf	0.03275	0.999803
Trdn	chr10:33083482-33476709	16.4301	1.21485	-3.75749	0.0331	0.999803
Fscn1	chr5:142960354-142973189	70.1763	40.0091	-0.81066	0.0337	0.999803
Clec4a2	chr6:123122689-123143999	8.30379	20.4947	1.30341	0.0341	0.999803
S100a5	chr3:90608521-90611780	2.1456	0	-inf	0.0342	0.999803
Pgm2	chr4:99929450-99987294	41.1049	20.3484	-1.01439	0.0344	0.999803
Pla2g7	chr17:43568450-43612201	46.1659	86.1717	0.900386	0.03455	0.999803
Cacng6	chr7:3424661-3434940	1.23926	0	-inf	0.0353	0.999803
Ak1	chr2:32621757-32635058	26.3035	2.79966	-3.23193	0.03585	0.999803
Tnnt3	chr7:142460811-142516009	1100.06	3.71488	-8.21006	0.0365	0.999803
Gpx3	chr11:54902853-54910382	34.9339	14.8877	-1.23051	0.0375	0.999803
Olfr728	chr14:50139701-50140637	2.79119	0	-inf	0.03905	0.999803
Gm1587	chr14:77793944-77798968	1.73329	0	-inf	0.03905	0.999803
Olfr92	chr17:37111041-37111980	2.77902	0	-inf	0.03905	0.999803

Table 7 continued

Olfr1031	chr2:85991818-85992829	2.5157	0	-inf	0.03905	0.999803
Skint8	chr4:111919554-111950356	1.86158	0	-inf	0.03905	0.999803
Pramef17	chr4:143991126-143994369	1.27962	0	-inf	0.03905	0.999803
Btg1-ps1	chrX:38013907-38018815	3.33108	0	-inf	0.03905	0.999803
Cacna2d1	chr5:15934690-16374511	2.36864	0.693171	-1.77278	0.0398	0.999803
Myl1	chr1:66924295-66945056	845.073	2.04866	-8.68825	0.0404	0.999803
Atp1a2	chr1:172271708-172298064	5.38849	1.35472	-1.99189	0.0405	0.999803
Ccr1	chr9:123962125-123968692	5.88944	16.3089	1.46946	0.0405	0.999803
Ctsc	chr7:88278092-88310875	83.2511	143.418	0.784688	0.04115	0.999803
4933415F23Rik	chr1:23100473-23102253	1.25786	0	-inf	0.0415	0.999803
Clec4a1	chr6:122921847-122934619	11.834	26.2801	1.15103	0.04205	0.999803
Atp6v1e2	chr17:86944108-86947887	0	2.5186	inf	0.043	0.999803
Vmn1r77	chr7:12041298-12042219	0	2.81906	inf	0.043	0.999803
H2-M2	chr17:37480850-37483529	38.9588	19.0987	-1.02848	0.0446	0.999803
Fas	chr19:34290658-34327770	22.9617	44.0506	0.939931	0.0452	0.999803
Nexn	chr3:152236983-152266320	6.47478	1.8935	-1.77378	0.0453	0.999803
Il18bp	chr7:102015076-102018155	24.7498	47.4827	0.939982	0.04555	0.999803
Slc25a4	chr8:46207340-46211009	287.314	159.866	-0.84576	0.04645	0.999803
Ifltd1	chr6:145397234-145434925	0	1.4075	inf	0.04665	0.999803
Ifnlr1	chr4:135686456-135708180	3.65885	1.08761	-1.75023	0.047	0.999803
Il1a	chr2:129297369-129309972	4.48178	29.4672	2.71697	0.0478	0.999803
Gzma	chr13:113093826-113100981	134.726	230.205	0.772892	0.04835	0.999803
Rrm2	chr12:24708253-24714146	27.8907	47.1693	0.758063	0.04905	0.999803
Olfr1000	chr2:85607963-85608908	0	2.99876	inf	0.0492	0.999803
1700028B04Rik	chr7:28496940-28497492	0	6.50168	inf	0.0492	0.999803
Mb	chr15:77015486-77057108	26.3153	0.299352	-6.45791	0.04935	0.999803
Gpt2	chr8:85492616-85527558	3.97369	1.22894	-1.69306	0.04985	0.999803

A.1.3. Supplementary videos

Supplementary Video 1: Example video of pIC exosome arrival in the collecting vessels of a mouse 10 cm downstream from the site of intradermal injection. The dominant vessel is seen below and the non-dominant vessel is seen above. Video is played at 10X speed

Supplemental Video 2: Example video of pIC exosome arrival in the draining (sciatic) lymph nodes of a mouse within minutes of intradermal exosome injection at the tip of the tail. The dominant node is seen below and the non-dominant vessel is seen above. Video is played at 10X speed

A.2. Supplementary information for Chapter 5

A.2.1. Supplementary figures

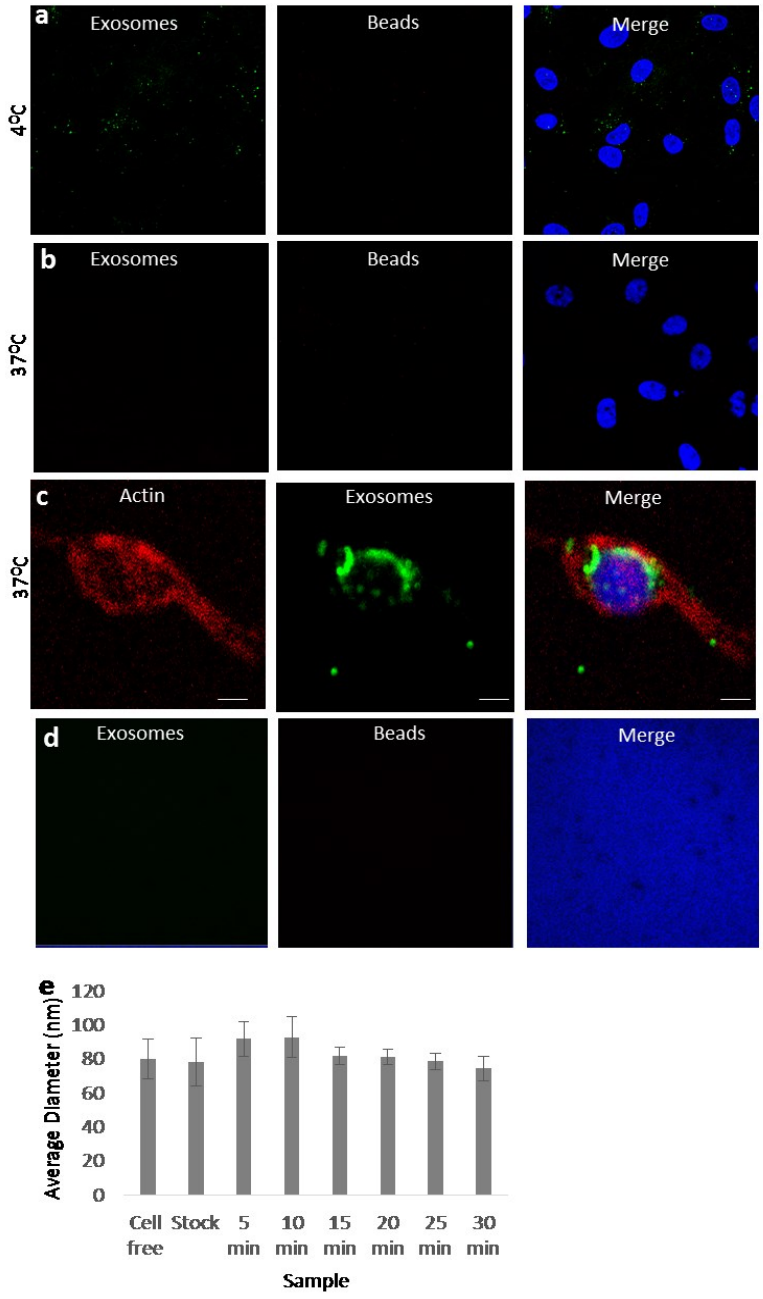

Figure 42: Transport of exosomes and beads across the lymphatic endothelium *in vitro* Confocal images showing a: exosomes and beads are not taken up the lymphatic endothelial cells at 4°C, b: exosomes but not beads are taken up at 37°C; c: intracellular localization of exosomes with actin; and d: the membrane does not bind to either exosomes or beads. e: Average diameter of exosome samples collected from the apical side at various time points during transport

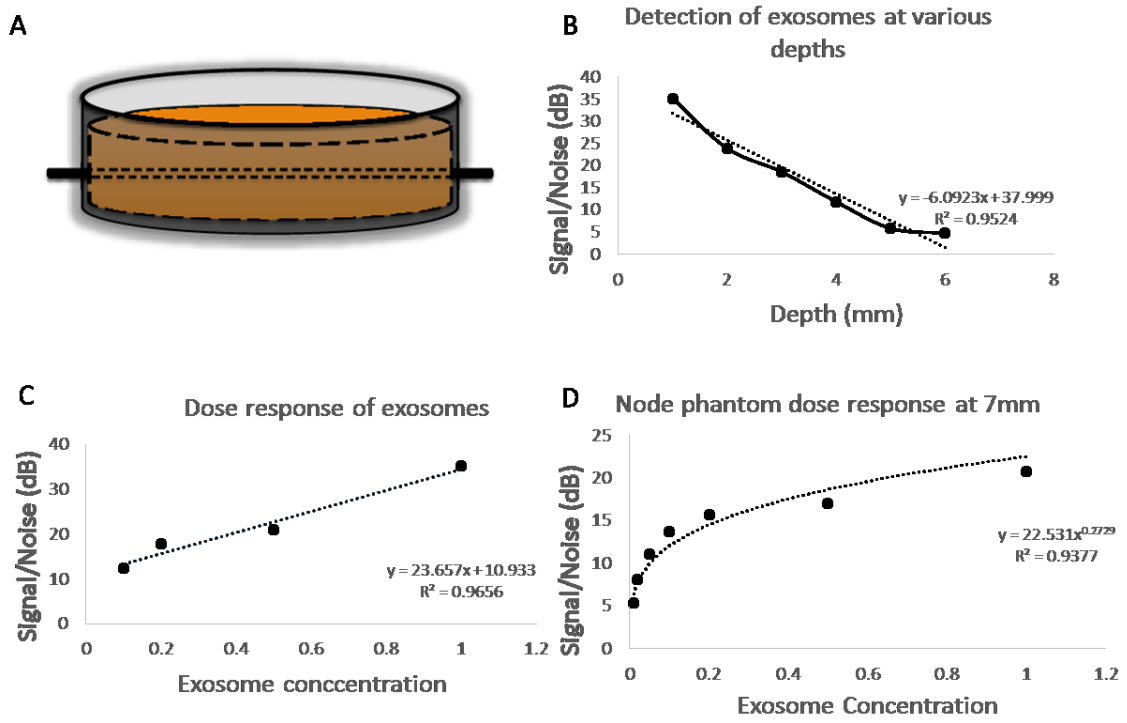

Figure 43 Characterization of System sensitivity of labeled exosome detection. A: Description of system setup (node and tissue phantoms), B: SNR in Tissue phantom at various depths, C: Dose response of exosomes (different concentrations at 2mm depth), D: Node phantom dose response to show limit of detection at node

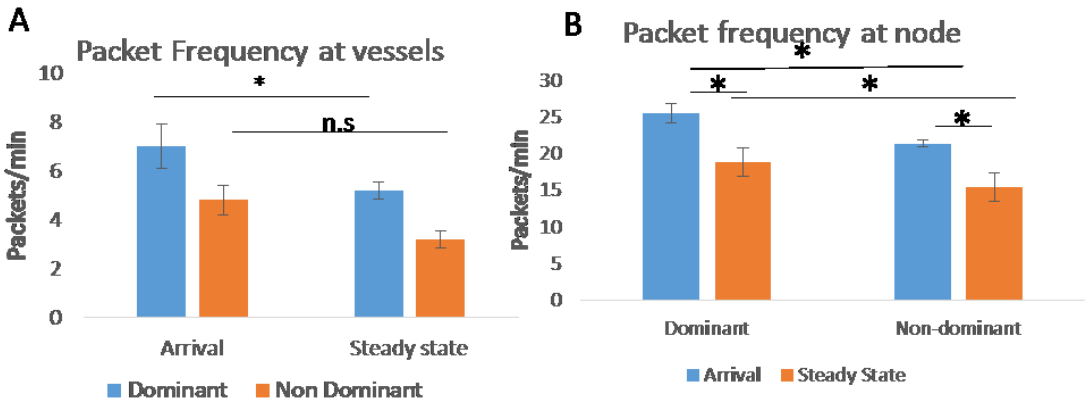

Figure 44: Packet frequency at collecting vessels and draining lymph node. Packet frequencies were calculated based on number of packets detected per minute from the line diagram at A) the collecting vessels and B) the draining lymph node

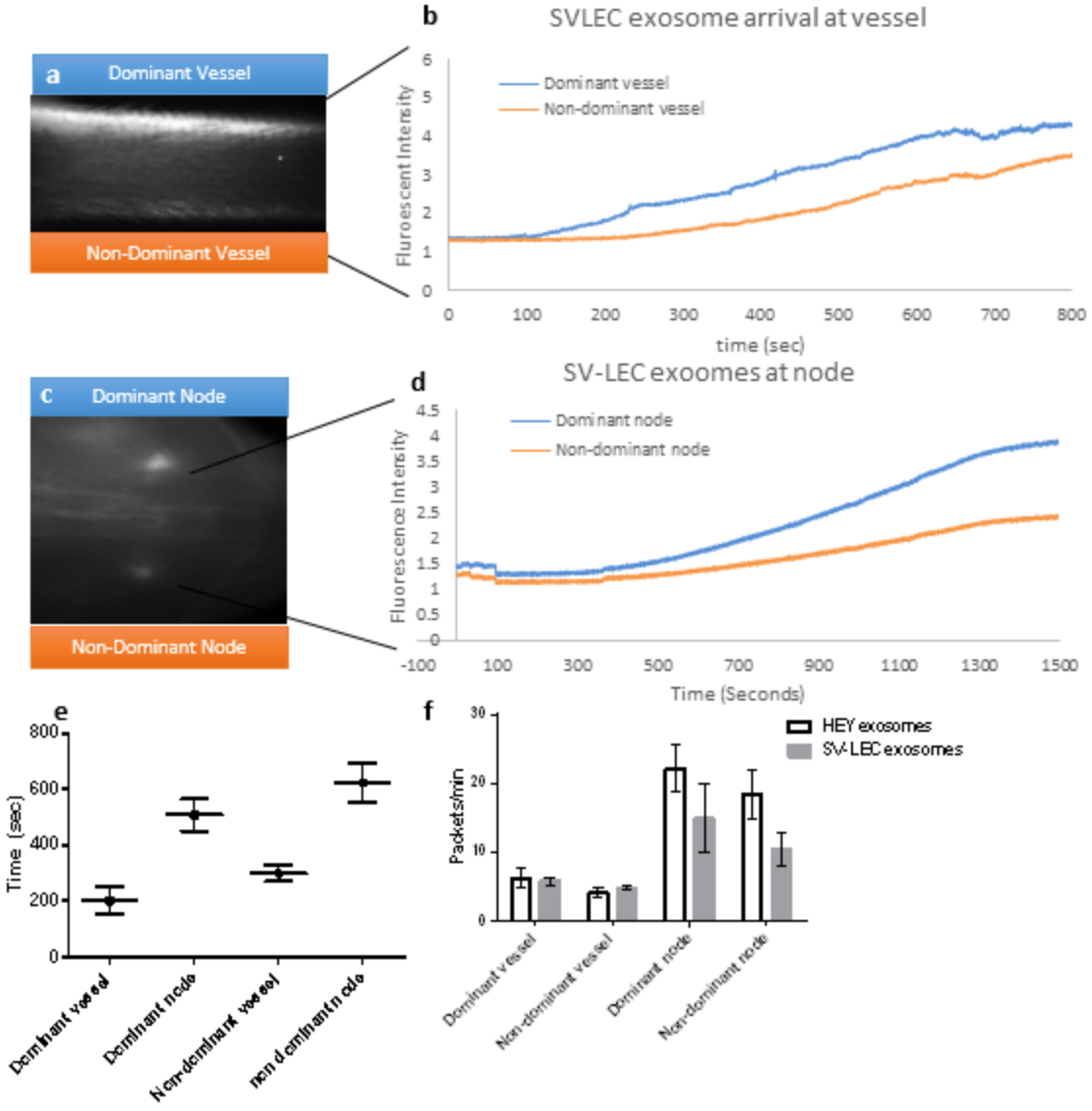

Figure 45: Characterizing SV-LEC exosome transport *in vivo* a) Steady state fluorescence in the lymphatic collecting vessel b) Intensity profile of a specified region of interest of exosome transport in a representative vessel over a 10 minute period, c) Steady state fluorescence in the draining lymph node, d) Intensity profile of a specified region of interest of exosome transport in a representative lymph node over a 10 minute period, e) Arrival time of detectable levels of fluorescence for dominant and non-dominant collecting vessels and draining lymph nodes. F) Packet frequency of HEY exosomes and SV-LEC exosomes at the collecting vessels and lymph nodes

A.2.2. Supplementary videos

Supplemental Video 1: Example video of exosome arrival in the collecting vessels of a mouse 10 cm downstream from the site of intradermal injection. The dominant vessel is seen below and the non-dominant vessel is seen above. Video is played at 10X speed

Supplemental Video 2: Example video of exosome arrival in the draining (sciatic) lymph nodes of a mouse within minutes of intradermal exosome injection at the tip of the tail. The dominant node is seen above and the non-dominant vessel is seen below. Video is played at 10X speed

REFERENCES

1. Murphy K, Travers P, Walport M, Janeway C. Janeway's immunobiology. 8th ed. New York: Garland Science; 2012. xix, 868 p. p.
2. Thomas SN, Vokali E, Lund AW, Hubbell JA, Swartz MA. Targeting the tumor-draining lymph node with adjuvanted nanoparticles reshapes the anti-tumor immune response. Biomaterials. 2014;35(2):814-24.
3. Gautier L, Cope L, Bolstad BM, Irizarry RA. affy--analysis of Affymetrix GeneChip data at the probe level. Bioinformatics. 2004;20(3):307-15.
4. Janeway CA, Jr., Medzhitov R. Innate immune recognition. Annual review of immunology. 2002;20:197-216.
5. Mogensen TH. Pathogen Recognition and Inflammatory Signaling in Innate Immune Defenses. Clinical microbiology reviews. 2009;22(2):240-73.
6. Janssens S, Beyaert R. Role of Toll-like receptors in pathogen recognition. Clinical microbiology reviews. 2003;16(4):637-46.
7. Akira S. Mammalian Toll-like receptors. Current opinion in immunology. 2003;15(1):5-11.
8. Thoma-Uszynski S, Stenger S, Takeuchi O, Ochoa MT, Engele M, Sieling PA, et al. Induction of direct antimicrobial activity through mammalian toll-like receptors. Science. 2001;291(5508):1544-7.
9. Medzhitov R, Preston-Hurlburt P, Janeway CA, Jr. A human homologue of the Drosophila Toll protein signals activation of adaptive immunity. Nature. 1997;388(6640):394-7.
10. Wright SD, Ramos RA, Tobias PS, Ulevitch RJ, Mathison JC. CD14, a receptor for complexes of lipopolysaccharide (LPS) and LPS binding protein. Science. 1990;249(4975):1431-3.
11. Wright SD, Tobias PS, Ulevitch RJ, Ramos RA. Lipopolysaccharide (LPS) binding protein opsonizes LPS-bearing particles for recognition by a novel receptor on macrophages. The Journal of experimental medicine. 1989;170(4):1231-41.
12. Beutler B. Innate immune responses to microbial poisons: discovery and function of the Toll-like receptors. Annual review of pharmacology and toxicology. 2003;43:609-28.
13. Pålsson-McDermott EM, O'Neill LAJ. Signal transduction by the lipopolysaccharide receptor, Toll-like receptor-4. Immunology. 2004;113(2):153-62.
14. Chung HY, Lee EK, Choi YJ, Kim JM, Kim DH, Zou Y, et al. Molecular inflammation as an underlying mechanism of the aging process and age-related diseases. Journal of dental research. 2011;90(7):830-40.
15. Akira S, Takeda K. Toll-like receptor signalling. Nature reviews Immunology. 2004;4(7):499-511.
16. Zhang G, Ghosh S. Negative Regulation of Toll-like Receptor-mediated Signaling by Tollip. Journal of Biological Chemistry. 2002;277(9):7059-65.
17. Lawrence T. The Nuclear Factor NF-κB Pathway in Inflammation. Cold Spring Harbor Perspectives in Biology. 2009;1(6):a001651.
18. Yeung F, Hoberg JE, Ramsey CS, Keller MD, Jones DR, Frye RA, et al. Modulation of NF-κB-dependent transcription and cell survival by the SIRT1 deacetylase. The EMBO Journal. 2004;23(12):2369-80.

19. Muzio M, Bosisio D, Polentarutti N, D'Amico G, Stoppacciaro A, Mancinelli R, et al. Differential expression and regulation of toll-like receptors (TLR) in human leukocytes: selective expression of TLR3 in dendritic cells. J Immunol. 2000;164(11):5998-6004.
20. Alexopoulou L, Holt AC, Medzhitov R, Flavell RA. Recognition of double-stranded RNA and activation of NF-kappaB by Toll-like receptor 3. Nature. 2001;413(6857):732-8.
21. Matsumoto M, Funami K, Tanabe M, Oshiumi H, Shingai M, Seto Y, et al. Subcellular localization of toll-like receptor 3 in human dendritic cells. Journal of Immunology. 2003;171(6):3154-62.
22. Sarkar SN, Elco CP, Peters KL, Chattopadhyay S, Sen GC. Two tyrosine residues of toll-like receptor 3 trigger different steps of NF-κB activation. Journal of Biological Chemistry. 2007;282(6):3423-7.
23. Gauzzi MC, Del Corno M, Gessani S. Dissecting TLR3 signalling in dendritic cells. Immunobiology. 2010;215(9-10):713-23.
24. Yoneyama M, Kikuchi M, Natsukawa T, Shinobu N, Imaizumi T, Miyagishi M, et al. The RNA helicase RIG-I has an essential function in double-stranded RNA-induced innate antiviral responses. Nat Immunol. 2004;5(7):730-7.
25. Borden EC, Sen GC, Uze G, Silverman RH, Ransohoff RM, Foster GR, et al. Interferons at age 50: past, current and future impact on biomedicine. Nat Rev Drug Discov. 2007;6(12):975-90.
26. Amit I, Regev A, Hacohen N. Strategies to discover regulatory circuits of the mammalian immune system. Nature reviews Immunology. 2011;11(12):873-80.
27. Reimer T, Brcic M, Schweizer M, Jungi TW. poly(I:C) and LPS induce distinct IRF3 and NF-κB signaling during type-I IFN and TNF responses in human macrophages. Journal of Leukocyte Biology. 2008;83(5):1249-57.
28. Adib-Conquy M, Scott-Algara D, Cavaillon J-M, Souza-Fonseca-Guimaraes F. TLR-mediated activation of NK cells and their role in bacterial/viral immune responses in mammals. Immunol Cell Biol. 2014;92(3):256-62.
29. Sandig H, Bulfone-Paus S. TLR signaling in mast cells: common and unique features. Front Immunol. 2012;3:185.
30. Gallego C, Golenbock D, Gomez MA, Saravia NG. Toll-Like Receptors Participate in Macrophage Activation and Intracellular Control of Leishmania (Viannia) panamensis. Infection and Immunity. 2011;79(7):2871-9.
31. Kaisho T, Akira S. Regulation of dendritic cell function through Toll-like receptors. Current molecular medicine. 2003;3(4):373-85.
32. Prince LR, Whyte MK, Sabroe I, Parker LC. The role of TLRs in neutrophil activation. Current opinion in pharmacology. 2011;11(4):397-403.
33. Pegu A, Qin S, Fallert Junecko BA, Nisato RE, Pepper MS, Reinhart TA. Human lymphatic endothelial cells express multiple functional TLRs. J Immunol. 2008;180(5):3399-405.
34. Venugopal PG, Nutman TB, Semnani RT. Activation and regulation of toll-like receptors (TLRs) by helminth parasites. Immunologic research. 2009;43(1-3):252-63.
35. Ishii KJ, Koyama S, Nakagawa A, Coban C, Akira S. Host Innate Immune Receptors and Beyond: Making Sense of Microbial Infections. Cell host & microbe. 2008;3(6):352-63.
36. Mantovani A, Allavena P, Sica A, Balkwill F. Cancer-related inflammation. Nature. 2008;454(7203):436-44.

37. Harmey JH, Bucana CD, Lu W, Byrne AM, McDonnell S, Lynch C, et al. Lipopolysaccharide-induced metastatic growth is associated with increased angiogenesis, vascular permeability and tumor cell invasion. International journal of cancer. 2002;101(5):415-22.
38. Jego G, Bataille R, Geffroy-Luseau A, Descamps G, Pellat-Deceunynck C. Pathogen-associated molecular patterns are growth and survival factors for human myeloma cells through Toll-like receptors. Leukemia : official journal of the Leukemia Society of America, Leukemia Research Fund, UK. 2006;20(6):1130-7.
39. Huang B, Zhao J, Li H, He KL, Chen Y, Chen SH, et al. Toll-like receptors on tumor cells facilitate evasion of immune surveillance. Cancer research. 2005;65(12):5009-14.
40. Grivennikov SI, Greten FR, Karin M. Immunity, inflammation, and cancer. Cell. 2010;140(6):883-99.
41. Kaczanowska S, Joseph AM, Davila E. TLR agonists: our best frenemy in cancer immunotherapy. Journal of Leukocyte Biology. 2013;93(6):847-63.
42. Kindt TJ, Goldsby RA, Osborne BA, Kuby J. Kuby immunology. 6th ed. / ed. New York :: W.H. Freeman; 2007.
43. Rockson SG. Diagnosis and management of lymphatic vascular disease. Journal of the American College of Cardiology. 2008;52(10):799-806.
44. Nipper ME, Dixon JB. Engineering the Lymphatic System. Cardiovascular engineering and technology. 2011;2(4):296-308.
45. Randolph GJ, Angeli V, Swartz MA. Dendritic-cell trafficking to lymph nodes through lymphatic vessels. Nature reviews Immunology. 2005;5(8):617-28.
46. Liao S, Cheng G, Conner DA, Huang Y, Kucherlapati RS, Munn LL, et al. Impaired lymphatic contraction associated with immunosuppression. Proceedings of the National Academy of Sciences of the United States of America. 2011;108(46):18784-9.
47. Dixon JB. Lymphatic lipid transport: sewer or subway? Trends in endocrinology and metabolism: TEM. 2010;21(8):480-7.
48. Swartz MA, Lund AW. Lymphatic and interstitial flow in the tumour microenvironment: linking mechanobiology with immunity. Nature reviews Cancer. 2012;12(3):210-9.
49. Kuan EL, Ivanov S, Bridenbaugh EA, Victora G, Wang W, Childs EW, et al. Collecting lymphatic vessel permeability facilitates adipose tissue inflammation and distribution of antigen to lymph node-homing adipose tissue dendritic cells. J Immunol. 2015;194(11):5200-10.
50. Margaris KN, Black RA. Modelling the lymphatic system: challenges and opportunities. Journal of the Royal Society Interface. 2012;9(69):601-12.
51. Stacker SA, Williams SP, Karnezis T, Shayan R, Fox SB, Achen MG. Lymphangiogenesis and lymphatic vessel remodelling in cancer. Nature reviews Cancer. 2014;14(3):159-72.
52. Swartz MA. The physiology of the lymphatic system. Advanced drug delivery reviews. 2001;50(1-2):3-20.
53. Haig DM, Hopkins J, Miller HRP. Local immune responses in afferent and efferent lymph. Immunology. 1999;96(2):155-63.
54. Roozendaal R, Mebius RE, Kraal G. The conduit system of the lymph node. International immunology. 2008;20(12):1483-7.
55. Van den Broeck W, Derore A, Simoens P. Anatomy and nomenclature of murine lymph nodes: Descriptive study and nomenclatory standardization in BALB/cAnNCrl mice. Journal of immunological methods. 2006;312(1–2):12-9.
56. Willard-Mack CL. Normal structure, function, and histology of lymph nodes. Toxicologic pathology. 2006;34(5):409-24.

57. Barrett T, Choyke PL, Kobayashi H. Imaging of the lymphatic system: new horizons. Contrast Media & Molecular Imaging. 2006;1(6):230-45.
58. Zhang F, Niu G, Lu G, Chen X. Preclinical Lymphatic Imaging. Molecular imaging and biology : MIB : the official publication of the Academy of Molecular Imaging. 2011;13(4):599-612.
59. Szuba A, Shin WS, Strauss HW, Rockson S. The third circulation: radionuclide lymphoscintigraphy in the evaluation of lymphedema. Journal of nuclear medicine : official publication, Society of Nuclear Medicine. 2003;44(1):43-57.
60. Sordillo LA, Pu Y, Pratavieira S, Budansky Y, Alfano RR. Deep optical imaging of tissue using the second and third near-infrared spectral windows. Journal of biomedical optics. 2014;19(5):056004.
61. Weiler M, Kassis T, Dixon JB. Sensitivity analysis of near-infrared functional lymphatic imaging. Journal of biomedical optics. 2012;17(6):066019.
62. Sharma R, Wang W, Rasmussen JC, Joshi A, Houston JP, Adams KE, et al. Quantitative imaging of lymph function. American Journal of Physiology - Heart and Circulatory Physiology. 2007;292(6):H3109-H18.
63. Sevick-Muraca EM. Translation of near-infrared fluorescence imaging technologies: emerging clinical applications. Annual review of medicine. 2012;63:217-31.
64. Weiler M, Dixon JB. Differential transport function of lymphatic vessels in the rat tail model and the long-term effects of Indocyanine Green as assessed with near-infrared imaging. Frontiers in physiology. 2013;4:215.
65. Nelson TS, Akin RE, Weiler MJ, Kassis T, Kornuta JA, Dixon JB. Minimally invasive method for determining the effective lymphatic pumping pressure in rats using near-infrared imaging. American journal of physiology Regulatory, integrative and comparative physiology. 2014;306(5):R281-90.
66. Brandon Dixon J, Weiler MJ. Bridging the divide between pathogenesis and detection in lymphedema. Seminars in Cell & Developmental Biology. 2015;38:75-82.
67. Buretta KJ, Brat GA, Christensen JM, Ibrahim Z, Grahammer J, Furtmuller GJ, et al. Near-infrared lymphography as a minimally invasive modality for imaging lymphatic reconstitution in a rat orthotopic hind limb transplantation model. Transplant international : official journal of the European Society for Organ Transplantation. 2013;26(9):928-37.
68. Ghoroghchian PP, Therien MJ, Hammer DA. In vivo fluorescence imaging: a personal perspective. Wiley interdisciplinary reviews Nanomedicine and nanobiotechnology. 2009;1(2):156-67.
69. Michalet X, Pinaud FF, Bentolila LA, Tsay JM, Doose S, Li JJ, et al. Quantum dots for live cells, in vivo imaging, and diagnostics. Science. 2005;307(5709):538-44.
70. Hama Y, Koyama Y, Urano Y, Choyke PL, Kobayashi H. Two-color lymphatic mapping using Ig-conjugated near infrared optical probes. The Journal of investigative dermatology. 2007;127(10):2351-6.
71. Shields JD, Fleury ME, Yong C, Tomei AA, Randolph GJ, Swartz MA. Autologous chemotaxis as a mechanism of tumor cell homing to lymphatics via interstitial flow and autocrine CCR7 signaling. Cancer cell. 2007;11(6):526-38.
72. Coghlin C, Murray GI. Current and emerging concepts in tumour metastasis. The Journal of pathology. 2010;222(1):1-15.

73. Phan TG, Green JA, Gray EE, Xu Y, Cyster JG. Immune complex relay by subcapsular sinus macrophages and noncognate B cells drives antibody affinity maturation. Nat Immunol. 2009;10(7):786-93.
74. Potin L, Maillat L, Dubrot J, Duraes F, Hugues S, Swartz M. Antigen presentation via MHC class II by lymphatic endothelial cells dampens CD4+ T cell response (IRC7P.436). The Journal of Immunology. 2015;194(1 Supplement):128.17.
75. Pan BT, Johnstone RM. Fate of the transferrin receptor during maturation of sheep reticulocytes in vitro: selective externalization of the receptor. Cell. 1983;33(3):967-78.
76. Trams EG, Lauter CJ, Salem N, Jr., Heine U. Exfoliation of membrane ecto-enzymes in the form of micro-vesicles. Biochimica et biophysica acta. 1981;645(1):63-70.
77. Raposo G, Nijman HW, Stoorvogel W, Liejendekker R, Harding CV, Melief CJ, et al. B lymphocytes secrete antigen-presenting vesicles. The Journal of experimental medicine. 1996;183(3):1161-72.
78. Blanchard N, Lankar D, Faure F, Regnault A, Dumont C, Raposo G, et al. TCR activation of human T cells induces the production of exosomes bearing the TCR/CD3/zeta complex. J Immunol. 2002;168(7):3235-41.
79. Thery C, Regnault A, Garin J, Wolfers J, Zitvogel L, Ricciardi-Castagnoli P, et al. Molecular characterization of dendritic cell-derived exosomes. Selective accumulation of the heat shock protein hsc73. J Cell Biol. 1999;147(3):599-610.
80. Raposo G, Tenza D, Mecheri S, Peronet R, Bonnerot C, Desaymard C. Accumulation of major histocompatibility complex class II molecules in mast cell secretory granules and their release upon degranulation. Molecular biology of the cell. 1997;8(12):2631-45.
81. Ismail N, Wang Y, Dakhlallah D, Moldovan L, Agarwal K, Batte K, et al. Macrophage microvesicles induce macrophage differentiation and miR-223 transfer. Blood. 2012.
82. Park JA, Sharif AS, Tschumperlin DJ, Lau L, Limbrey R, Howarth P, et al. Tissue factor-bearing exosome secretion from human mechanically stimulated bronchial epithelial cells in vitro and in vivo. The Journal of allergy and clinical immunology. 2012.
83. Chivet M, Hemming F, Pernet-Gallay K, Fraboulet S, Sadoul R. Emerging role of neuronal exosomes in the central nervous system. Frontiers in physiology. 2012;3:145.
84. Muller G, Schneider M, Biemer-Daub G, Wied S. Microvesicles released from rat adipocytes and harboring glycosylphosphatidylinositol-anchored proteins transfer RNA stimulating lipid synthesis. Cellular signalling. 2011;23(7):1207-23.
85. Peinado H, Aleckovic M, Lavotshkin S, Matei I, Costa-Silva B, Moreno-Bueno G, et al. Melanoma exosomes educate bone marrow progenitor cells toward a pro-metastatic phenotype through MET. Nat Med. 2012;18(6):883-91.
86. Li T, Yan Y, Wang B, Qian H, Zhang X, Shen L, et al. Exosomes derived from human umbilical cord mesenchymal stem cells alleviate liver fibrosis. Stem Cells Dev. 2012.
87. Vlassov AV, Magdaleno S, Setterquist R, Conrad R. Exosomes: current knowledge of their composition, biological functions, and diagnostic and therapeutic potentials. Biochimica et biophysica acta. 2012;1820(7):940-8.
88. Thery C, Zitvogel L, Amigorena S. Exosomes: composition, biogenesis and function. Nature reviews Immunology. 2002;2(8):569-79.
89. Futter CE, Pearse A, Hewlett LJ, Hopkins CR. Multivesicular endosomes containing internalized EGF-EGF receptor complexes mature and then fuse directly with lysosomes. J Cell Biol. 1996;132(6):1011-23.

90. Thery C, Ostrowski M, Segura E. Membrane vesicles as conveyors of immune responses. Nature reviews Immunology. 2009;9(8):581-93.
91. Lasser C, Eldh M, Lotvall J. Isolation and characterization of RNA-containing exosomes. Journal of visualized experiments : JoVE. 2012(59):e3037.
92. Clayton A, Court J, Navabi H, Adams M, Mason MD, Hobot JA, et al. Analysis of antigen presenting cell derived exosomes, based on immuno-magnetic isolation and flow cytometry. Journal of immunological methods. 2001;247(1-2):163-74.
93. Katzmann DJ, Sarkar S, Chu T, Audhya A, Emr SD. Multivesicular body sorting: ubiquitin ligase Rsp5 is required for the modification and sorting of carboxypeptidase S. Molecular biology of the cell. 2004;15(2):468-80.
94. Claas C, Stipp CS, Hemler ME. Evaluation of prototype transmembrane 4 superfamily protein complexes and their relation to lipid rafts. The Journal of biological chemistry. 2001;276(11):7974-84.
95. Geminard C, De Gassart A, Blanc L, Vidal M. Degradation of AP2 during reticulocyte maturation enhances binding of hsc70 and Alix to a common site on TFR for sorting into exosomes. Traffic. 2004;5(3):181-93.
96. Mobius W, van Donselaar E, Ohno-Iwashita Y, Shimada Y, Heijnen HF, Slot JW, et al. Recycling compartments and the internal vesicles of multivesicular bodies harbor most of the cholesterol found in the endocytic pathway. Traffic. 2003;4(4):222-31.
97. Laulagnier K, Motta C, Hamdi S, Roy S, Fauvelle F, Pageaux JF, et al. Mast cell- and dendritic cell-derived exosomes display a specific lipid composition and an unusual membrane organization. The Biochemical journal. 2004;380(Pt 1):161-71.
98. Wubbolts R, Leckie RS, Veenhuizen PT, Schwarzmann G, Mobius W, Hoernschemeyer J, et al. Proteomic and biochemical analyses of human B cell-derived exosomes. Potential implications for their function and multivesicular body formation. The Journal of biological chemistry. 2003;278(13):10963-72.
99. Yáñez-Mó M, Siljander PRM, Andreu Z, Zavec AB, Borràs FE, Buzas EI, et al. Biological properties of extracellular vesicles and their physiological functions. Journal of Extracellular Vesicles; Vol 4 (2015) incl supplements. 2015.
100. Zappaterra MD, Lisgo SN, Lindsay S, Gygi SP, Walsh CA, Ballif BA. A comparative proteomic analysis of human and rat embryonic cerebrospinal fluid. Journal of proteome research. 2007;6(9):3537-48.
101. Berckmans RJ, Sturk A, van Tienen LM, Schaap MC, Nieuwland R. Cell-derived vesicles exposing coagulant tissue factor in saliva. Blood. 2011;117(11):3172-80.
102. Asea A, Jean-Pierre C, Kaur P, Rao P, Linhares IM, Skupski D, et al. Heat shock protein-containing exosomes in mid-trimester amniotic fluids. Journal of reproductive immunology. 2008;79(1):12-7.
103. Lopera-Vásquez R, Hamdi M, Fernandez-Fuertes B, Maillo V, Beltrán-Breña P, Calle A, et al. Extracellular Vesicles from BOEC in <italic>In Vitro</italic> Embryo Development and Quality. PloS one. 2016;11(2):e0148083.
104. Lai RC, Arslan F, Lee MM, Sze NS, Choo A, Chen TS, et al. Exosome secreted by MSC reduces myocardial ischemia/reperfusion injury. Stem cell research. 2010;4(3):214-22.
105. Thery C, Duban L, Segura E, Veron P, Lantz O, Amigorena S. Indirect activation of naive CD4+ T cells by dendritic cell-derived exosomes. Nat Immunol. 2002;3(12):1156-62.

106. Zitvogel L, Regnault A, Lozier A, Wolfers J, Flament C, Tenza D, et al. Eradication of established murine tumors using a novel cell-free vaccine: dendritic cell-derived exosomes. Nat Med. 1998;4(5):594-600.
107. Admyre C, Johansson SM, Paulie S, Gabrielsson S. Direct exosome stimulation of peripheral human T cells detected by ELISPOT. European journal of immunology. 2006;36(7):1772-81.
108. Walker JD, Maier CL, Pober JS. Cytomegalovirus-infected human endothelial cells can stimulate allogeneic CD4+ memory T cells by releasing antigenic exosomes. J Immunol. 2009;182(3):1548-59.
109. Schorey JS, Cheng Y, Singh PP, Smith VL. Exosomes and other extracellular vesicles in host–pathogen interactions. EMBO reports. 2015;16(1):24-43.
110. Lenassi M, Cagney G, Liao M, Vaupotic T, Bartholomeeusen K, Cheng Y, et al. HIV Nef is secreted in exosomes and triggers apoptosis in bystander CD4+ T cells. Traffic. 2010;11(1):110-22.
111. Silverman JM, Clos J, Horakova E, Wang AY, Wiesgigl M, Kelly I, et al. Leishmania exosomes modulate innate and adaptive immune responses through effects on monocytes and dendritic cells. J Immunol. 2010;185(9):5011-22.
112. Oliveira DL, Rizzo J, Joffe LS, Godinho RM, Rodrigues ML. Where do they come from and where do they go: candidates for regulating extracellular vesicle formation in fungi. International journal of molecular sciences. 2013;14(5):9581-603.
113. Karlsson M, Lundin S, Dahlgren U, Kahu H, Pettersson I, Telemo E. "Tolerosomes" are produced by intestinal epithelial cells. European journal of immunology. 2001;31(10):2892-900.
114. Peche H, Heslan M, Usal C, Amigorena S, Cuturi MC. Presentation of donor major histocompatibility complex antigens by bone marrow dendritic cell-derived exosomes modulates allograft rejection. Transplantation. 2003;76(10):1503-10.
115. Wolfers J, Lozier A, Raposo G, Regnault A, Thery C, Masurier C, et al. Tumor-derived exosomes are a source of shared tumor rejection antigens for CTL cross-priming. Nat Med. 2001;7(3):297-303.
116. Andre F, Schartz NE, Movassagh M, Flament C, Pautier P, Morice P, et al. Malignant effusions and immunogenic tumour-derived exosomes. Lancet. 2002;360(9329):295-305.
117. Andreola G, Rivoltini L, Castelli C, Huber V, Perego P, Deho P, et al. Induction of lymphocyte apoptosis by tumor cell secretion of FasL-bearing microvesicles. The Journal of experimental medicine. 2002;195(10):1303-16.
118. Clayton A, Mitchell JP, Court J, Linnane S, Mason MD, Tabi Z. Human tumor-derived exosomes down-modulate NKG2D expression. J Immunol. 2008;180(11):7249-58.
119. Hong BS, Cho JH, Kim H, Choi EJ, Rho S, Kim J, et al. Colorectal cancer cell-derived microvesicles are enriched in cell cycle-related mRNAs that promote proliferation of endothelial cells. BMC genomics. 2009;10:556.
120. Del Tatto M, Ng T, Aliotta JM, Colvin GA, Dooner MS, Berz D, et al. Marrow cell genetic phenotype change induced by human lung cancer cells. Experimental hematology. 2011;39(11):1072-80.
121. Renzulli JF, 2nd, Del Tatto M, Dooner G, Aliotta J, Goldstein L, Dooner M, et al. Microvesicle induction of prostate specific gene expression in normal human bone marrow cells. The Journal of urology. 2010;184(5):2165-71.

122. Skog J, Wurdinger T, van Rijn S, Meijer DH, Gainche L, Sena-Esteves M, et al. Glioblastoma microvesicles transport RNA and proteins that promote tumour growth and provide diagnostic biomarkers. Nat Cell Biol. 2008;10(12):1470-6.
123. Wolf P. The nature and significance of platelet products in human plasma. British journal of haematology. 1967;13(3):269-88.
124. Saunderson SC, Dunn AC, Crocker PR, McLellan AD. CD169 mediates the capture of exosomes in spleen and lymph node. Blood. 2014;123(2):208-16.
125. Takahashi Y, Nishikawa M, Shinotsuka H, Matsui Y, Ohara S, Imai T, et al. Visualization and in vivo tracking of the exosomes of murine melanoma B16-BL6 cells in mice after intravenous injection. Journal of biotechnology. 2013;165(2):77-84.
126. Sarker S, Scholz-Romero K, Perez A, Illanes SE, Mitchell MD, Rice GE, et al. Placenta-derived exosomes continuously increase in maternal circulation over the first trimester of pregnancy. Journal of Translational Medicine. 2014;12(1):1-19.
127. Hood JL, San RS, Wickline SA. Exosomes released by melanoma cells prepare sentinel lymph nodes for tumor metastasis. Cancer research. 2011;71(11):3792-801.
128. Belting M, Wittrup A. Nanotubes, exosomes, and nucleic acid-binding peptides provide novel mechanisms of intercellular communication in eukaryotic cells: implications in health and disease. J Cell Biol. 2008;183(7):1187-91.
129. Camussi G, Deregibus MC, Bruno S, Cantaluppi V, Biancone L. Exosomes/microvesicles as a mechanism of cell-to-cell communication. Kidney international. 2010;78(9):838-48.
130. Bang C, Thum T. Exosomes: New players in cell-cell communication. Int J Biochem Cell Biol. 2012;44(11):2060-4.
131. Meckes DG, Jr., Raab-Traub N. Microvesicles and viral infection. Journal of virology. 2011;85(24):12844-54.
132. Bobrie A, Colombo M, Raposo G, Thery C. Exosome secretion: molecular mechanisms and roles in immune responses. Traffic. 2011;12(12):1659-68.
133. Reddy ST, Rehor A, Schmoekel HG, Hubbell JA, Swartz MA. In vivo targeting of dendritic cells in lymph nodes with poly(propylene sulfide) nanoparticles. Journal of controlled release : official journal of the Controlled Release Society. 2006;112(1):26-34.
134. Eldh M, Ekstrom K, Valadi H, Sjostrand M, Olsson B, Jernas M, et al. Exosomes communicate protective messages during oxidative stress; possible role of exosomal shuttle RNA. PloS one. 2010;5(12):e15353.
135. Amit I, Garber M, Chevrier N, Leite AP, Donner Y, Eisenhaure T, et al. Unbiased reconstruction of a mammalian transcriptional network mediating pathogen responses. Science. 2009;326(5950):257-63.
136. Kwissa M, Nakaya HI, Oluoch H, Pulendran B. Distinct TLR adjuvants differentially stimulate systemic and local innate immune responses in nonhuman primates. Blood. 2012;119(9):2044-55.
137. Loo YM, Gale M, Jr. Immune signaling by RIG-I-like receptors. Immunity. 2011;34(5):680-92.
138. Kawai T, Akira S. Toll-like receptors and their crosstalk with other innate receptors in infection and immunity. Immunity. 2011;34(5):637-50.
139. Guermonprez P, Valladeau J, Zitvogel L, Théry C, Amigorena S. ANTIGEN PRESENTATION AND T CELL STIMULATION BY DENDRITIC CELLS. Annual Review of Immunology. 2002;20(1):621-67.

140. Verbeek FP, Troyan SL, Mieog JS, Liefers GJ, Moffitt LA, Rosenberg M, et al. Near-infrared fluorescence sentinel lymph node mapping in breast cancer: a multicenter experience. Breast cancer research and treatment. 2014;143(2):333-42.
141. Oliver G, Alitalo K. The lymphatic vasculature: recent progress and paradigms. Annual review of cell and developmental biology. 2005;21:457-83.
142. van den Boorn JG, Dassler J, Coch C, Schlee M, Hartmann G. Exosomes as nucleic acid nanocarriers. Advanced drug delivery reviews. 2012.
143. Li L. Regulation of innate immunity signaling and its connection with human diseases. Current drug targets Inflammation and allergy. 2004;3(1):81-6.
144. Xie Y, Bagby TR, Cohen MS, Forrest ML. Drug delivery to the lymphatic system: importance in future cancer diagnosis and therapies. Expert opinion on drug delivery. 2009;6(8):785-92.
145. Gerner MY, Torabi-Parizi P, Germain RN. Strategically localized dendritic cells promote rapid T cell responses to lymph-borne particulate antigens. Immunity. 2015;42(1):172-85.
146. Schorey JS, Bhatnagar S. Exosome function: from tumor immunology to pathogen biology. Traffic. 2008;9(6):871-81.
147. Chevrier N, Mertins P, Artyomov MN, Shalek AK, Iannacone M, Ciaccio MF, et al. Systematic discovery of TLR signaling components delineates viral-sensing circuits. Cell. 2011;147(4):853-67.
148. Tian T, Wang Y, Wang H, Zhu Z, Xiao Z. Visualizing of the cellular uptake and intracellular trafficking of exosomes by live-cell microscopy. Journal of cellular biochemistry. 2010;111(2):488-96.
149. Ozinsky A, Underhill DM, Fontenot JD, Hajjar AM, Smith KD, Wilson CB, et al. The repertoire for pattern recognition of pathogens by the innate immune system is defined by cooperation between toll-like receptors. Proceedings of the National Academy of Sciences of the United States of America. 2000;97(25):13766-71.
150. Dixon JB, Raghunathan S, Swartz MA. A tissue-engineered model of the intestinal lacteal for evaluating lipid transport by lymphatics. Biotechnology and bioengineering. 2009;103(6):1224-35.
151. Ando T, Jordan P, Joh T, Wang Y, Jennings MH, Houghton J, et al. Isolation and characterization of a novel mouse lymphatic endothelial cell line: SV-LEC. Lymphatic research and biology. 2005;3(3):105-15.
152. Lualdi M, Colombo A, Farina B, Tomatis S, Marchesini R. A phantom with tissue-like optical properties in the visible and near infrared for use in photomedicine. Lasers in surgery and medicine. 2001;28(3):237-43.
153. Sokolova V, Ludwig AK, Hornung S, Rotan O, Horn PA, Epple M, et al. Characterisation of exosomes derived from human cells by nanoparticle tracking analysis and scanning electron microscopy. Colloids and surfaces B, Biointerfaces. 2011;87(1):146-50.
154. Cario E, Podolsky DK. Intestinal epithelial TOLLerance versus inTOLLerance of commensals. Molecular immunology. 2005;42(8):887-93.
155. Shibolet O, Podolsky DK. TLRs in the Gut. IV. Negative regulation of Toll-like receptors and intestinal homeostasis: addition by subtraction. American journal of physiology Gastrointestinal and liver physiology. 2007;292(6):G1469-73.
156. Valadi H, Ekstrom K, Bossios A, Sjostrand M, Lee JJ, Lotvall JO. Exosome-mediated transfer of mRNAs and microRNAs is a novel mechanism of genetic exchange between cells. Nat Cell Biol. 2007;9(6):654-9.

157. Singh PP, LeMaire C, Tan JC, Zeng E, Schorey JS. Exosomes released from M. tuberculosis infected cells can suppress IFN-gamma mediated activation of naive macrophages. PloS one. 2011;6(4):e18564.
158. Nitschke M, Aebischer D, Abadier M, Haener S, Lucic M, Vigl B, et al. Differential requirement for ROCK in dendritic cell migration within lymphatic capillaries in steady-state and inflammation. Blood. 2012;120(11):2249-58.
159. Lai CP, Mardini O, Ericsson M, Prabhakar S, Maguire CA, Chen JW, et al. Dynamic Biodistribution of Extracellular Vesicles in Vivo Using a Multimodal Imaging Reporter. ACS nano. 2014;8(1):483-94.
160. Chan JK, Cheung MK, Husain A, Teng NN, West D, Whittemore AS, et al. Patterns and Progress in Ovarian Cancer Over 14 Years. Obstetrics & Gynecology. 2006;108(3, Part 1):521-8.
161. Lengyel E. Ovarian Cancer Development and Metastasis. The American Journal of Pathology. 2010;177(3):1053-64.
162. Milane L, Singh A, Mattheolabakis G, Suresh M, Amiji MM. Exosome mediated communication within the tumor microenvironment. Journal of controlled release : official journal of the Controlled Release Society. 2015;219:278-94.
163. Valapala M, Vishwanatha JK. Lipid Raft Endocytosis and Exosomal Transport Facilitate Extracellular Trafficking of Annexin A2. Journal of Biological Chemistry. 2011;286(35):30911-25.
164. Tian T, Zhu Y-L, Zhou Y-Y, Liang G-F, Wang Y-Y, Hu F-H, et al. Exosome Uptake through Clathrin-mediated Endocytosis and Macropinocytosis and Mediating miR-21 Delivery. Journal of Biological Chemistry. 2014;289(32):22258-67.
165. Mulcahy LA, Pink RC, Carter DRF. Routes and mechanisms of extracellular vesicle uptake. Journal of Extracellular Vesicles. 2014;3:10.3402/jev.v3.24641.
166. Hirosue S, Vokali E, Raghavan VR, Rincon-Restrepo M, Lund AW, Corthesy-Henrioud P, et al. Steady-state antigen scavenging, cross-presentation, and CD8+ T cell priming: a new role for lymphatic endothelial cells. J Immunol. 2014;192(11):5002-11.
167. Lim HY, Thiam CH, Yeo KP, Bisoendial R, Hii CS, McGrath KC, et al. Lymphatic vessels are essential for the removal of cholesterol from peripheral tissues by SR-BI-mediated transport of HDL. Cell metabolism. 2013;17(5):671-84.
168. Reed AL, Rowson SA, Dixon JB. Demonstration of ATP-dependent, transcellular transport of lipid across the lymphatic endothelium using an in vitro model of the lacteal. Pharmaceutical research. 2013;30(12):3271-80.
169. Baluk P, Fuxe J, Hashizume H, Romano T, Lashnits E, Butz S, et al. Functionally specialized junctions between endothelial cells of lymphatic vessels. The Journal of experimental medicine. 2007;204(10):2349-62.
170. Miteva DO, Rutkowski JM, Dixon JB, Kilarski W, Shields JD, Swartz MA. Transmural flow modulates cell and fluid transport functions of lymphatic endothelium. Circulation research. 2010;106(5):920-31.
171. Beyer M, Mallmann MR, Xue J, Staratschek-Jox A, Vorholt D, Krebs W, et al. High-Resolution Transcriptome of Human Macrophages. PloS one. 2012;7(9):e45466.
172. Unanue ER, Cerottini JC, Bedford M. Persistence of antigen on the surface of macrophages. Nature. 1969;222(5199):1193-5.
173. Li XB, Zhang ZR, Schluesener HJ, Xu SQ. Role of exosomes in immune regulation. Journal of cellular and molecular medicine. 2006;10(2):364-75.

174. Mittelbrunn M, Gutierrez-Vazquez C, Villarroya-Beltri C, Gonzalez S, Sanchez-Cabo F, Gonzalez MA, et al. Unidirectional transfer of microRNA-loaded exosomes from T cells to antigen-presenting cells. Nature communications. 2011;2:282.
175. Didierlaurent A, Brissoni B, Velin D, Aebi N, Tardivel A, Käslin E, et al. Tollip Regulates Proinflammatory Responses to Interleukin-1 and Lipopolysaccharide. Molecular and Cellular Biology. 2006;26(3):735-42.
176. Yeung F, Hoberg JE, Ramsey CS, Keller MD, Jones DR, Frye RA, et al. Modulation of NF-κB-dependent transcription and cell survival by the SIRT1 deacetylase. The EMBO Journal. 2004;23(12):2369-80.
177. Scott I, Norris KL. The Mitochondrial Antiviral Signaling Protein, MAVS, Is Cleaved During Apoptosis. Biochemical and biophysical research communications. 2008;375(1):101-6.
178. Srinivasan S, Vannberg FO, Dixon JB. Lymphatic transport of exosomes as a rapid route of information dissemination to the lymph node. Scientific Reports. 2016;6:24436.
179. Kawai T, Adachi O, Ogawa T, Takeda K, Akira S. Unresponsiveness of MyD88-deficient mice to endotoxin. Immunity. 1999;11(1):115-22.
180. Aderem A, Ulevitch RJ. Toll-like receptors in the induction of the innate immune response. Nature. 2000;406(6797):782-7.
181. Robbins PD, Morelli AE. Regulation of immune responses by extracellular vesicles. Nature reviews Immunology. 2014;14(3):195-208.
182. Greening DW, Gopal SK, Xu R, Simpson RJ, Chen W. Exosomes and their roles in immune regulation and cancer. Seminars in Cell & Developmental Biology. 2015;40:72-81.
183. Liu TF, Yoza BK, El Gazzar M, Vachharajani VT, McCall CE. NAD+-dependent SIRT1 deacetylase participates in epigenetic reprogramming during endotoxin tolerance. The Journal of biological chemistry. 2011;286(11):9856-64.
184. Carson WF, Cavassani KA, Dou Y, Kunkel SL. Epigenetic regulation of immune cell functions during post-septic immunosuppression. Epigenetics. 2011;6(3):273-83.
185. Medzhitov R. Toll-like receptors and innate immunity. Nature reviews Immunology. 2001;1(2):135-45.
186. Heffelfinger C, Pakstis AJ, Speed WC, Clark AP, Haigh E, Fang R, et al. Haplotype structure and positive selection at TLR1. European journal of human genetics : EJHG. 2014;22(4):551-7.
187. Grossman SR, Andersen KG, Shlyakhter I, Tabrizi S, Winnicki S, Yen A, et al. Identifying recent adaptations in large-scale genomic data. Cell. 2013;152(4):703-13.
188. Chapman SJ, Hill AVS. Human genetic susceptibility to infectious disease. Nat Rev Genet. 2012;13(3):175-88.
189. Pucci F, Garris C, Lai CP, Newton A, Pfirschke C, Engblom C, et al. SCS macrophages suppress melanoma by restricting tumor-derived vesicle–B cell interactions. Science. 2016.
190. MacMicking J, Xie QW, Nathan C. Nitric oxide and macrophage function. Annual review of immunology. 1997;15:323-50.
191. Fukumura D, Kashiwagi S, Jain RK. The role of nitric oxide in tumour progression. Nature reviews Cancer. 2006;6(7):521-34.
192. Jelovac D, Armstrong DK. Recent progress in the diagnosis and treatment of ovarian cancer. CA: A Cancer Journal for Clinicians. 2011;61(3):183-203.
193. Vaughan S, Coward JI, Bast Jr RC, Berchuck A, Berek JS, Brenton JD, et al. Rethinking Ovarian Cancer: Recommendations for Improving Outcomes. Nature reviews Cancer. 2011;11(10):719-25.

194. Coussens LM, Werb Z. Inflammation and cancer. Nature. 2002;420(6917):860-7.
195. Karin M, Cao Y, Greten FR, Li Z-W. NF-[kappa]B in cancer: from innocent bystander to major culprit. Nature reviews Cancer. 2002;2(4):301-10.
196. Muccioli M, Benencia F. Toll-like Receptors in Ovarian Cancer as Targets for Immunotherapies. Frontiers in Immunology. 2014;5:341.
197. Rakoff-Nahoum S, Medzhitov R. Toll-like receptors and cancer. Nature reviews Cancer. 2009;9(1):57-63.
198. Nagato T, Celis E. A novel combinatorial cancer immunotherapy: poly-IC and blockade of the PD-1/PD-L1 pathway. Oncoimmunology. 2014;3:e28440.
199. Zhang L, Wang CC. Inflammatory response of macrophages in infection. Hepatobiliary Pancreat Dis Int. 2014;13(2):138-52.
200. Powell DR, Huttenlocher A. Neutrophils in the Tumor Microenvironment. Trends in immunology.37(1):41-52.
201. Granot Z, Jablonska J. Distinct Functions of Neutrophil in Cancer and Its Regulation. Mediators of Inflammation. 2015;2015:11.
202. El Andaloussi S, Lakhal S, Mager I, Wood MJ. Exosomes for targeted siRNA delivery across biological barriers. Advanced drug delivery reviews. 2012.